

UNIVERSITEIT ANTWERPEN
UNIVERSITAIRE INSTELLING ANTWERPEN

Departement Schelkunde

Instituut voor Zeewetenschappelijk onderzoek
Institute for Marine Scientific Research
Prinses Elisabethlaan 69
8401 Brodene - Belgium - Tel. 059 / 80 37 15

**Automated electron probe X-ray microanalysis
combined with multivariate analysis for application
in marine research**

Proefschrift ter verkrijging van de graad van Doctor in de Wetenschappen aan
de Universitaire Instelling Antwerpen te verdedigen door Paul BERNARD

Promotor :

Prof. Dr. R. Van Grieken

Antwerpen, 1989

kech ok
cot.
2 dag helen
Mueler

universitaire
instelling
antwerpen



11.10.89

universiteit antwerpen

NB#15

universiteitsplein 1
b-2610 wilrijk
tel. (03) 820 20 20

10 oktober 1989

Geachte Mevrouw Jaspers,
Gelieve, voor de bibliotheek van het IZWO,
een exemplaar van mijn doctoraatsproefschrift te vinden, dat
ik 6 oktober heb verdedigd. Met dit werk behaalde ik
de titel van Doctor in de Wetenschappen richting scheikunde
met de grootste onderscheiding

Met de groeten van

Paul BERNARD

UNIVERSITEIT ANTWERPEN
UNIVERSITAIRE INSTELLING ANTWERPEN
Departement Schelkunde

66384

**Automated electron probe X-ray microanalysis
combined with multivariate analysis for application
in marine research**

Proefschrift ter verkrijging van de graad van Doctor in de Wetenschappen aan
de Universitaire Instelling Antwerpen te verdedigen door Paul BERNARD

Promotor :

Prof. Dr. R. Van Grieken

Antwerpen, 1989

Dankwoord

Mijn zeer oprechte dank gaat uit naar mijn promotor, Prof. Dr. R. Van Grieken, voor zijn wetenschappelijke begeleiding en constructieve raadgevingen tijdens het tot stand komen van dit werk.

Ik wens Dr. L. Brüggmann, Dr. F. Dehairs en Dr. D. Eisma te danken voor hun stimulerende en verhelderende discussies aangaande het mariene suspensie onderzoek, en voor de mogelijkheden die ze me boden om te participeren in onderzoeksprojecten.

Mijn legerdienst, die ik via de dienst Studie en Onderzoek van de Zeemacht bij de Beheerseenheid Mathematisch Model (BMM) heb doorgebracht, heeft mijn horizon aangaande het mariene onderzoek verruimd. Hiervoor ben ik in het bijzonder Dr. G. Pichot en ir. A. Pollentier dankbaar, die mij deze kans hebben gegeven.

Verder wens ik alle collega's van de Universitaire Instelling Antwerpen mijn dank te betuigen voor de vlotte samenwerking en de stimulerende wetenschappelijke conversaties.

Het Instituut tot Aanmoediging van het Wetenschappelijk Onderzoek in Nijverheid en Landbouw (IWONL) ben ik erkentelijk voor de financiële steun die ik gedurende drie jaar heb genoten.

Tenslotte wil ik graag mijn ouders en mijn vrouw danken voor de morele steun en de mogelijkheden die ze me hebben geboden om mijn studie te volbrengen.

TABLE OF CONTENTS

<u>Chapter 1 : Introduction</u>	1
<u>Chapter 2 : Electron probe X-ray microanalysis</u>	5
2.1 The Jeol Superprobe JXA-733	9
2.1.1 Working conditions.	11
2.1.2 Electron-solid interactions and the detector systems.	11
2.2 Automated individual particle analysis	21
2.2.1 The Tracor Northern particle recognition and characterization program.	21
2.2.2 The 733b particle analysis program.	23
2.3 Deconvolution techniques for X-ray spectra	25
2.3.1 Regions of interest.	25
2.3.2 Fast filter algorithm.	26
2.3.3 AXIL program.	27
2.3.4 Comparison of the deconvolution techniques.	28
2.4 Quantitative electron microprobe analysis	35
2.5 References	39
<u>Chapter 3 : Multivariate analysis</u>	41
3.1 Principal component analysis	43
3.1.1 Theoretical background.	43
3.1.2 Applications.	47
3.2 Cluster analysis	51
3.2.1 Hierarchical cluster techniques.	51
3.2.2 Nonhierarchical cluster techniques.	57
3.2.3 Comparison and parameter evaluation of hierarchical cluster techniques.	58

3.2.4 Applications.	96
3.3 References	107
<u>Chapter 4 : Geochemistry of individual suspension particles</u>	
4.1 Estuarine processes	113
4.2 The Ems estuary	119
4.2.1 Results and discussion.	122
4.3 The Gironde estuary	135
4.3.1 Results and discussion.	138
4.4 The Scheldt estuary	145
4.4.1 Results and discussion.	145
4.5 The Baltic Sea	155
4.5.1 Experimental.	157
4.5.2 Results and discussion.	160
4.6 References	187
<u>Chapter 5 : Summary</u>	193
<u>Chapter 6 : Samenvatting</u>	199
<u>Appendix : Publications</u>	205

Chapter 1

Introduction

In modern electron microprobe instruments a variety of signals rapidly provide information about the chemical composition and surface topography of micro-meter size regions of a specimen or of individual microscopic particles. The computer control of these instruments plays a significant role in improving the quality and quantity of the obtained data, and in increasing the flexibility and efficiency of the analysis. Recently it became possible to automatically localize, size and perform an X-ray analysis of a particle on a sequential base. This kind of particle analysis allows the analyses of a large number of features in a relatively short time. Applications were for instance found in studies of atmospheric aerosols, asbestos fibers, mineral inclusions in coal and marine suspended particulate matter. Because such an automated analysis rapidly yields a very large data matrix, a straightforward interpretation is only possible when the individual particles are classified into particle types. In the past, before 1985, all these studies had in common that a preset number of particle types were made in which the measured particles were classified. This approach is preferable if the system under study is well known, as previous knowledge about the system can then be used for the classification of the obtained data and estimations of the accuracy of the procedure can be made. If, however, the information on the system under study is limited or lacking, it is necessary to use non-parametric classification techniques. In a general analysis scheme these techniques should be included and their performance for the study of the data structure and the classification of the data into various particle types should be evaluated. Initially the present study aimed at developing a classification scheme capable of processing the huge amount of data generated by Automated Electron Probe X-ray MicroAnalysis (EPXMA) of particulate samples. For this purpose hierarchical and nonhierarchical cluster analyses were applied.

A large number of hierarchical cluster analyses have been used. In order to select the best method for the classification of the EPXMA data, known mineral mixtures were made and the performance of the different hierarchical cluster

analyses was evaluated on the basis of the cluster results. Kappa statistics were applied to measure quantitatively the degree of correct classification. In this way not only different hierarchical cluster techniques could be tested for a number of mixtures, but it was also possible to elaborate the influence of a number of experimental parameters of the cluster and EPXMA on the cluster results. With regard to the cluster analysis the merits of normalized/unnormalized and of correlated/uncorrelated variables were studied. In the case of the EPXMA it is expected that the quantification of the data can have an influence on the cluster result. To study this effect cluster analyses were applied to relative X-ray data obtained by three different deconvolution techniques and to quantitative Armstrong-Buseck ZAF-corrected data. This allows to predict the effect of the used experimental variables on the final cluster result. Finally a generalized scheme for the multivariate analysis of large EPXMA data sets is given.

For the practical applications of this work, research topics in the aquatic environmental field were chosen. In this field the use of automated EPXMA of suspended particulate matter can have great perspectives but have seldomly been used hitherto. Most single particle analyses in the past were manually performed, with the disadvantage of being enormously time consuming. The use of automated EPXMA allows the fast identification of the particles present in a certain sample. By the use of EPXMA and multivariate analysis particles of different samples can be classified into particle types, and the abundance of the particle types can be followed throughout the study area, to provide information about physical and biogeochemical processes that influence the abundance of certain groups. In this way not only an advanced characterization of the suspended particulate matter is acquired, but processes influencing its composition can be studied.

In practice, the composition of the suspended particulate matter of some estuaries, namely the Ems, Gironde and Scheldt was investigated. By sampling

throughout the whole estuary, the estuarine processes influencing the abundance of some of the identified particle types were studied. These estuarine processes are important with respect to the fate of the suspended particulate matter, which in some cases carries a significant amount of pollutants. Furthermore suspended particulate matter from all over the Baltic Sea was analyzed to identify the individual suspension particles, and to elaborate the influence of some geochemical processes on to the composition of the suspended particulate matter.

Chapter 2

Electron probe X-ray microanalysis

In our rapidly expanding technology, the scientist today is more frequently required to observe and correctly explain phenomena occurring on a micrometer (μm) and submicrometer scale. The electron microprobe is a powerful instrument which permits the characterization of heterogeneous materials, surfaces and particles on such a local scale. In the instrument, the area to be examined is irradiated with a finely focused electron beam, which may be static, or swept in a raster across the surface of the specimen. The types of signals which are produced when the focused electron beam impinges on a specimen surface include secondary electrons, backscattered electrons, Auger electrons, characteristic X-rays, Bremsstrahlung X-ray and photons of various energies. They are obtained from specific emission volumes within the sample and are used to measure many characteristics of the sample.

The primary signals of interest in the Electron Probe X-ray MicroAnalyzer (EPXMA) are the characteristic X-rays. The analysis of the characteristic X-rays, which are emitted from the region at which the electron beam impinges, yields compositional information of both a qualitative and quantitative nature. Variations in the emissions of secondary electrons, backscattered electrons, and characteristic X-rays take place as the electron beam is swept in a raster across the surface of a specimen, due to differences in surface topography and composition, and allow imaging of the sample. A relatively high resolution is obtained by secondary electron imaging, as the secondary electron yield is confined near the beam impact area. The three-dimensional appearance of the images is due to the large depth of focus. Compositional and topographical viewing is obtained by processing the backscattered electron signal. X-ray scanning pictures of the sample allow the study of the elemental distribution in the area of interest.

In general, the variety of signals available in the EPXMA can provide rapid information about composition and surface topography in small regions of the specimen.

The use of a computer controlled instrument improves significantly the quality and quantity of the obtained data. Control of the electron beam, specimen stage, and spectrometers and on-line possibilities for quantitative analysis increases the flexibility of the analysis. The greatest advantage of automation is in particular that it greatly facilitates repetitive-type analysis, which increases the efficiency. Recently it became possible to localize, size and perform an X-ray analysis of a particle on a sequential base. This fully automated EPXMA of particles allows the analysis of a large number of particles within a relatively short time.

This chapter includes a description of :

- the used EPXMA instrument with respect to the working conditions, the electron solid interactions of interest and the required detector systems to measure the generated signals.
- the measurement methodology of automated individual particle analysis for a commercially available and a home-made probe automation software package. The differences between the searching and sizing routines will be discussed.
- the available methods for the deconvolution of the acquired X-ray spectra. First the methods are explained theoretically, while practically the different methods are compared by applying them to clay mineral standards. This was achieved by comparing them in relation to the number of detected (generated) peaks, the percentage of outliers, and the correlation, linear regression, between the obtained intensities.
- the philosophy of the different methods for the correction for the matrix effects in EPXMA. Applying these methods to the net peak intensities obtained by one of the deconvolution techniques leads to quantitative EPXMA results.

A large part of the basic methodology for EPXMA analysis is described in detail in textbooks by Goldstein and Yakowitz (1977), Holt et al. (1974) and Reed (1975). Instrument specifications and the available methods at the University of Antwerp have in most cases already been outlined in the Ph. D. Dissertations of Raeymakers (1986) and Storms (1988). Therefore most of the discussions will be brief but provide all necessary information in a comprehensive way.

2.1 THE JEOL SUPERPROBE JXA - 733

The instrument used in this work at the Department of Chemistry, University of Antwerp (UIA) is a Jeol Superprobe JXA - 733 Electron Probe X-ray MicroAnalyzer. A schematic drawing of the electron microprobe is given in Figure 2.1.

The instrument is equipped with a 30 mm² energy-dispersive Si(Li) detector, a wavelength-dispersive X-ray spectrometer, secondary electron, absorbed electron and transmission electron detectors, and backscattered electron detectors (for composition and topographic viewing).

The microprobe is automated with the Tracor Northern TN-2000 system and is controlled by a LSI 11/23 minicomputer with two double density floppy disk drives. A 9-track 800 bpi magnetic tape unit, connected as an extra bulk storage device, allows the storage of data and provides a convenient medium for transfer of the data to a VAX 11/780 computer for (additional) data analysis.

The sample stage can accurately be positioned in the x, y, z - directions, either manually or under computer control .

The coaxial optical microscope, magnification 414 x, allows the examination of the sample, and more important, allows to control the working distance, which is the distance between the objective lens and the sample. In this way it is possible to adjust the space angles between the sample and the detectors, hence to keep the detection efficiencies constant.

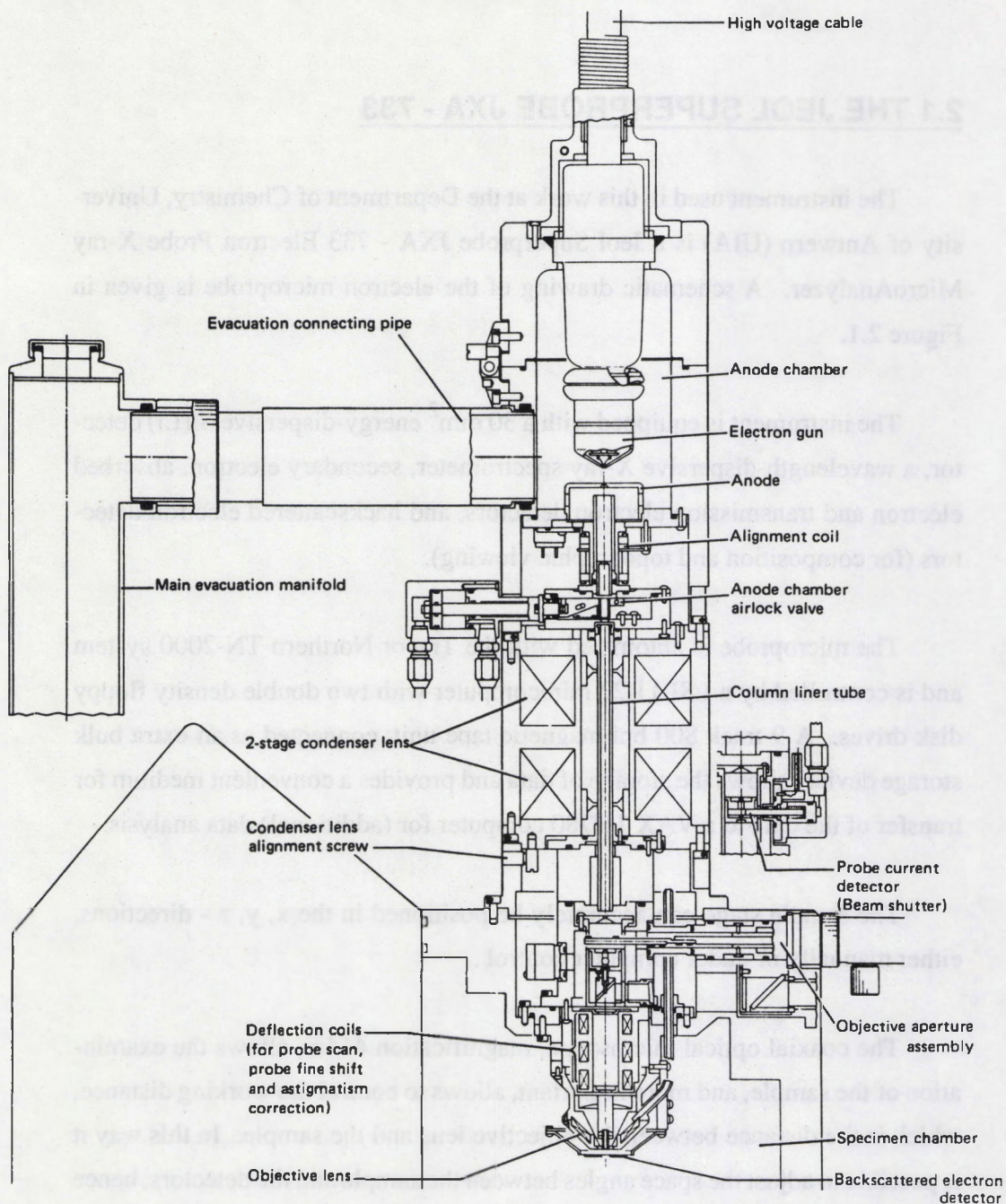


Figure 2.1 : Schematic drawing of the Jeol Superprobe JXA - 733.

2.1.1 Working conditions.

The electron source is a thermionic tungsten filament in an electron gun. At working conditions the filament is heated, by passing a current through it, to about 2800 K. At this temperature the filament releases thermionic electrons which are accelerated toward the anode by a voltage difference of 0-50 kV. The Wehnelt cylinder, which is negatively charged with respect to the cathode, converges the emitted electrons to a crossover of 25-100 μm diameter. A magnetic lens system, composed of a double stage condenser lens and an objective lens system, is used to demagnify the electron image formed at the crossover in the electron gun to the final probe size on the sample. The final spot size is a function of the electron current, the acceleration voltage and some instrumental parameters. Figure 2.2 gives, for the Jeol JXA - 733, the final spot size as a function of the electron current for an accelerating voltage of 30 kV. The decision on the probe current and accelerating voltage to be used for a certain application is in most cases a compromise between : a) a good lateral and depth resolution for imaging and X-ray analysis, and b) the required intensities of the signals to be measured by the different detectors in a reasonable time.

2.1.2 Electron-solid interactions and the detector systems.

Due to electron-matter interactions in the sample under study, a wide range of characteristic specimen-related signals is produced and can be measured by appropriate detectors. The X-ray and electron detectors of the Jeol JXA - 733 will be discussed.

2.1.2.1 Emitted X-rays and X-ray detectors.

Any sufficiently energetic electron beam impinging on a solid specimen generates X-rays. The generated X-rays can be divided in continuum (brem-

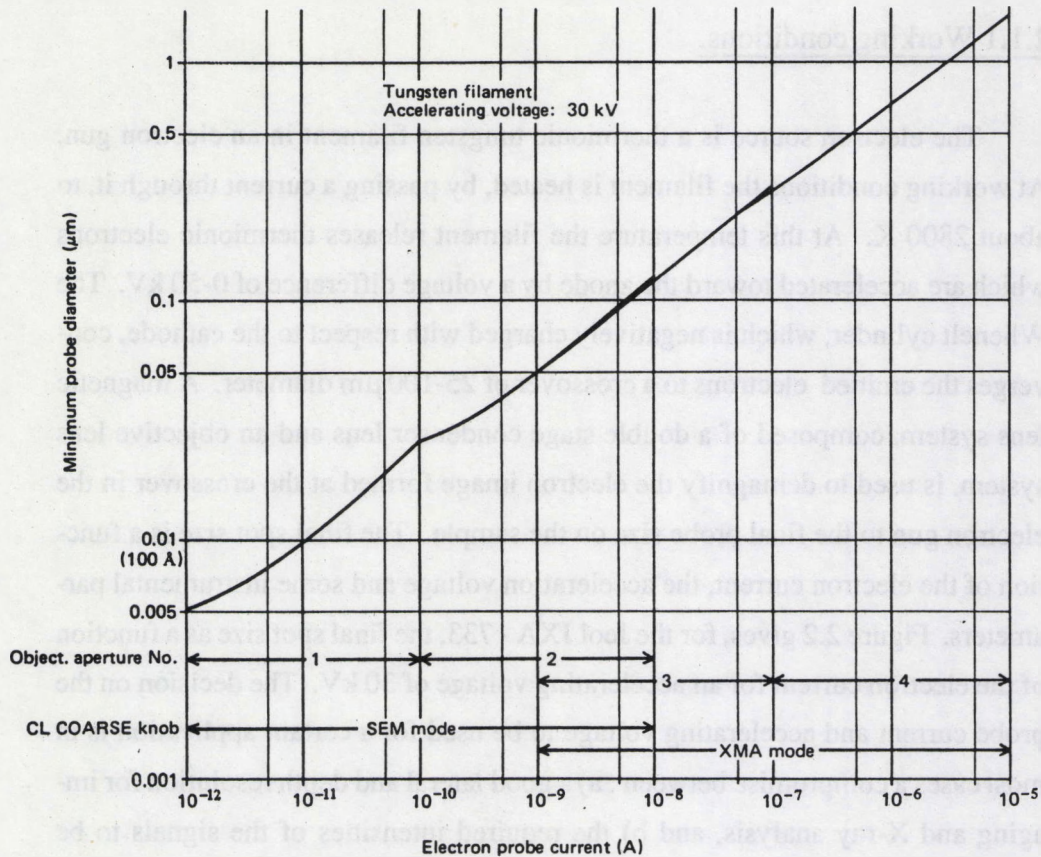


Figure 2.2 : The final electron beam spot size as a function of the electron beam current by an acceleration voltage of 30 kV.

strahlung) and characteristic X-rays, respectively due to elastic and inelastic scattering. The continuous X-ray spectrum is described by the relation of Kramers. This relation determines the continuum intensity as a function of X-ray energy by the probe current, the incident electron energy and the mean atomic number of the specimen. The characteristic X-rays are only emitted when the critical excitation energy is exceeded by the primary electron energy. In which case inner shell ionization of the atom is possible. A characteristic X-ray or Auger electron is emitted when the excited ion returns to its ground level. This process is schematically showed in Figure 2.3. The energy of the emitted X-ray is characteris-

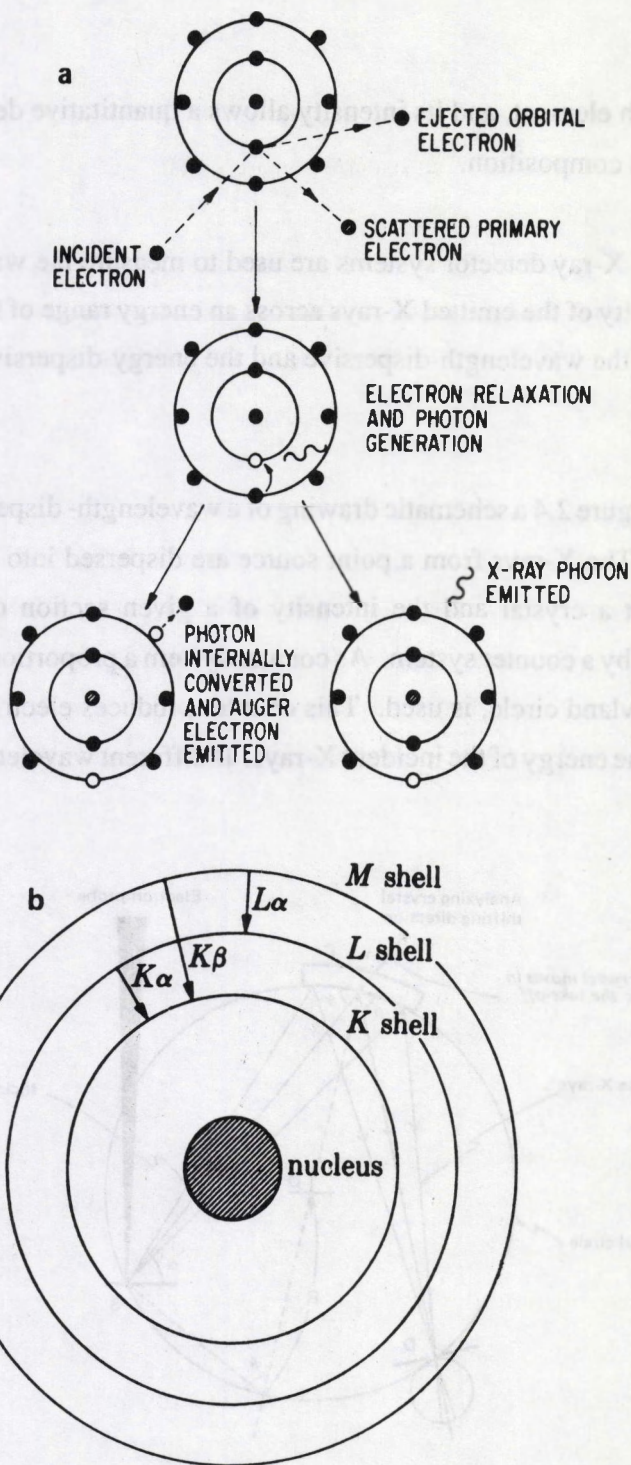


Figure 2.3 : a) Process of electron excitation producing characteristic X-rays or Auger electrons. b) Electronic transitions in an atom (schematic).

tic for each element, and its intensity allows a quantitative determination of the specimens composition.

Two X-ray detector systems are used to measure the wavelength (energy) and intensity of the emitted X-rays across an energy range of 0.2 keV to 20 keV. These are the wavelength-dispersive and the energy-dispersive "solid state" detectors.

In Figure 2.4 a schematic drawing of a wavelength-dispersive spectrometer is given. The X-rays from a point source are dispersed into a spectrum by diffraction at a crystal and the intensity of a given section of the spectrum is measured by a counter system. As counter system a proportional counter, placed at the Rowland circle, is used. This counter produces electrical pulses proportional to the energy of the incident X-rays. If different wavelengths are diffracted

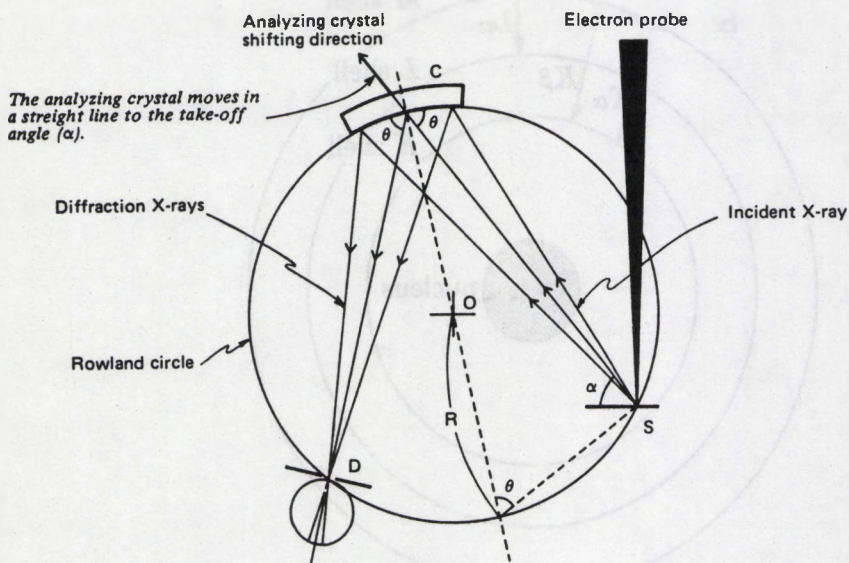


Figure 2.4 : Schematic drawing of a wavelength-dispersive spectrometer.

through the same angle, because of the higher order of reflections, the resultant pulses have different heights and can be separated electronically. The Jeol JXA - 733 is equipped with two wavelength-dispersive spectrometers, each with two different diffraction crystals. In this way the full wavelength range, as shown in Figure 2.5, is covered.

Analyzing crystal	Detection wavelength range (Å)	Atomic number									
		10	20	30	40	50	60	70	80	90	100
STE	21.2 ~ 88.9	⁵ B, ⁸ O, ²⁰ Ca, ²⁴ Cr Kα, Lα, Lβ									
TAP	5.57 ~ 23.4	⁹ F, ¹⁵ P, ²⁴ Cr, ⁴¹ Nb, ⁵⁷ La, ⁸⁰ Hg Kα, Lα, Lβ, Mα									
PET	1.89 ~ 7.93	¹⁴ Si, ²⁶ Fe, ³⁶ Kr, ⁶⁶ Dy, ⁷¹ Lu, ⁹² U Kα, Kβ, Lα, Lβ, Mα									
LIF	0.870 ~ 3.65	¹⁹ K, ³⁸ Sr, ⁴⁸ Cd, ⁹³ Np Kα, Kβ, Lα, Lβ									

STE : Stearate

TAP : Thallium acid phtalate

PET : Pentaerythritol

LIF : Lithium fluoride

Figure 2.5 : Wavelength and element range of the available diffraction crystals.

The energy-dispersive X-ray detector is a solid state detector of silicon treated with lithium, which is held at liquid nitrogen temperature, to prevent migration of the lithium and to reduce electrical noise. The surface of the detector is protected from contaminants in the microprobe vacuum system by a beryllium window of 12 μm thickness. The X-rays passing through the window interact with the silicon and produce electrical pulses. The pulses are amplified and fed into a multichannel pulse height analyzer for analysis, storage and subsequent display.

An intercomparison of the two detector systems is given in Table 2.1. By using the energy-dispersive system and analyzing all the X-rays simultaneously, the analysis time is low but the energy resolution is poor. Using the wavelength-dispersive system the analysis time is high, due to the necessity of scanning the whole spectrum, but the energy resolution is good.

	Wavelength-dispersive	Energy-dispersive
Energy resolution	< 10 eV	150 eV
Solid angle	~ 0.001 ster, variable	~ 0.01 ster, fixed
Detector efficiency	< 30 %	100 % (for ~ 3–15 keV)
Focusing requirements	Focusing circles	Minimal
Mechanical design	Complex	No moving parts
Scanning	Required	Not required
Speed of analysis	Minutes to hours	Seconds to minutes

Table 2.1 : Comparison of the wavelength-dispersive and energy-dispersive systems.

2.1.2.2 Emitted electrons and electron detectors.

The typical form of an energy spectrum of electrons emitted from a target is shown in Figure 2.6.

The first part of the spectrum, the electrons with an energy less than 50 eV, are defined as secondary electrons. The origin of the secondary electrons is the large number of low energy electrons generated in the energy dissipation process. Those electrons reaching the surface with an energy greater than the work-

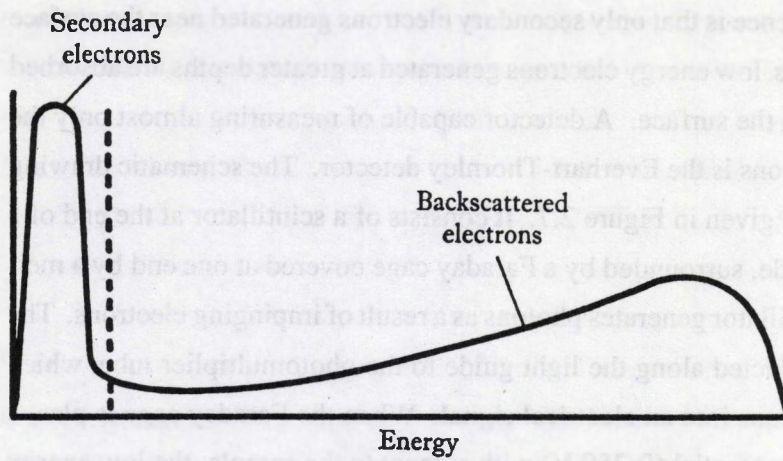
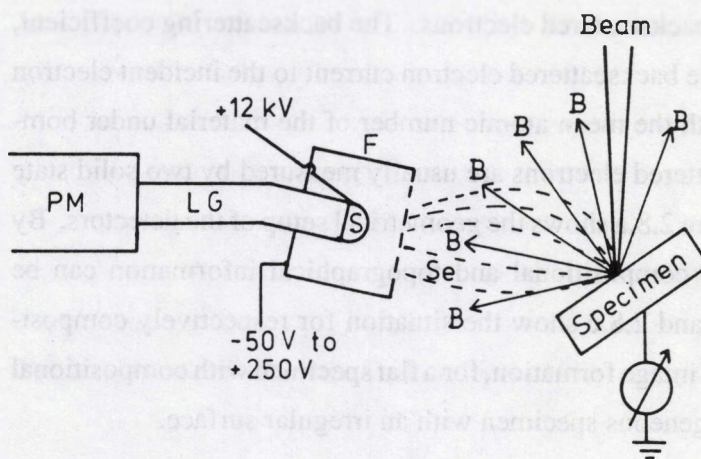


Figure 2.6 : Schematic energy spectrum of the emitted secondary and backscattered electrons from an irradiated target.



- | | |
|-----------------------------|--------------------------|
| F : Faraday cage | Se : Secondary electrons |
| S : Scintillator | LG : Light Guide |
| B : Backscattered electrons | PM : Photo Multiplier |

Figure 2.7 : Everhart-Thornley detector, with biased grid to control secondary electron collection.

ing function of the target material have a finite change of escaping the surface. A direct consequence is that only secondary electrons generated near the surface are measurable, as low energy electrons generated at greater depths are absorbed before they reach the surface. A detector capable of measuring almost only the low energy electrons is the Everhart-Thornley detector. The schematic drawing of this detector is given in Figure 2.7. It consists of a scintillator at the end of a perspex light guide, surrounded by a Faraday cage covered at one end by a metal grid. The scintillator generates photons as a result of impinging electrons. The photons are conducted along the light guide to the photomultiplier tube, which converts the photons into an electrical signal. When the Faraday cage is placed at a low positive potential (0-250 V) with respect to the sample, the low energy electrons are deflected and collected. They are accelerated toward the scintillator by a high voltage, about 12 kV, because the scintillator process is only effective for high energy electrons.

The second part of the electron energy spectrum, electron energy higher than 50 eV, consists of backscattered electrons. The backscattering coefficient, defined as the ratio of the backscattered electron current to the incident electron beam current, varies with the mean atomic number of the material under bombardment. The backscattered electrons are usually measured by two solid state electron detectors. Figure 2.8.a shows the geometrical setup of the detectors. By proper signal treatment compositional and topographical information can be derived. Figures 2.8.b and 2.8.c show the situation for respectively compositional and topographical image formation, for a flat specimen with compositional differences and a homogeneous specimen with an irregular surface.

2.1.2.3 Other electron detectors.

To measure the transmitted and absorbed electron current the Jeol JXA - 733 is equipped with a transmitted electron detector, while the absorbed current

is measured directly after amplification.

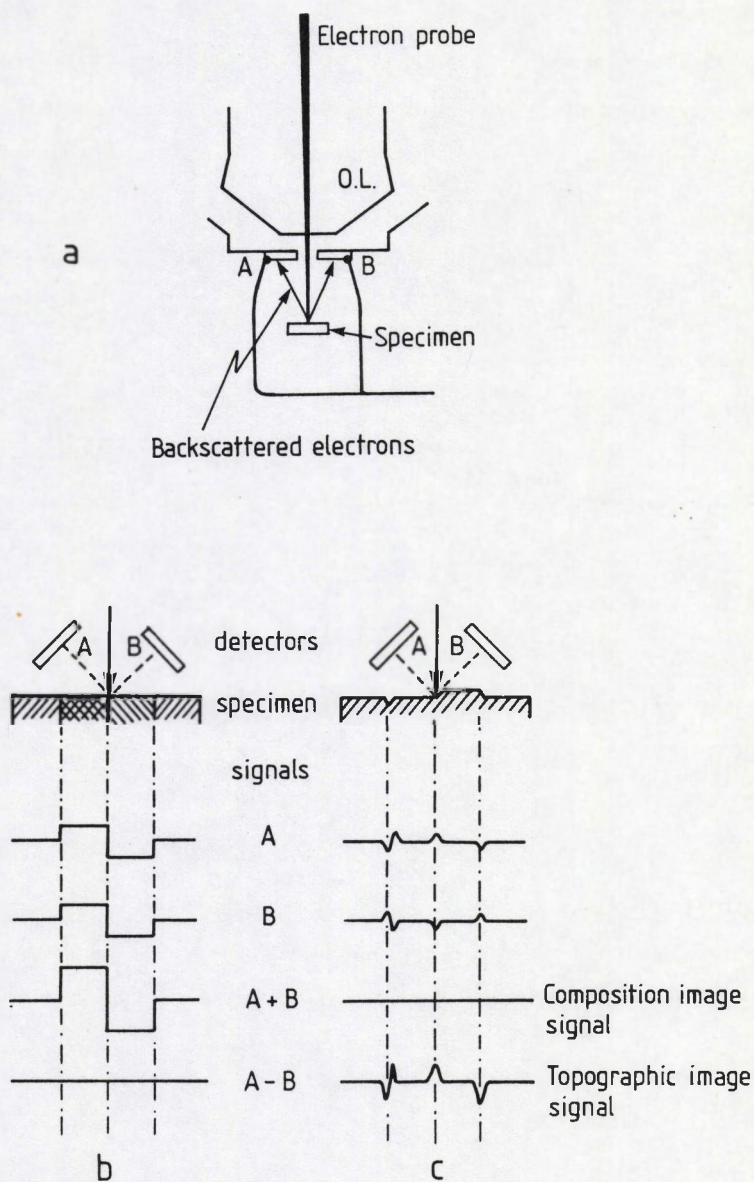


Figure 2.8 : a) Geometrical setup of the solid state detectors for the detection of back-scattered electrons. b) Compositional image formation. c) Topographical image formation.

2.2 AUTOMATED INDIVIDUAL PARTICLE ANALYSIS

The combination of Automated Image Analysis and chemical analysis in electron microscopes and probes was introduced in the last decennia. The image analysis is used to extract quantitative information from the electron microprobe images. The size, shape, intensity and position may be measured from an almost infinite variety of sources, as long as the contrast is sufficient. However artifacts can occur (Kelly et al., 1980) due to :

- a small contrast difference between the particle and the matrix.
- a high matrix noise level or a particle thickness or diameter in the range of the penetration depth of the primary electrons.

These result in :

- not finding and measuring these particles.
- analyzing one particle as several smaller particles.
- a decrease of the total measured particle area.

The computer controlled electron beam is used for the localization of the features and their subsequent X-ray analysis. Tracor Northern Inc. has a commercially available SEM-based automatic image analysis system, the Particle Recognition and Characterization (PRC) program (Fritz, 1982) for the morphological and chemical characterization of individual features. Besides the commercial Tracor Northern software, a home-made 733b particle analysis program was used, with the advantages of a greater flexibility and an improved image analysis. The basic measurement methodology of the two software packages will be outlined in this section.

2.2.1 The Tracor Northern particle recognition and characterization program.

In this system, the digital beam control moves the electron beam across the area to be analyzed according to a 410 x 410 point grid while monitoring a de-

detector signal. The computer moves the electron beam according to the measuring grid until a detector signal above an adjustable lower threshold and below an upper limit is detected. The particle boundary is defined as the location where the detector signal falls outside the selected intensity limits. When a particle is detected, the scan grid resolution is increased 10-fold, and the particle centroid is searched. After the detection of a particle a scan is made over the particle in a direction normal to the previous scan starting from the midpoint between the observed particle boundaries. Such scans normal to the previous one are made subsequently until a stable midpoint position is obtained; this is taken as the centroid. From this point eight diagonal scans over the particle are made, and the coordinates of these 16 contour points are determined. From these coordinates the mean, maximum and minimum diameter, the area, and the circumference (or perimeter) are calculated. A shape factor is calculated as the ratio of the square of the perimeter to 4π times the area. Table 2.2 gives, for a few geometrical figures, the theoretical shape factor. When X-ray analysis is required an energy-

Geometrical figure	Length / width	Shape factor
Circle	1 : 1	1.00
Square	1 : 1	1.27
Rectangular	2 : 1	1.43
	5 : 1	2.29
	10 : 1	3.85
	15 : 1	5.43
	20 : 1	7.00

Table 2.2 : Theoretical shape factor for some geometrical figures.

dispersive X-ray spectrum is collected, for a preset time, at the particle centroid, or while the electron beam rasters over the particle. After a first pretreatment (deconvolution) of the spectrum the size information and the energies and intensities of the characteristic X-rays are stored on a floppy disk as an object vector for each individual particle. The entire X-ray spectrum can also be stored simultaneously on magnetic tape. After a particle is processed, the program goes back to the search mode and moves the beam again across the grid points until the next particle is detected. To avoid reanalysis, the coordinates of the centroids of the detected particles are stored in memory.

2.2.2 The 733b particle analysis program.

The 733b particle analysis program is part of the 733b probe automation package, which also includes automated wavelength-dispersive, energy-dispersive, image acquisition, and subroutines for the (pre)treatment of the data.

The 733b particle analysis differs from the PRC software in the particle searching and sizing methodology. The localization of the particles is achieved by consecutive horizontal line scans over the area of interest. During this process the contour grid points, with an image intensity which meets the threshold requirements, are stored. A particle is totally defined if all the contour grid points are determined. Then the area, perimeter and the equivalent diameter are calculated. The equivalent diameter is defined as the diameter of a circle which corresponds with the measured particle area. If required an X-ray spectrum can be accumulated, while the electron beam is fixed at the center or scans with a choice of several possible patterns across the particle. After a particle is measured the program proceeds with the line scans. The X-ray spectra can be stored on magnetic tape, or on-line deconvolution of the spectrum can be performed after which the data per particle are stored on floppy disk.

The main advantages of the 733b particle analysis program are the faster searching mode and the more accurate sizing routine. Even complex particle structures, as for instance diatoms, can accurately be localized and sized, while the PRC program can measure only holomorphic particles correctly.

2.2.2 The 733b particle analysis program

The 733b particle analysis program is part of the 733b probe automation package which also includes associated waveform-discriminator, energy-discriminator, image acquisition and software for the (pre)processing of the data.

The 733b particle analysis differs from the PRC software in the particle searching and sizing methodology. The localization of the particles is achieved by consecutive horizontal line scans over the area of interest. During the process the contour grid points, with an image intensity which meets the threshold requirements, are stored. A particle is totally defined if all the contour grid points are determined. Then the area, perimeter, and the equivalent diameter are calculated. The equivalent diameter is defined as the diameter of a circle which corresponds with the measured particle area. It is reported in X-ray spectra can be accumulated, while the electron beam is fixed at the center of scans with a choice of several possible patterns across the particle. After a particle is measured, the program proceeds with the first scan. The X-ray spectra can be stored on magnetic tape or on the hardcopy output of the spectrum can be performed after which the data per particle are stored on floppy disk.

2.3 DECONVOLUTION TECHNIQUES FOR X-RAY SPECTRA

During this work three different types of deconvolution techniques were used. The two software packages for automated analysis allow the on-line processing of the spectrum by fast deconvolution algorithms, and/or the storage of the spectrum on magnetic tape. The storage of the spectra permits the off-line use of slower deconvolution algorithms, which otherwise would slow down the automated analysis too much. Two fast deconvolution techniques are the Regions Of Interest (ROI) and the Fast Filter Algorithm (FFA). A slower off-line program is the so called Analytical X-ray analysis by Iterative Least squares (AXIL)-program which uses non-linear least squares fitting of the spectrum with a calculated background and a set of Gaussian peaks (Van Espen et al. (1977), Nullens et al. (1979)). These three methods will be described and the major drawbacks and advantages will be discussed. Finally the methods will be compared practically by applying them to a set of clay mineral standards.

2.3.1 Regions of Interest.

The characteristic X-ray peaks of the elements under study are limited by a higher and lower X-ray energy of a number of ROI. These higher and lower X-ray energies are expected to be the peak boundaries. The net peak intensities are calculated by subtracting the linearly interpolated background contributions from the total counts in the ROI. A peak is retained, if its net peak intensity is greater than three times the standard deviation of the background intensity. Otherwise the peak is assumed to be noise, and is rejected. If the low energy resolution energy-dispersive detector is used, the ROI does not produce accurate results, as the method is sensitive to peak overlap and energy shifts of the detector. In case of on-line automated analysis the operator has to be well informed about the elements to be measured in the total sample. Missing an element (ROI) can

lead to severe errors in the final result. If elements are measured for which peak overlap occurs it is still necessary to process the data off-line.

2.3.2 Fast Filter Algorithm.

The energy-dispersive spectrum is altered by the Hardeman transformation (Op de Beeck and Hoste, 1975). For all channel numbers (k) a new intensity is calculated by the expression :

$$H_k = \sum_{j=-m}^m h(j) S_{k+j}$$

where H_k is the Hardeman transform of channel k , $h(j)$ is the symmetrical convolution function with a square wave of period $2m$ with a value between -1 and

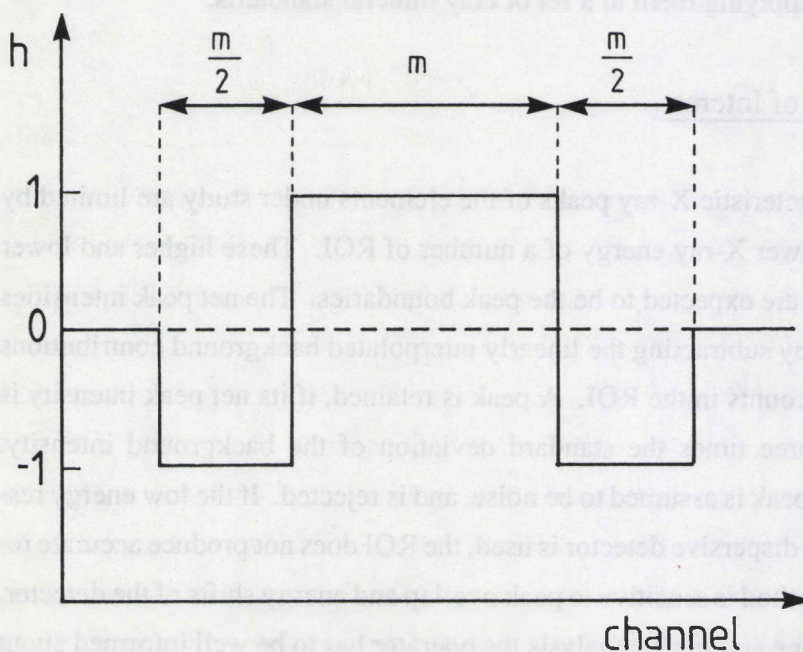


Figure 2.9 : Symmetrical convolution function with a square wave of period $2m$.

1. Figure 2.9 represents the symmetrical convolution function used by the Hardeeman transformation. S_{k+j} is the number of counts in the $k+j$ channel number. In this way the spectrum is transformed into a form which is smaller or equal to zero, except in the neighborhood of characteristic X-ray peaks where high positive values are encountered. The positions and intensities of the peaks are then determined on the hand of this new spectrum. In general, as explained by Janssens (1985), the method is fast in relation to calculation time and reliable for detecting the characteristic X-ray peaks. Small peaks can however be neglected by the routine, with possible consequences for the further data analysis. It is clear that, for instance, in case of the binary cluster algorithm, described by Raeymakers (1986), used to classify particles with respect to the occurrence of elements, the use of the FFA as deconvolution technique can introduce some errors.

To execute the FFA no a priori knowledge of the elements under study is required. However for large particle populations an expert system for the element identification is needed. Making the peak-element association manually would be too time consuming. In the case of marine and river suspended and sediment material an expert system for a limited number of elements was developed. The system will deal minimally with these elements most commonly encountered, with a significant concentration, in single marine particles. The elements included in the program are Na, Mg, Al, Si, P, S, Cl, K, Ca, Sc, Ti, V, Cr, Mn, Fe, Co, Ni, Cu, Zn, Ba. Recently a more general and advanced expert system became available (Janssens, 1989).

2.3.3 AXIL program.

The spectrum deconvolution is based on the least square fitting using a modified Marquardt algorithm (Bevington (1969), Nullens et al. (1979)). In this procedure the parameters of a non-linear analytical function, the fitting function, are iteratively refined in order to minimize the difference in a weighted least

square sense between the model and the observed spectrum. The background is calculated by a linear polynomial model for small energy regions or by an exponential polynomial model for the entire X-ray spectrum. The calculated background is modified by the X-ray attenuation term. In practice, the AXIL program is only used off-line as the calculation time is high. The need of input from the operator to select the elements under study is in this case not a serious drawback. This because the quality of the fit is controlled, and by working off-line the user can alter the setup for some special particles under study. In this way the net peak intensities are accurately calculated, even for complex X-ray spectra with peak overlap.

2.3.4 Comparison of the deconvolution techniques.

For the comparison of the deconvolution techniques, they were applied to the analysis of clay mineral standard spectra. The used clay minerals were dickite, montmorillonite, nontronite, illite and pyrophyllite of the American Petroleum Institute (API standards). The bulk composition of the mineral standards, water excluded and the total iron content converted to Fe_2O_3 , is represented in Table 2.3. The grained minerals were measured by the 733b automated individual particle analysis program. For all the mineral standards the deconvolution techniques were compared in relation to the percentage of outliers, on a 3σ criteria for every variable, and in relation to the number of the identified (generated) peaks. The intensities obtained by the different deconvolution techniques were compared in a single case. The influence of the used deconvolution technique on further data treatment by the use of cluster analysis is discussed in section 3.2.3.3.

2.3.4.1 EPXMA measurements of the mineral standards.

The grained mineral standards were suspended in Milli-Q-water. Aliquots

of these suspensions were filtered over a 25 mm diameter, 0.4 μm pore-size Nuclepore membrane filter. Care was taken to obtain a sufficient loading for analysis while maintaining a low percentage (less than 5%) of overlapping particles (Kelly et al., 1980). After air drying, in a laminar flow box, the filters were vacuum coated with carbon.

The measurements were performed at an electron beam energy of 20 keV and a beam current of 1 nA. The magnification was 1000 x, allowing particles larger than 0.28 μm to be analyzed. The FFA was used on-line and the results were stored on a floppy disk. Meanwhile the collected energy-dispersive X-ray spectra were stored on a magnetic tape. This allowed off-line peak deconvolution of the spectra with ROI and AXIL.

2.3.4.2 Results and discussion.

Table 2.4 gives for each measured mineral standard, the number of measured particles, the percentage of outliers and the percentage of the detected peaks (detection frequency) for the ROI, FFA and AXIL deconvolution technique. The detection frequency is defined as the number of detected peaks divided by the total number of particles multiplied by hundred.

The percentage of outliers, which were rejected on a 3σ criteria for each variable, was highest when the deconvolution was performed with the ROI. When using the FFA a minimum of outliers was found, except for the montmorillonite case where the lowest number of outliers was obtained by using AXIL. For the ROI deconvolution technique it is assumed that the number of outliers is increased due to statistical fluctuations of the intensities measured at the ROI boundaries. By performing a linear interpolation this sometimes leads to the generation of outliers in the case of low abundance elements.

Mineral	Concentration (w%)								
	Na_2O	MgO	Al_2O_3	SiO_2	K_2O	CaO	TiO_2	MnO_2	$Fe_2O_3^*$
Dickite	0.14	—	46.8	52.5	0.18	0.60	0.02	—	0.01
Montmorillonite	0.22	6.06	21.6	66.4	0.61	2.95	0.42	0.01	2.11
Nontronite	0.18	0.08	6.55	51.2	0.30	2.42	—	—	40.0
Illite	0.47	2.27	20.3	62.4	5.59	1.74	0.88	—	5.76
Pyrophyllite	0.23	0.05	17.1	80.2	1.31	0.42	0.19	—	0.49

— Trace content.

* Total metal content converted to Fe_2O_3 .

Table 2.3 : Bulk composition of the standard clay minerals, water excluded and the total iron content converted to Fe_2O_3 .

Mineral	Number of measured particles	Deconvolution technique	Outliers (%)	Number of detected peaks (%)								
				Na	Mg	Al	Si	K	Ca	Ti	Mn	Fe
Dickite	298	ROI	8.7	3.4	0	99.7	96.6	7.0	10.7	6.0	5.4	8.7
		FFA	5.0	0	0	99.0	95.6	0.3	4.0	0	0	1.3
		AXIL	7.0	0	32.6	99.3	97.7	0.7	6.4	21.8	1.0	33.6
Montmorillonite	300	ROI	13	3.7	17.3	99.7	99.7	7.0	44.0	6.0	7.7	73.3
		FFA	7.7	0.3	1.3	98.0	99.7	1.0	10.3	0.7	0	67.3
		AXIL	4.0	0	6.7	99.7	100	1.3	57.7	32.3	0	100
Nontronite	298	ROI	16	5.0	9.4	78.9	99.3	11.7	28.2	6.4	7.4	94.3
		FFA	10	0.7	1.3	42.6	99.0	3.4	5.0	1.7	0	93.0
		AXIL	14	0	14.4	88.6	99.3	7.4	29.2	21.8	0	98.3
Illite	292	ROI	22	5.8	11.6	79.8	93.5	78.1	8.9	12.7	6.5	78.1
		FFA	14	0	0.7	75.3	90.1	65.8	3.1	4.1	0	67.5
		AXIL	14	0.3	39.7	84.2	91.1	78.8	9.9	28.8	0	97.6
Pyrophyllite	286	ROI	11	5.2	3.5	80.8	98.6	42.7	8.4	7.7	8.0	17.8
		FFA	6.6	0	0.7	77.6	97.6	25.9	2.4	1.0	0.7	11.2
		AXIL	7.0	0	22.4	87.4	98.3	34.6	2.8	20.6	0.7	47.2

Table 2.4 : Comparison of the deconvolution techniques with respect to the percentage of outliers and the detected peak frequency.

The lowest number of peaks for each standard and each element was detected by the FFA. Comparing Table 2.3 with Table 2.4 reveals that the differences between the number of detected peaks for the FFA and the other deconvolution techniques increases for the relatively low abundance elements. This phenomenon is seen best for the elements Al and Fe, as their concentration ranges from 6.6 % to 46.8 % and 0.01 % to 40.0 %, respectively. The difference becomes only significant for low element concentrations. This is probably due to the FFA property of sometimes neglecting small peaks, which increases the detection limit of the method. In the case of high element concentrations, as for instance in the case of Si, the differences between the different deconvolution methods are negligible.

For the montmorillonite measurements the net peak intensities of the three methods were also compared. This was done by using linear regression analysis, for the elements with relatively high concentrations, e.g. Al, Si, Ca and Fe. The linear regression analysis was performed for the unnormalized intensities and for the normalized intensities, between ROI and AXIL, and between FFA and AXIL. The results of these analyses are summarized in Table 2.5. It is seen that, except for Ca, the measured intensities have the following order : $I_{(FFA)} > I_{(AXIL)} > I_{(ROI)}$. Actually the FFA intensity is not the net peak intensity of the X-ray spectrum but of the transformed spectrum. The use of the transformed spectrum increased the net peak intensity. The differences between the ROI and AXIL is assumed to be due to the inaccurate determination of the net peak intensities by the ROI. Normalization of the intensities decreased the correlation coefficient, probably because the normalized intensity is also a function of all the uncertainties of all the elements.

Equation	Element	A_0	A_1	r
$I_{(ROI)} = A_0 + A_1 \cdot I_{(AXIL)}$	<i>Al</i>	-11	0.86	0.98
	<i>Si</i>	-11	0.72	0.99
	<i>Ca</i>	2.9	0.55	0.73
	<i>Fe</i>	-1.6	0.42	0.91
$I_{norm(ROI)} = A_0 + A_1 \cdot I_{norm(AXIL)}$	<i>Al</i>	2.6	1.0	0.93
	<i>Si</i>	4.9	0.92	0.89
	<i>Ca</i>	0.39	0.72	0.68
	<i>Fe</i>	-1.6	0.81	0.92
$I_{(FFA)} = A_0 + A_1 \cdot I_{(AXIL)}$	<i>Al</i>	-17	1.3	0.97
	<i>Si</i>	-26	1.2	0.99
	<i>Ca</i>	-9.0	0.75	0.64
	<i>Fe</i>	-1.1	1.09	0.93
$I_{norm(FFA)} = A_0 + A_1 \cdot I_{norm(AXIL)}$	<i>Al</i>	0.83	1.0	0.85
	<i>Si</i>	2.1	0.99	0.87
	<i>Ca</i>	-0.7	0.70	0.71
	<i>Fe</i>	-1.2	0.98	0.88

Table 2.5 : Linear regression analysis for the net and normalized peak intensities obtained by ROI - FFA - AXIL.

2.4 QUANTITATIVE ELECTRON MICROPROBE ANALYSIS

The characteristic net peak intensities obtained by applying a deconvolution technique at the X-ray spectrum, can be converted by different methods to elemental concentrations. A distinction is made between the conventional methods used for the quantitative X-ray microanalysis of bulk flat specimen and these methods dealing with the quantitative X-ray microanalysis of irregularly shaped microscopic particles.

The conventional methods are in their turn divided into empirical techniques and the ZAF-correction procedures. Most of these methods are described in detail in textbooks by Goldstein and Yakowitz (1977), Heinrich (1981), and Maurice et al. (1978). In most of these techniques the relative X-ray intensity ratio between the elements of interest in the specimen and the same element in a standard is measured. Both unknown and standard are examined under identical experimental conditions. The X-ray intensities measured on the unknown specimen differ only from those from the standard because of differences in composition. The obtained X-ray intensity ratio has to be corrected for several effects, including :

- the differences in electron scattering and retardation in the specimen and the standard, i.e., the so called atomic number effect, expressed as the correction factor k_Z .
- absorption of X-rays within the specimen, correction factor k_A .
- fluorescence effect as expressed by the factor k_F .

The concentration of an element present in the sample is then calculated as follows :

$$\frac{I_u}{I_s} = \frac{C_u}{C_s} k_Z k_A k_F$$

I_u and I_s are the X-ray intensities of the element for the specimen and the standard, C_u and C_s are the concentration of the element of interest in the specimen and the standard. k_Z , k_A and k_F are respectively the correction factors for the atomic number effect, the absorption effect and the fluorescence effect. Because the correction factors k_Z , k_A and k_F are all dependent upon the true unknown composition of the specimen, the X-ray intensity ratio specimen standard is taken as a first estimation of the composition. An iteration procedure is started until convergence of the results occur. A standardless correction procedure can be applied if instrumental parameters are included; Henoc and Maurice (1978), Wernisch (1985) and Raeymakers (1986).

In the case of individual unpolished microparticles, the measured X-ray intensities differ from those of the flat standards not only because of compositional differences but also because of the so-called "geometrical effect". The geometrical effect becomes important when the dimension of the particle is smaller than the X-ray production volume. The geometrical effect is subdivided into a mass effect, the absorption effect and the fluorescence effect. The mass effect occurs when the dimension of the particle is smaller than the excitation volume of the primary electrons for the element under study in a bulk solid. The electrons may escape the sides and bottom of the particle, which results in a smaller particle to bulk X-ray intensity ratio. This is shown in Figure 2.10 where the mass effect is illustrated. The absorption effect becomes important when the average X-ray absorption path length for a particle is different from that in a bulk material. Secondary fluorescence normally takes place across large volumes, a few hundreds μm^3 . The secondary fluorescence yield will therefore be reduced for small particles.

A preferred correction method for the geometrical effect is the method of Armstrong and Buseck (1975), since it shows less limitations and uncertainties than any other available method at this time (Storms, 1988). This method is

based on the geometrical modelling of the particle shape. Storms (1988) showed that when the results are normalized to 100 %, the use of a spherical particle model for the absorption correction of particles with a different shape gave satisfactory results.

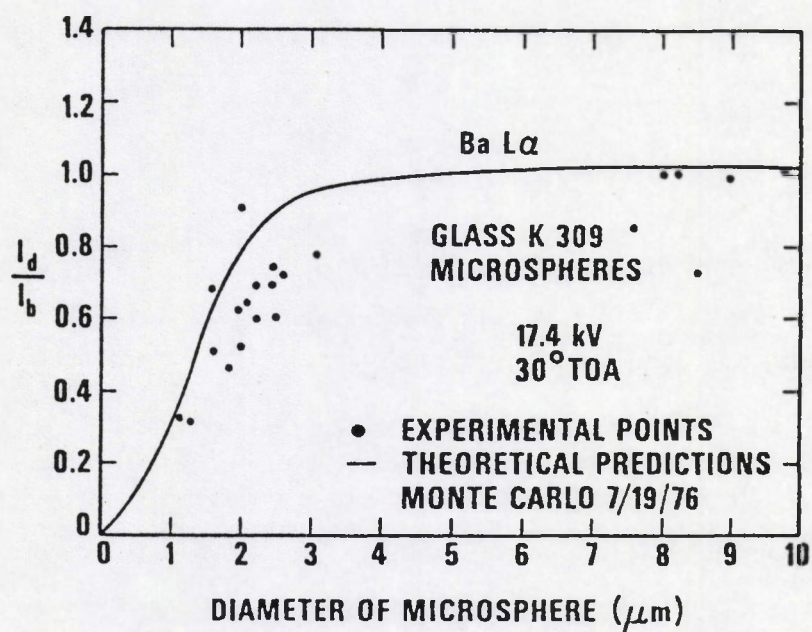


Figure 2.10 : The mass effect as demonstrated by the $\text{Ba } L\alpha$ X-ray intensity for glass spheres (I_d) relative to the bulk X-ray intensity (I_b) as a function of the sphere diameter (adapted from Small et al., 1980).

2.5 REFERENCES

- Armstrong, J. T., and Buseck, P. R., 1975. Quantitative chemical analysis of individual microparticles using the electron microprobe : theoretical. *Anal. Chem.*, 47 : 2178-2192.
- Bevington, P. R., 1969. *Data Reduction and Error Analysis for the Physical Sciences*, Mc. Graw-Hill, New York, 336 pp.
- Fritz, G., 1982. Particle recognition and characterization (TN-1912), Tracor Northern, Inc., 51 pp.
- Goldstein, J. I., and Yakowitz, H., 1977. *Practical scanning electron microscopy*, Plenum Press, New York, 582 pp.
- Heinrich, K. F. J., 1981. *Electron Beam X-Ray Microanalysis*, Van Nostrand Reinhold Company, New York, 578 pp.
- Henoc, J., and Maurice, F., 1978. Practical quantitative analysis of bulk specimens. In : F. Maurice, L. Meny and R. Tixier (Editors), *Microanalysis and Scanning Electron Microscopy*, Les Editions de Physique, Orsay, pp. 281-317.
- Holt, D. B., Muir, M. D., Grant, P. R., and Boswarva, I. M., 1974. *Quantitative Scanning Electron Microscopy*, Academic Press, London, 570 pp.
- Kelly, J. F., Lee, R. J., and Lentz, S., 1980. Automated characterization of fine particulates. *Scanning Electron Microscopy*, I : 311-322.
- Lifshin, E., Ciccarelli, M. F., and Bolon, R. B., 1977. X-ray spectral measurements and interpretation. In : J. I. Goldstein and H. Yakowitz (Editors), *Practical Scanning Electron Microscopy*, Plenum Press, New York, pp. 263-297.
- Janssens, K., 1985. Een expert systeem voor de kwalitatieve interpretatie van energiedispersieve X-stralen spectra. Ms. Dissertation - University of Antwerp (in Dutch).
- Janssens, K., 1989. *Automated Data Handling in X-ray Analysis : An integration of expert systems and conventional software*. Ph. D. Dissertation - University of Antwerp.

- Maurice, F., Meny, L., and Tixier, R., 1978. *Microanalysis and Scanning Electron Microscopy*, Les Editions de Physique, Orsay, 530 pp.
- Nullens, H., Van Espen, P., and Adams, F., 1979. Linear and non-linear peak fitting in energy-dispersive X-ray fluorescence. *X-ray Spectrometry*, 8 : 104-109.
- Op de Beeck, J. P., and Hoste, J., 1975. The application of computer techniques to instrumental neutron activation analysis. *Atomic Energy Review*, 13 : 151-189.
- Raeymakers, B., 1986. *Characterization of Particles by Automated Electron Probe Microanalysis*. Ph. D. Dissertation - University of Antwerp.
- Reed, S. J. B., 1975. *Electron Microprobe Analysis*, Cambridge University Press, Cambridge, 400 pp.
- Small, J. A., Heinrich, K. F. J., Newbury, D. E., Myklebust, R. L., and Fiori, C. E., 1980. Procedure for the quantitative analysis of single particles with the electron probe. In : K. F. J. Heinrich (Editor), *Characterization of Particles* NBS Special Publication 533, pp. 29-38.
- Storms, H., 1988. *Quantification of Automated Electron Microprobe X-ray Analysis and Application in Aerosol Research*, Ph. D. Dissertation - University of Antwerp.
- Van Espen, P., Nullens, H., and Adams, F., 1977. A computer analysis of X-ray fluorescence spectra. *Nuclear Instruments and Methods*, 142 : 243-250.
- Wernisch, J., 1985. Quantitative electron microprobe analysis without standard samples. *X-ray Spectrometry*, 14 : 109-119.

Chapter 3

Multivariate analysis

In most scientific disciplines, multivariate analysis is used to help in the interpretation of large multidimensional arrays. It is needed to describe the relationships between the variables and the samples (objects) in a rigorous and comprehensive way. In the previous chapter, it was seen how powerful the automated electron probe X-ray microanalyzer is in gathering a large amount of data. It was shown that it is possible to transfer the results of the EPXMA to a VAX 11/780 computer for (additional) analysis. The data matrix consists of subsequent rows in which the results of the X-ray analysis and the morphological data of a particle are listed. In the first instance the multivariate analysis was used to elaborate the data structure of the single samples measured by automated EPXMA, and the relation between the individual samples. The use of multivariate analysis was however not limited to the EPXMA results alone, but was expanded to the interpretation of hydrographic and bulk analytical data. The applications of the different multivariate techniques outlined in this chapter are however restricted to their use for the EPXMA results. The other applications can be found in some specific case studies in the following chapter.

In this work some of the frequently used multivariate analysis techniques, as principal component analysis, several hierarchical and a nonhierarchical cluster analysis technique, are described theoretically and with some illustrative examples, their advantages and disadvantages are discussed in relation to their performance to the EPXMA results. The theory of these techniques and their applications in different fields of science are discussed in detail in the textbooks of Anderberg (1973), Massart et al. (1978), Massart and Kaufman (1983) and Mather (1976).

Most of the data presentation, the principal component analysis and the hierarchical cluster analysis was done using a software package, the so-called "Data Processing Program (DPP)", developed by Van Espen (1984). Hierarchical and non-hierarchical cluster analysis was used to accomplish the classifica-

tion or grouping of the analyzed particles. In this way the existing geochemically relevant particle types are identified in the studied sample(s). Because of the existence and the easy availability of a great number of hierarchical cluster analyses the "best" method for the classification of the EPXMA data has to be chosen. Indeed, mostly the different cluster techniques provide also different cluster results. Therefore most authors suggest to use several cluster techniques on the same data set and to confront the obtained results, or to apply in parallel to the cluster analysis a different multivariate technique. Besides the choice of a method, a decision on the used similarity measurement, the use of unnormalized or normalized variables, and the use of correlated or uncorrelated variables is required. Furthermore it is necessary to predict the effect of the measurement errors on the classification. To study this cluster analyses were applied to data consisting of relative peak intensities (obtained by the Regions Of Interest (ROI), the Fast Filter Algorithm (FFA) and by the Analytical X-ray analysis by Iterative Least squares (AXIL) deconvolution techniques) and of the quantitative Armstrong-Buseck ZAF-corrected results. The influence of all these parameters was investigated by constructing mixture models. The mixtures consist of with the automated EPXMA measured standard minerals. For all these mixtures kappa statistics were used to measure the amount of correct classification. The effect of some of these parameters was also studied on aqueous suspension data. Because in this case the correct classification is unknown, the evaluation was necessarily rather intuitive and based on the experience gained.

At the end of the chapter a generalized scheme is given for the multivariate analysis of the EPXMA data and the representativeness of the analysis is discussed.

3.1 PRINCIPAL COMPONENT ANALYSIS

The purpose of the principal component method is to represent the variation present in the data in such a way that, without losing significant information, the dimensionality is reduced. To achieve this, new variables are constructed, according to a linear combination of the original variables, in such a way that :

- the newly formed principal components are uncorrelated, i.e. orthogonal in the n -dimensional space, where n is the number of principal components.
- the principal components are constructed with decreasing degree of importance, i.e. the first principal component represents as much variation as possible, the second represents as much variation as possible after the variation explained by the first component have been removed, etc.

The principal components obtained in this way represent the linear independent variance present in the data of the original variables. Studying the first principal components the most important sources for the variance in the data are examined.

3.1.1 Theoretical background.

The covariance or the correlation matrix is used to calculate the principal components. These matrices are derived from the original data matrix $X(m,n)$ with m objects (particles) and n variables, in which x_{ij} is the value of the i^{th} object of the j^{th} variable. An element of the covariance matrix is given by :

$$C_{kl} = \frac{1}{m-1} \sum_{i=1}^m (x_{ik} - \bar{x}_{.k})(x_{il} - \bar{x}_{.l})$$

where

$$\bar{x}_{.k} = \frac{1}{m} \sum_{i=1}^m x_{ik} \quad \text{and} \quad \bar{x}_{.l} = \frac{1}{m} \sum_{i=1}^m x_{il}$$

are the means of the variables k and l .

The covariance matrix can be written as :

$$C = \begin{pmatrix} c_{11} & c_{12} & \dots & c_{1n} \\ c_{21} & c_{22} & & c_{2n} \\ \vdots & & & \vdots \\ c_{n1} & c_{n2} & \dots & c_{nn} \end{pmatrix}$$

Which is an $n \times n$ matrix. The diagonal elements of the matrix are the variances of the n variables, and their sum is equal to the total variance in the data set.

The relation between the covariance matrix and the correlation matrix is given by :

$$r_{kl} = \frac{c_{kl}}{\sqrt{c_{kk} c_{ll}}}$$

and the correlation matrix is written as :

$$R = \begin{pmatrix} r_{11} & r_{12} & \dots & r_{1n} \\ r_{21} & r_{22} & & r_{2n} \\ \vdots & & & \vdots \\ r_{n1} & r_{n2} & \dots & r_{nn} \end{pmatrix}$$

The correlation coefficient r_{kl} is in fact a standardized covariance, so that its value lies between -1 and +1. The sum of the diagonal elements is now equal to the number of variables.

The linear transformation of the correlated variables \mathbf{Z} to the uncorrelated variables \mathbf{U} can be written for the element u_k as :

$u_k = v_{k1} z_1 + v_{k2} z_2 + v_{k3} z_3 + \dots + v_{kn} z_n$ in matrix form this becomes

$$\mathbf{U} = \mathbf{V} \cdot \mathbf{Z}$$

where

$$\mathbf{Z} = \begin{pmatrix} z_1 \\ z_2 \\ \vdots \\ z_n \end{pmatrix} \quad \mathbf{U} = \begin{pmatrix} u_1 \\ u_2 \\ \vdots \\ u_n \end{pmatrix}$$

and

$$\mathbf{V} = \begin{pmatrix} v_{11} & v_{12} & \dots & v_{1n} \\ v_{21} & v_{22} & & v_{2n} \\ \vdots & & & \vdots \\ v_{n1} & v_{n2} & \dots & v_{nn} \end{pmatrix}$$

The covariance matrix of the new variables is calculated as :

$$\mathbf{C}_u = \mathbf{V} \cdot \mathbf{C}_z \cdot \mathbf{V}'$$

because \mathbf{U} are uncorrelated variables, \mathbf{C}_u is a diagonal matrix, which is a restriction for \mathbf{V} . Furthermore it is required that the first component has maximum variance. Because it is possible to increase the variance of the elements \mathbf{C}_u by increasing the elements of \mathbf{V} another restriction has to be introduced, namely that

the vector V_k is a normalized vector.

$$V_k \cdot V'_k = 1$$

Therefore it is necessary that

$$V'_1 \cdot C \cdot V_1 \text{ is maximized subject to } V'_1 \cdot V_1 = 1$$

These requirements are fulfilled if V_1 is an eigenvector of matrix C , with the largest corresponding eigenvalue λ_1 . The second row of matrix V is obtained by maximizing the variance of U_2 subject to the following restrictions

1. U_2 and U_1 are uncorrelated
2. $V'_2 \cdot V_2 = 1$

Which is an eigenvector corresponding to the second largest eigenvalue. In the same way successive eigenvectors yield successive rows of matrix V . The eigenvectors are obtained in a descending order

$$\lambda_1 \geq \lambda_2 \geq \lambda_3 \cdots \geq \lambda_n$$

The new variables U are called the principal components. These variables are uncorrelated linear functions of the original variables. The total variance of the original data set is retained.

$$\sum_{i=1}^n \lambda_i = \sum_{i=1}^n c_{ii}$$

Because the first principal components explain a great part of the total variance of the sample, studying these few components is essential to elaborate the orig-

inal data structure. The percentage variance explained by a component is defined as :

$$\% \text{ variance of the component} = 100 \cdot (\text{eigenvalue of the component} / \text{total variance})$$

and gives an idea about the component significance.

3.1.2 Applications.

A typical example of a PCA applied to a data set of automated EPXMA of estuarine suspended particulate matter will be outlined. A covariance matrix on the basis of the elemental concentrations, in this case on 9 variables namely Mg, Al, Si, P, S, K, Ca, Ti and Fe, was used to construct the eigenvectors and eigenvalues. The relation between the original variables and the principal components is given in the component loading matrix (Table 3.1). For the first two components this is also shown in Figure 3.1. The components scores, which are the values of the components for the m objects, are also represented graphically for the first two components in Figure 3.2. In this way the data structure can be visualized and studied, as 81 % of the total sample variance is represented in this plot.

The PCA of this kind of material shows that the variance in the compositional data set is mainly due to the occurrence of particles rich in Si, Fe, Ti, Al-Si-K, Al-Si-Ca. The division between the different particle types is not clear (Figure 3.2), and therefore the method is seldomly used to classify the particles in their respective particle types. The method is however mainly used :

- as a display method, to elaborate the data structure, and
- for the transformation of the original data into the principal component space, in which one can work with orthogonal principal components.

	Principal components								
	1	2	3	4	5	6	7	8	9
Cum. Per.	65	81	90	95	98	99	100	100	100
Variables	Loadings								
<i>Mg</i>	-0.22	-0.41	-0.14	0.12	-0.05	0.46	-0.28	0.67	0.00
<i>Al</i>	-0.01	-0.46	0.78	-0.26	-0.31	-0.06	0.00	-0.02	0.00
<i>Si</i>	0.96	0.27	-0.03	-0.02	-0.02	-0.02	0.00	0.00	0.00
<i>P</i>	-0.25	-0.28	-0.31	-0.06	0.03	0.53	0.69	-0.01	0.00
<i>S</i>	-0.22	-0.32	-0.04	0.21	0.23	0.76	-0.35	-0.25	0.00
<i>K</i>	0.01	-0.37	0.42	0.00	0.80	-0.22	0.01	0.00	0.00
<i>Ca</i>	-0.27	-0.54	-0.70	-0.36	-0.08	-0.13	-0.03	-0.02	0.00
<i>Ti</i>	-0.26	-0.26	-0.14	0.88	-0.21	-0.17	0.01	-0.02	0.00
<i>Fe</i>	-0.85	0.53	0.01	-0.05	-0.02	-0.03	0.00	0.00	0.00

Table 3.1 : Component loading matrix of the PCA, on the basis of the covariance matrix, of EPXMA results of suspended particulate matter (Dordogne sample 02B).

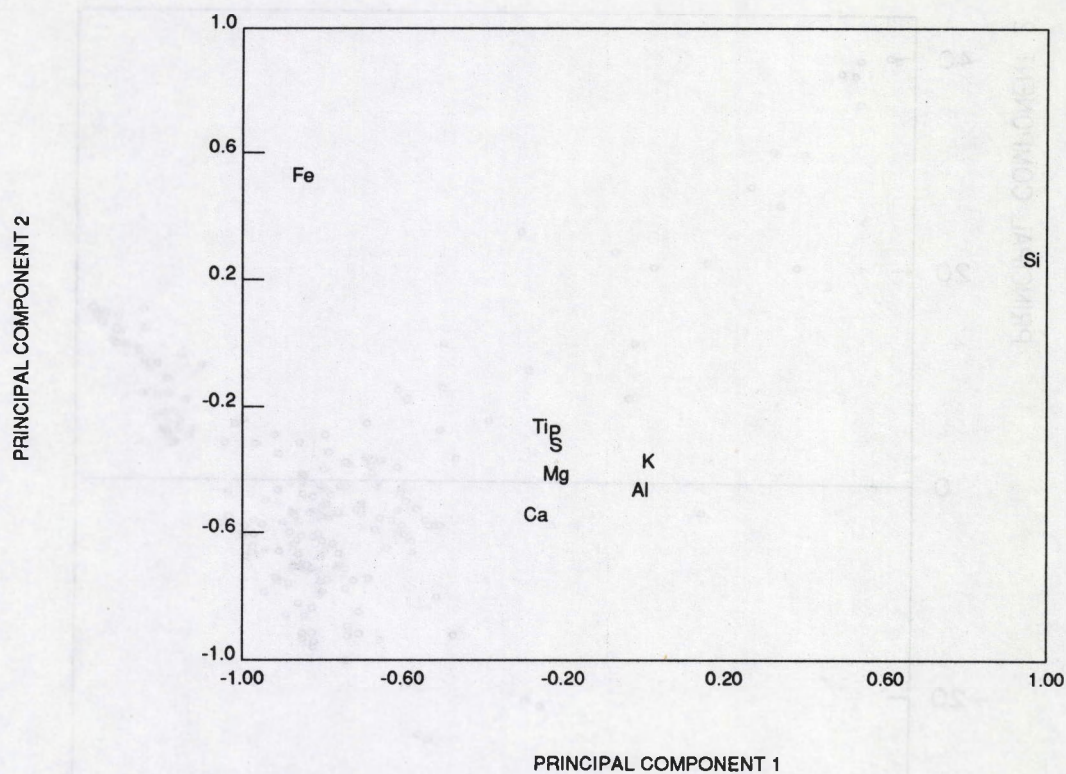


Figure 3.1 : Loadings of the first two principal components, of the PCA of EPXMA results of suspended matter (Dordogne sample 02B).

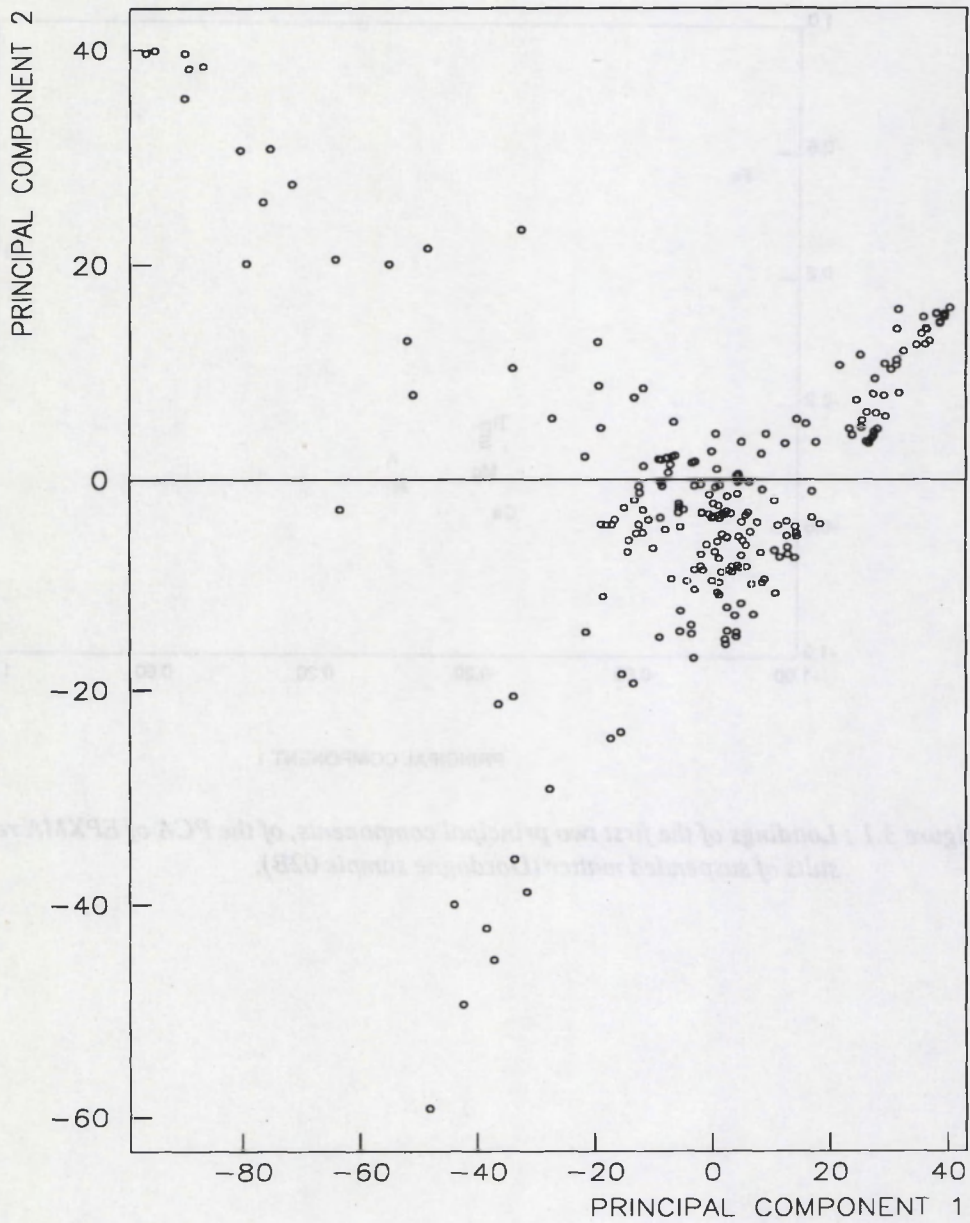


Figure 3.2 : Component scores of the objects for the first two principal components of the PCA of EPXMA results of suspended particulate matter (Dordogne sample 02B).

3.2 CLUSTER ANALYSIS

Cluster analysis is a generic term for a number of statistical procedures which create a classification from a data set, with m objects and n variables. These methods are also often called numerical taxonomy methods or methods for unsupervised pattern recognition. The general philosophy is that without prior knowledge of the data structure, the objects are grouped in K classes in such a way that the objects of a certain group are, in some sense, similar to one another. In most cases the number of classes have to be derived also.

3.2.1 Hierarchical cluster techniques.

The agglomerative hierarchical procedures are perhaps the most popular cluster techniques, and are used in many areas of science. These methods start from m objects that are to be classified and at each step the two most similar objects or clusters are merged into a single cluster. Every object or cluster is a subgroup of a larger group. After $m-1$ steps all objects and clusters belong to one large cluster, namely the whole sample. The different hierarchical methods differ in the decision criteria of which objects and/or clusters are merged and in the calculation of the similarity of the newly obtained cluster and the remaining objects and/or clusters. The similarity between two objects or clusters, can for instance be derived from the Euclidean distance between the objects or clusters in the n -dimensional space (with n = number of variables). Two objects or clusters close to each other will be more similar to each other than two objects or clusters far from each other. In general however instead of using the Euclidean distance, the Euclidean distance coefficient or average distance is used. The Euclidean distance coefficient is defined as :

$$d_{ij} = \sqrt{\frac{\sum_{k=1}^n (x_{ik} - x_{jk})^2}{p}}$$

This for an n -dimensional orthogonal space. If the Euclidean distance coefficient is determined via correlated variables, errors can be introduced. If there are missing data for some variables, then $p < n$. This is a compensation for missing data and for the fact that the Euclidean distance increases with increasing number of variables. The original data matrix is used to derive the similarity matrix or in case the Euclidean distance coefficient is used, the distance matrix. Standardization can be accomplished by a z -transform

$$z_{ij} = \frac{(x_{ij} - \bar{x}_{.j})}{S_j}$$

where $\bar{x}_{.j} = \frac{1}{m} \sum_{i=1}^m (x_{ij})$ with m objects, and $S_j^2 = \frac{1}{m-1} \sum_{i=1}^m (x_{ij} - \bar{x}_{.j})^2$

All the newly formed z_{ij} variables have a mean of zero and a variance 1, e.g. there covariance matrix is equal to their correlation matrix. The overall effect of standardization is that all variables have equal weight, which is sometimes desirable.

The Euclidean distance coefficient is calculated for every pair of objects, e.g. $m \cdot (m-1) / 2$ Euclidean distance coefficients have to be calculated. With increasing m , the number of required calculations rises quadratically and can become prohibitively large, which limits the number of objects that can be considered in practice.

The procedure for an hierarchical clustering is as follows :

1. find the smallest element d_{ij} in the similarity matrix.
2. fuse i and j into a single group r .
3. compute new distances d_{rk} , k represents each of the remaining objects and/or clusters. These distances replace d_{ik} and d_{jk} .
4. repeat for $(m-1)$ cycles.

The hierarchical strategies used in this study were the following : Furthest Neighbor (complete linkage), Nearest Neighbor (single linkage), Group Average (unweighted average linkage), Simple Average (weighted average linkage), Centroid sorting (unweighted centroid method), Median method (weighted centroid sorting) and the Ward's method (error sum of squares method). Lance and Williams (1967) showed that for all these methods the distances between the newly formed cluster (r) and the remaining objects and/or clusters (k) can be calculated from the existing elements of the similarity matrix and the parameters d_{ik} , d_{jk} , d_{ij} , m_i and m_j , where i and j are groups, with respectively m_i and m_j objects at the smallest distance d_{ij} of the similarity matrix. The distance of the new cluster (r) and the remaining objects and/or clusters (k) can then be calculated by :

$$d_{rk} = \alpha_i d_{ik} + \alpha_j d_{jk} + \beta d_{ij} + \gamma |d_{ik} - d_{jk}|$$

with d_{xy} as the distance between cluster x and y .

The different cluster algorithms are characterized by the values of α_i , α_j , β and γ . These values are summarized in Table 3.2.

Furthest Neighbor : the distance between two clusters i and j is defined as the largest distance between two objects, one of each cluster. The distance of the new cluster r to the k remaining groups is then given by

$$d_{rk} = 0.5d_{ik} + 0.5d_{jk} + 0.5|d_{ik} - d_{jk}|$$

Nearest Neighbor : this method is actually the opposite of the Furthest Neighbor method. The distance between two clusters i and j is defined as the smallest distance between two objects, one of each cluster. The distance of the new cluster r to the k remaining groups is given by :

$$d_{rk} = 0.5d_{ik} + 0.5d_{jk} - 0.5|d_{ik} - d_{jk}|$$

Method	α_i	α_j	β	γ
Furthest Neighbor	$\frac{1}{2}$	$\frac{1}{2}$	0	$\frac{1}{2}$
Nearest Neighbor	$\frac{1}{2}$	$\frac{1}{2}$	0	$-\frac{1}{2}$
Group Average	$\frac{m_i}{m_r}$	$\frac{m_j}{m_r}$	0	0
Simple Average	$\frac{1}{2}$	$\frac{1}{2}$	0	0
Centroid	$\frac{m_i}{m_r}$	$\frac{m_j}{m_r}$	$-\frac{m_i m_j}{m_r^2}$	0
Median	$\frac{1}{2}$	$\frac{1}{2}$	$-\frac{1}{4}$	0
Ward's	$\frac{m_i + m_k}{m_r + m_k}$	$\frac{m_j + m_k}{m_r + m_k}$	$-\frac{m_k}{m_r + m_k}$	0

Table 3.2 : Characterization of the hierarchical cluster methods by the coefficient values of the Lance and Williams formula.

Group Average : is the unweighted pair group variant of the average linkage methods. The distance between two clusters i and j is the arithmetical mean of the distance between the objects of the clusters i and j . The distance of the new cluster r to the k remaining groups is given by :

$$d_{rk} = \frac{m_i}{m_r} d_{ik} + \frac{m_j}{m_r} d_{jk}$$

Simple Average : is the weighted pair group variant of the average linkage methods. The distance of the new cluster r to the k remaining clusters is given by :

$$d_{rk} = 0.5d_{ik} + 0.5d_{jk}$$

Centroid sorting : this methods defines the distance between two clusters i and j as the distance between the centroids of the clusters. The distance of the new cluster r to the k remaining groups is given by :

$$d_{rk} = \frac{m_i}{m_r} d_{ik} + \frac{m_j}{m_r} d_{jk} - \frac{m_i m_j}{m_r^2} d_{ij}$$

Median method : is the weighted centroid method, for which the distance of the new cluster r to the k remaining groups is given by :

$$d_{rk} = 0.5d_{ik} + 0.5d_{jk} - \frac{1}{4}d_{ij}$$

Ward's method : this method minimizes the sum of squares, defined as the squared distance of an object to the centroid of its cluster. The clusters that might be formed are considered, and the one for which the increase of the sum of squares is least is retained. Wishart (1969) showed that the distances between the new cluster r and the remaining k groups can be calculated as :

$$d_{rk} = \frac{(m_i + m_k)}{(m_r + m_k)} d_{ik} + \frac{(m_j + m_k)}{(m_r + m_k)} d_{jk} - \frac{m_k}{(m_r + m_k)} d_{ij}$$

The result of a hierarchical cluster analysis is represented in a table or a dendrogram. In such a table, of which an example is given in Table 3.3, the objects and/or clusters are given in the order of the minimal distance at which they are merged in the subsequent steps. In a dendrogram (Figure 3.6) the same information is represented; the distance at which two branches come together is proportional to the distance d_{ij} , e.g. the smallest distance of the similarity matrix at that level. The dendrogram visualizes the relationship between all the objects. Cutting the tree at a certain similarity level generates clusters.

Number of clusters	Min. Dist. d_{ij}						
239	0	179	1.2	119	2.3	59	4.4
238	0	178	1.2	118	2.3	58	4.4
237	0	177	1.3	117	2.3	57	4.7
236	0	176	1.3	116	2.4	56	4.9
235	0	175	1.3	115	2.4	55	5.0
234	0	174	1.3	114	2.4	54	5.5
233	0	173	1.3	113	2.4	53	5.6
232	0	172	1.3	112	2.4	52	5.6
231	0	171	1.3	111	2.4	51	5.6
230	0.01	170	1.4	110	2.4	50	5.6
229	0.01	169	1.4	109	2.4	49	5.6
228	0.46	168	1.4	108	2.4	48	5.7
227	0.46	167	1.4	107	2.5	47	6.1
226	0.48	166	1.4	106	2.5	46	6.2
225	0.48	165	1.4	105	2.5	45	6.2
224	0.48	164	1.4	104	2.6	44	6.3
223	0.48	163	1.4	103	2.6	43	6.8
222	0.49	162	1.5	102	2.6	42	6.8
221	0.51	161	1.5	101	2.6	41	6.8
220	0.57	160	1.5	100	2.6	40	7.0
219	0.61	159	1.5	99	2.6	39	7.2
218	0.70	158	1.5	98	2.7	38	7.6
217	0.71	157	1.5	97	2.7	37	7.8
216	0.73	156	1.5	96	2.9	36	8.0
215	0.74	155	1.6	95	2.9	35	8.3
214	0.75	154	1.6	94	3.0	34	10
213	0.75	153	1.6	93	3.0	33	10
212	0.76	152	1.6	92	3.0	32	11
211	0.80	151	1.6	91	3.1	31	11
210	0.82	150	1.6	90	3.1	30	11
209	0.84	149	1.7	89	3.1	29	11
208	0.85	148	1.7	88	3.1	28	11
207	0.85	147	1.7	87	3.1	27	12
206	0.86	146	1.7	86	3.1	26	12
205	0.93	145	1.7	85	3.2	25	14
204	0.93	144	1.8	84	3.3	24	14
203	0.96	143	1.8	83	3.3	23	14
202	0.98	142	1.8	82	3.4	22	15
201	0.98	141	1.8	81	3.4	21	15
200	0.98	140	1.8	80	3.4	20	15
199	0.99	139	1.8	79	3.4	19	16
198	1.0	138	1.8	78	3.4	18	16
197	1.0	137	1.8	77	3.4	17	17
196	1.0	136	1.8	76	3.4	16	18
195	1.0	135	1.8	75	3.5	15	19
194	1.0	134	1.8	74	3.5	14	20
193	1.1	133	1.8	73	3.5	13	24
192	1.1	132	1.9	72	3.6	12	24
191	1.1	131	1.9	71	3.7	11	27
190	1.1	130	2.0	70	3.7	10	27
189	1.1	129	2.0	69	3.7	9	30
188	1.1	128	2.0	68	3.8	8	33
187	1.1	127	2.0	67	3.8	7	36
186	1.2	126	2.1	66	3.8	6	54
185	1.2	125	2.1	65	3.9	5	57
184	1.2	124	2.1	64	4.0	4	81
183	1.2	123	2.1	63	4.0	3	130
182	1.2	122	2.2	62	4.2	2	160
181	1.2	121	2.2	61	4.2		
180	1.2	120	2.2	60	4.3		

Table 3.3 : The results of the hierarchical cluster analysis of the EPXMA results of suspended particulate matter in table form (Dordogne sample 02B).

3.2.2 Nonhierarchical cluster techniques.

Nonhierarchical or partitioning clustering algorithms search for a division of the set of objects into a number (K) of clusters, in such a way that the elements of the same cluster are close to each other, in one or another sense, and the different clusters are well separated. These K clusters are generated simultaneously resulting in a nonhierarchical classification. The Nearest Centroid Sorting is a group of nonhierarchical cluster methods, which classifies the objects in clusters according to their distance from the centroids of the clusters. The sum of squares of the distances to the centroids are minimized, for a fixed number of clusters. The simplest of these methods is the method of Forgy (1965). This procedure involves the following steps :

1. select an initial clustering.
2. compute the centroids of the clusters and the distance from all objects to all centroids.
3. relocate all objects that were incorrectly classified, e.g. not located with the nearest centroid.

Steps 2 and 3 are repeated until convergence appears and a stable partition has been obtained.

The selection of an initial clustering can be done in a variety of ways. In this study, a method which is outlined in the application section 3.2.4, is used. This method results in a well-balanced centroid configuration by a sequence of hierarchical cluster analyses.

3.2.3 Comparison and parameter evaluation of hierarchical cluster techniques.

In the preceding section the most common hierarchical cluster techniques were described. One of the hitherto unresolved problems in cluster analysis is the choice of the "best" method in some sense (Everitt, 1979). To elaborate this problem there have been two approaches. One of a theoretical nature is by Jardine and Sibson (1968), and by Fisher and Van Ness (1971). In these cases the cluster techniques were compared with each other according to a set of theoretical criteria. On the other hand there has been a tendency to use a mixing model (Wolfe, 1970) to describe data sets. The effectiveness of the cluster methods are compared across a variety of constructed data sets. These constructed sets are extremely useful for executing validation studies since the criterion, the true data structure, is known and the performance of the clustering algorithms can be objectively evaluated. The reports by Blashfield (1976), Gross (1972), Kuiper and Fisher (1975), Cunningham and Ogilvie (1971) and Rand (1971) are some of these studies. These authors constructed artificial data sets, with two or more multivariate normal distributions. Some of these authors perturbed their distributions to approximate natural data (measurements). However none of these authors used real data. Nevertheless they all seem to warn the future users to be skeptical while considering the results of their specific application. Or they suggest that any use of a cluster algorithm should be accompanied by other validation information.

In the first instance the evaluation of the hierarchical cluster techniques, used for the classification of estuarine and marine particles, were compared with respect to their applicability in the context of the geochemical studies. This evaluation was necessarily rather intuitive and based on the experience gained : a satisfactory compromise was pursued between, on the one hand, describing the large data set using a minimum number of groups and, on the other hand, main-

taining a maximum of geochemically relevant information avoiding the fusion of geochemical important groups (Bernard et al., 1986). From this study it appeared that Ward's classification method served the present purpose best. Somewhat less preferable seemed to be the Furthest Neighbor method, closely followed by the Simple Average and the Group Average method. The Nearest Neighbor method was clearly the least satisfactory. The Centroid and the Median method were not included in the comparison.

In a more rigorous approach mineral standards were measured to serve as populations (particle types). The minerals were pulverized and measured by the automated electron microprobe. After investigation of the data structure and the removal of outliers, the data were used to construct artificial data sets, which were used to evaluate the performance of the different cluster techniques. The different cluster techniques were evaluated in relation to a number of parameters. As a matter of fact, we studied the influence of the relative mixing ratio of the minerals, the size (number of particles) of the mixtures, the use of unnormalized and normalized data and the use of a principal component space. Furthermore to predict the effect of the measurement errors the influence of different deconvolution techniques, and the effect of the degree of accuracy and quantification (e.g. difference between the relative intensities data and the ZAF-corrected elemental weight composition data) were investigated.

The accuracy of the cluster solution with respect to the actual classification was measured by the statistic kappa (Cohen, 1960). The different cluster procedures are then compared on basis of their kappa values. In order to provide some identification of the difficulty of the mixture for the cluster analysis, Linear Discriminant Analysis (LDA) was conducted on each constructed data set.

3.2.3.1 Accuracy of the cluster solution.

To measure the agreement of the obtained cluster solution with the actual classification the statistic kappa (Cohen, 1960) was used. This statistic was introduced to provide a coefficient of agreement between two raters of nominal scales, but is also used to describe the agreement among multiple observers (Landis and Koch, 1977). As the true classification is known, determined by the procedure for the generation of the mixture, kappa is a good measure of how good the cluster solution resembles the true classification. Kappa is defined as:

$$\kappa = \frac{p_o - p_c}{1 - p_c}$$

where p_o is the observed proportions of agreements and p_c is the proportion of agreements expected by chance. The variation of kappa was calculated by a formula of Fleis et al. (1969).

$$\begin{aligned} Var(\kappa) = \frac{1}{N(1 - p_c)^4} & \left\{ \sum_{i=1}^k p_{ii} \left[(1 - p_c) - (p_{\cdot i} + p_{i \cdot})(1 - p_o) \right]^2 + \right. \\ & \left. (1 - p_o)^2 \sum_{i=1}^k \sum_{j=1}^k p_{ij} (p_{\cdot i} + p_{j \cdot})^2 - (p_o p_c - 2p_c + p_o)^2 \right\} \end{aligned}$$

where N is the number of subjects and p_{ij} is the proportion of subjects placed in the i_j^{th} cell of the contingency table. Kappa ranges from -1 to 1, with larger values indicating a better agreement. A kappa value of 1 indicates a perfect agreement, hence the cluster solution matches the true classification. When the observed agreement equals change agreement a kappa value of 0 is obtained. To illustrate the calculations of kappa and its variance, an example on the hand of a hypothetical data set (Table 3.4) is given. In the table 200 ($= N$) subjects are distributed into 9 (k^2) cells by each of them being assigned to one of 3 (k) categories

Rater B	Statistic	Rater A			p_i
		1	2	3	
1	a	0.53	0.05	0.02	0.60
	b	0.39	0.15	0.06	
2	a	0.11	0.14	0.05	0.30
	b	0.195	0.075	0.03	
3	a	0.01	0.06	0.03	0.10
	b	0.065	0.025	0.01	
	p_j	0.65	0.25	0.10	1.00

Table 3.4 : Hypothetical data set for the calculation of kappa and the variance of kappa (after Fleis et al., 1969).

by one rater and, independently, to one of the same k categories by a second rater.

Let p_{ij} be the proportion of subjects placed in the i_j^{th} cell, let

$$p_i = \sum_{j=1}^k p_{ij}$$

the proportion of subjects placed in the i^{th} row; and let

$$p_j = \sum_{i=1}^k p_{ij}$$

the proportion of subjects placed in the j^{th} column.

The a entry in each cell is the observed proportion out of $N = 200$, p_{ij} . The b entry is the proportion expected by chance, $p_i p_j$.

The observed proportion of agreement is obtained by summing the a entries for the agreement cells; e.g. only those with $i = j$. This is

$$p_0 = \sum_{i=1}^k p_{ii} = 0.700$$

The chance proportion of agreement is obtained by summing the b entries for the agreement cells, this becomes

$$p_c = \sum_{i=1}^k p_i \cdot p_{\cdot i} = 0.475$$

κ is then

$$\kappa = \frac{0.700 - 0.475}{1 - 0.475} = 0.429$$

and the variance becomes

$$Var(\kappa) = 0.003$$

A difficulty in the determination of a kappa value for a cluster analysis is the fact that $n!$, with n the number of populations (clusters), kappa values can be calculated for a single cluster solution. This is because, for each generated cluster, a population from the mixture has to be determined. If it is expected that the user of the cluster techniques is able to select the appropriate population for each generated cluster, the maximum for kappa is obtained. Therefore the largest kappa value is used for the comparison of the cluster techniques. When, however the user makes a wrong decision, on which population matches a cluster, the listed kappa values are overestimated. On the other hand, randomly matching clusters and populations would lead to severe underestimates of the accuracy of the cluster solutions (Blashfield, 1976).

3.2.3.2 Creation of the data sets.

Different clay mineral standards were measured by EPXMA to build up homogeneous data sets. Afterwards these data sets were used to build up the mixtures mathematically.

EPXMA measurements of the standard minerals.

The used standard minerals, the sample preparation and the EPXMA measurement conditions are described in section 2.3.4. There, for these standards, the comparison of deconvolution techniques in relation to the number of identified (generated) peaks, the percentage of outliers, and the correlation between the obtained intensities of the mineral standard was discussed in detail. As was shown in that section, a difficulty arises by the removal of outliers at a 3σ level as sometimes different outliers are generated by the different deconvolution techniques. Therefore only real (robust) outliers are removed. These are defined as these particles which are outliers for the three techniques. In this way "homogeneous" data sets are generated, which are used to create the mixtures.

Design of the mixtures.

In a first series of experiments, combinations of the five standard minerals, per two minerals, were made to build up the mixtures. This results in ten different mineral combinations. For this purpose only the "homogeneous" AXIL-derived data of the minerals was used. For all these combinations the different cluster techniques were evaluated as a function of the mixing ratio of the two minerals. The mixing ratio expressed as the number of particles of mineral type i divided by the total number of particles in the mixture composed of mineral type i and j multiplied by hundred, was divided into five intervals, namely 1-10 %, 10-30 %, 30-70 %, 70-90 % and 90-99 %. For each of these intervals

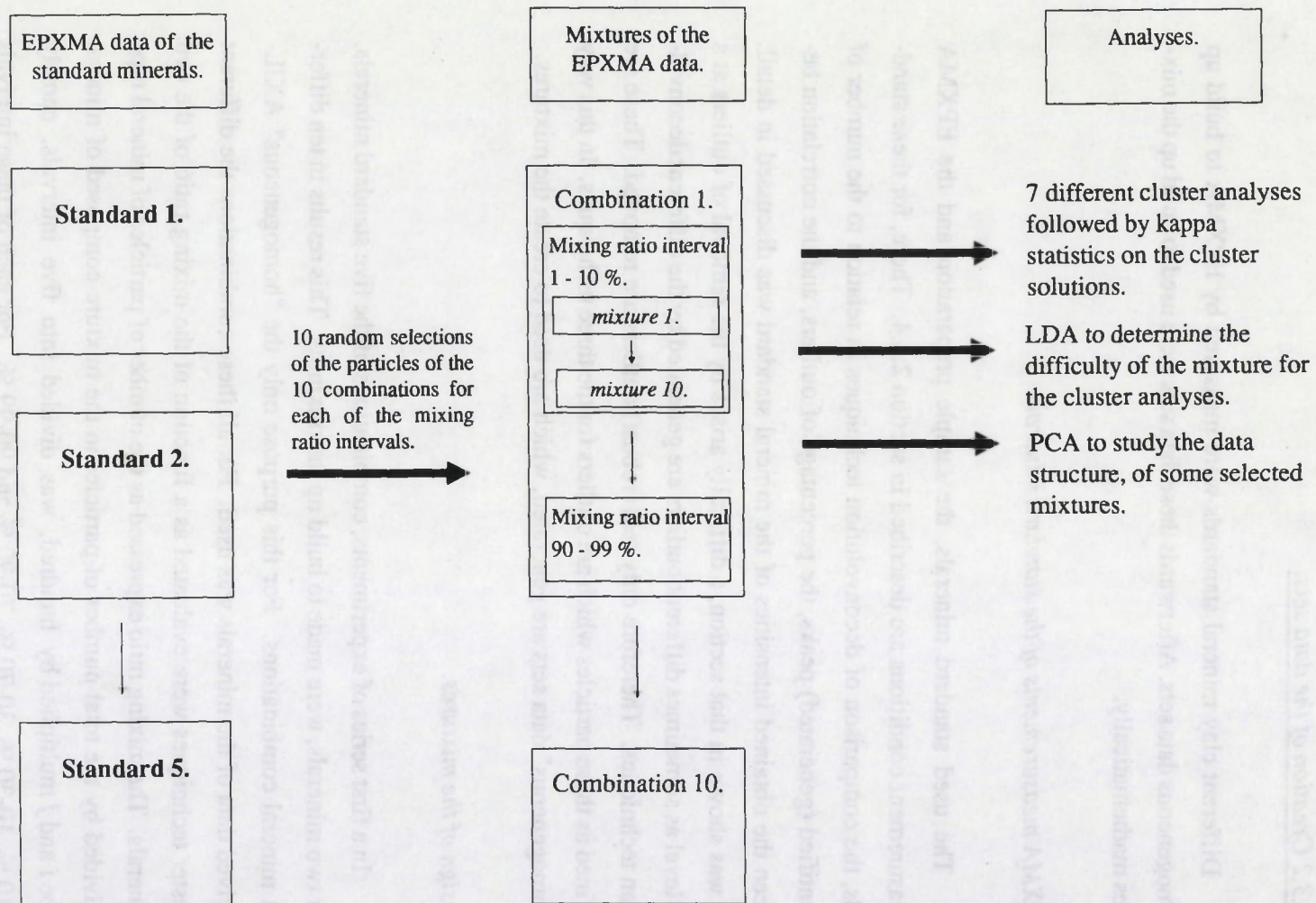


Figure 3.3 : Scheme for the creation of the different mixtures and of the performed analysis on the mixtures.

10 random relative proportions are calculated, and out of the pure (homogeneous) mineral data sets, objects (particles) are randomly chosen to build up the cluster structures while fulfilling the relative proportion criteria. The size of these newly formed mixtures was 100 objects (particles), which makes the mixing ratio equal to the number of particles of mineral type i . Cluster analyses were performed with unstandardized and standardized (normalized) variables for each generated mixture, and the difficulty of the created mixture for the cluster analysis was checked by conducting linear discriminant analysis. The data structure of some selected mixtures was elaborated by the use of principal component analysis. Figure 3.3 illustrates the scheme for the creation of the different mixtures of each mixing ratio interval for every combinations and of the analyses performed on the mixtures. These experiments allowed the study of the performance of the different cluster techniques for the 10 different mineral combinations, the influence of the mixing ratio and the use of normalized variables.

In a second series of experiments the mixtures were so constructed to study the influence of the total number of particles of the mixture, the use of uncorrelated variables (e.g. the use of a principal component space), the effect of the different deconvolution techniques and the effect of the degree of quantification. To build up these different kinds of mixtures the "homogeneous" dickite and montmorillonite data sets were selected. Table 3.5 summarizes these experiments and lists the experimental parameters.

To study the influence of	Data normalization	Mixture size (# particles)	Deconvolution technique
the mixture size	Unst. - Stand.	200	FFA
different deconvolution techniques	Unst. - Stand.	100	ROI
	Unst. - Stand.	100	FFA
	Unst. - Stand.	100	AXIL
clustering in the PC space	Unst. - Stand.	100	FFA
quantification of the data	Unst. - Stand.	100	ZAF-corrected AXIL

Unst. = Unstandardized variables.

Stand.= Standardized variables.

Table 3.5 : Experimental parameters and mixture types used for the second series of experiments.

3.2.3.3 Results and discussion.

For the first series of experiments the "homogeneous" data sets, obtained by the AXIL deconvolution technique, of the standard minerals were used. The complete results of such an analysis with unstandardized variables, for the dickite/nontronite combination is shown once to clarify the obtained results. For the mixing ratio interval 30-70 % the results are given in Table 3.6. Linear discriminant analysis found for all the mixtures the correct classification, while the different cluster techniques give in about 50 % of the cases a cluster solution which did match the actual classification. The mean kappa value of the cluster solutions seems to approximate a probability of good classification. Indeed, in most cases the kappa value is either near to one or zero, which means that either the correct classification was found or a totally wrong one. This also leads to high relative standard deviations. To elaborate the differences in performance

of the different cluster techniques, two mixtures will be studied in detail. Namely mixtures 1 and 3, having respectively 65 dickite - 35 nontronite, and 31 dickite - 69 nontronite particles. The correct cluster solution was found, if the cluster techniques were applied to mixture 1. For mixture 3 the correct cluster solution was only obtained by the Ward's method, while all the other techniques gave a wrong cluster solution. PCA was used to study the data structures of these mixtures. The scores of the first two principal components are plotted in Figure 3.4 and Figure 3.5, for mixture 1 and 3 respectively. These figures show a clear distinction between the two mineral types, confirming the LDA results where it was seen that no particle overlap occurred between the two groups. However it is seen that the variance of the nontronite mineral particles is higher than of the dickite particles. The cluster result of the Ward's method in dendrogram form is represented in Figure 3.6. For the distance scale a logarithmic distance is used. It appeared that the first part of the dendrogram, particle S1 to particle S42, consisted of nontronite particles and the second part of dickite particles. A clear division between the dickite and the nontronite particles is obtained, as shown by the minimum distance (d_{ij}) increase, logarithmic scale, when going from three to two clusters. For comparison the cluster result of the Furthest Neighbor method is given in Figure 3.7. The Furthest Neighbor dendrogram resembles the Ward's dendrogram quite well, and if the tree is cut at the two cluster level the same cluster result is obtained. The division between the dickite and the nontronite group seems to be better for the Ward's method, but care has to be taken as the logarithmic distance axis does not have the same absolute values. The dendrograms of the cluster results of the Ward's and the Furthest Neighbor methods of mixture 3 are respectively represented in Figure 3.8 and 3.9. In these figures the first 38 objects, S1 to S31, are the dickite particles. The main difference between the Ward's and the Furthest Neighbor cluster solution is the fact that by the Furthest Neighbor method the dickite group is joined with the nontronite group before this last group was complete. A single particle group, particle S97, and a group of 99 particles is obtained, containing dickite and nontronite par-

ticles. In practice a specialist probably finds the correct, or nearly the correct, classification by studying the dendrogram and the properties of the particles in the clusters. But in this study no a priori knowledge is assumed to find the correct classification, and the kappa value of the cluster result is near zero.

It is seen that on the average the cluster solutions of the Ward's method have the highest probability of correct classification (0.97+/-0.02, Table 3.6). For five mixtures, mixture 2, 5, 6, 8 and 10, kappa values lower than one were obtained. The only mixture for which all the cluster techniques gave the correct classification is mixture 1. It was also the only mixture for which the Nearest Neighbor method was successful. For all other mixtures the Nearest Neighbor method gave kappa values near zero. For the other mixtures it is seen that the Group Average, Centroid, Furthest Neighbor, Median and the Simple Average methods do find the correct classification in some cases.

The summarized results of the first series of experiments for the cluster analysis performed with unstandardized variables are given in Tables 3.7 a-e. Each of these tables represents the results for each mixing ratio interval, for the ten combinations, hence the result of 700 cluster and kappa analyses. Each value represents the mean of ten analyses. The standard deviation on the mean is given between brackets.

On the basis of the LDA it was seen that the dickite/montmorillonite, the dickite/nontronite and the dickite/illite mixtures were clearly distinguished. All other mixtures have particle overlap, the dickite/pyrophyllite, montmorillonite/nontronite, montmorillonite/illite to a lesser degree than the remaining, last four, mixtures. The difficulty of the mixtures for the cluster techniques is directly reflected in the cluster solutions and the kappa results. Relatively good results are obtained for the mixtures with no, or little, particle overlap.

In general, for all the mixtures, it seems that the Ward's method was, in most cases, most successful in finding the correct classification. Except for the nontronite/pyrophyllite mixture where the Nearest Neighbor and the Simple Average method have significantly higher mean kappa values. This is probably due to their ability to form chained clusters. In this way the complete elongated pyrophyllite cluster is formed before the nontronite particles are joined. In the case of the other cluster methods the nontronite particles are joined with a part of the pyrophyllite group at an earlier stage, leading to a wrong cluster solution. For mixtures with a low difficulty for the cluster techniques, as for instance the dickite/montmorillonite mixtures, the mean kappa values of all the cluster techniques approach each other near the upper limit of one. For the more difficult mixtures, the Ward's method has in most cases a significantly better mean kappa value. The Furthest Neighbor, the Group Average and the Centroid methods seem to be slightly better than the Simple Average, the Median and the Nearest Neighbor methods. However the differences are not always significant, and the rule is not generally applicable.

The influence of the mixing ratio can be studied by comparing Table 3.7 a-e. The differences between the mean kappa values for the different mixing ratio intervals are sometimes significant. These differences can be understood via the data structure of the mixtures. For instance, all the dickite mixtures show high mean kappa values, when a high amount of the more compact dickite group is present. Maximum kappa values are encountered for the 90-99 % relative mixing ratio interval. This is also the fact for the montmorillonite mixtures, for which in the case of the mixtures with nontronite, illite, and pyrophyllite the montmorillonite group is not only more compact but the particle overlap is also reduced for the higher mixing ratio intervals. The nontronite/illite and nontronite/pyrophyllite mixtures seem to have a maximum mean kappa value for the 30-70 % mixing ratio interval. In the case of the illite/pyrophyllite mixture very low kappa values were determined for all the mixing ratio intervals.

The results of the first series of experiments for the cluster analysis performed with standardized variables are represented in Table 3.8 a-e. By comparing Tables 3.7 a-e and 3.8 a-e, one can assess the influence of the variable normalization. For the mixtures, which have low abundance variables, and/or with low variations, with discriminatory power, between the minerals, the cluster solution, of in most cases only these of the Ward's method are improved when standardized variables are used. This is the case for the mixtures nontronite/pyrophyllite, dickite/illite, montmorillonite/illite, nontronite/illite and montmorillonite/pyrophyllite for some of the mixing ratio intervals. Normalization makes the low abundance variables, and/or low variation more important in the calculation of the similarity matrix. For some mixtures under study these were the K, Al, Ca and Fe variables. On the other hand, the possibility exists that due to variables with no relevant variation and/or data subject to a high experimental error, the normalization of the data leads to a data matrix in which these "insignificant" variables become relatively more important. Cluster analysis on such a matrix will result in worse cluster results.

The results of the second series of experiments (Table 3.5) for the cluster analysis, performed on the dickite/montmorillonite mixtures, with unstandardized variables, are given in Tables 3.9 a-e. Each of these tables represents the result of 420 cluster and kappa analyses, while each value is the mean of 10 kappa analyses. The listed standard deviations are the standard deviations on the mean.

It seems that the highest kappa values, or kappa values not significantly different from the highest ones, are obtained for all the Ward's cluster solutions, which means that these resemble the correct classification most. The other cluster techniques seem to perform as good as the Ward's method or worse, but their results are not significantly different from each other, for the mixing ratio intervals 1-10 %, 10-30 %, 30-70 %, except for the cluster results in the PC space.

For the mixing ratio intervals 70-90 % and 90-99 % the Furthest Neighbor, Group Average and in some cases the Centroid method seem to perform better than the other methods, as was already shown by the first series of experiments.

Influence of the mixing ratio.

The influence of the relative mixing ratio of the dickite and montmorillonite mineral particles can be studied by comparing Tables 3.9 a-e. It is seen that significant differences are encountered for the mixing ratio intervals 70-90 % and 90-99 %. The lowest kappa values were obtained for the 1-10 % and 10-30 % intervals. Relatively good results were obtained for the other mixing ratio intervals. A reason for this must probably be searched in the data structures of the mixtures. However none of the mixtures gave the linear discriminant analysis any problem to find the correct classification. It is however assumed that, as in the case of the discussed dickite/nontronite mixtures of the 30-70 % interval that due to the data structure in the intervals 1-10 % and 10-30 % the cluster analysis gives a solution with a single particle (montmorillonite) cluster.

Influence of the mixture size.

By comparing the cluster solutions of the 200 and 100 particle size mixtures (FFA derived), it is seen that in most cases, no significant variations were encountered. Only the Nearest Neighbor method seems to perform worse in the case of the 200 particle mixtures, for higher mixing ratios.

In general this leads to the conclusion that for this kind of mixtures, the obtained results of a limited data set can be extrapolated to greater data sets.

Influence of the used deconvolution technique.

By the comparison of the different deconvolution techniques, for all the relative mixing ratio intervals, no significant differences were measured in case the Ward's method was used. For the other cluster techniques it was seen that in most cases the ROI and AXIL gave comparable results. Using the FFA reduced, in some cases, the probability of a good classification, especially when cluster techniques other than Ward's method were used. This example shows that the choice of the deconvolution technique not only influences the number of detected peaks and the accuracy of the peak intensities (see section 2.3.4) but also the results of the hierarchical cluster analysis.

Influence of working in the principal component space.

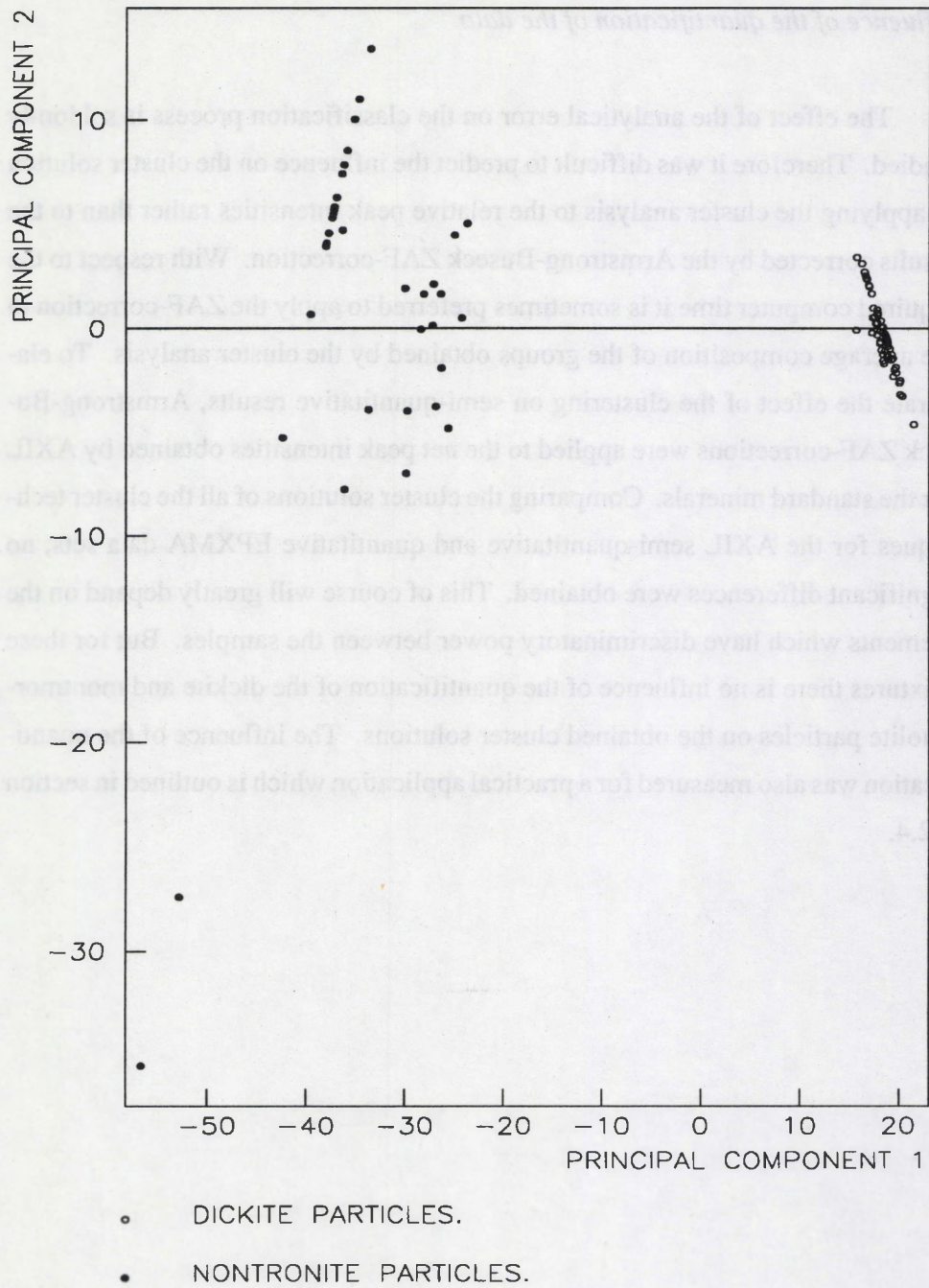
Applying a principal component analysis to the data, before a clustering is performed has sometimes been introduced to:

- eliminate redundant information by obtaining a small number of variables, i.e. removing noise by only working with the most important principal components.
- eliminate the introduced errors, when the Euclidean distance is calculated with correlated variables, by using the uncorrelated principal components for the calculation of the similarity matrix.

To elaborate the influence of working in a principal component space, a principal component analysis was performed on the generated mixtures (mixture size = 100, deconvolution technique = FFA). The component scores of the principal components were used to determine the similarity matrix. The mean kappa values for the clustering in the PC space are significantly smaller than for the original variable space. It seems that while the total variance is preserved by the PCA analysis, the use of uncorrelated variables reduced the mean kappa values. In this case study it is preferable to work with the original variables.

Influence of the quantification of the data.

The effect of the analytical error on the classification process is seldomly studied. Therefore it was difficult to predict the influence on the cluster solution of applying the cluster analysis to the relative peak intensities rather than to the results corrected by the Armstrong-Buseck ZAF-correction. With respect to the required computer time it is sometimes preferred to apply the ZAF-correction to the average composition of the groups obtained by the cluster analysis. To elaborate the effect of the clustering on semi-quantitative results, Armstrong-Buseck ZAF-corrections were applied to the net peak intensities obtained by AXIL for the standard minerals. Comparing the cluster solutions of all the cluster techniques for the AXIL semi-quantitative and quantitative EPXMA data sets, no significant differences were obtained. This of course will greatly depend on the elements which have discriminatory power between the samples. But for these mixtures there is no influence of the quantification of the dickite and montmorillonite particles on the obtained cluster solutions. The influence of the quantification was also measured for a practical application which is outlined in section 3.2.4.



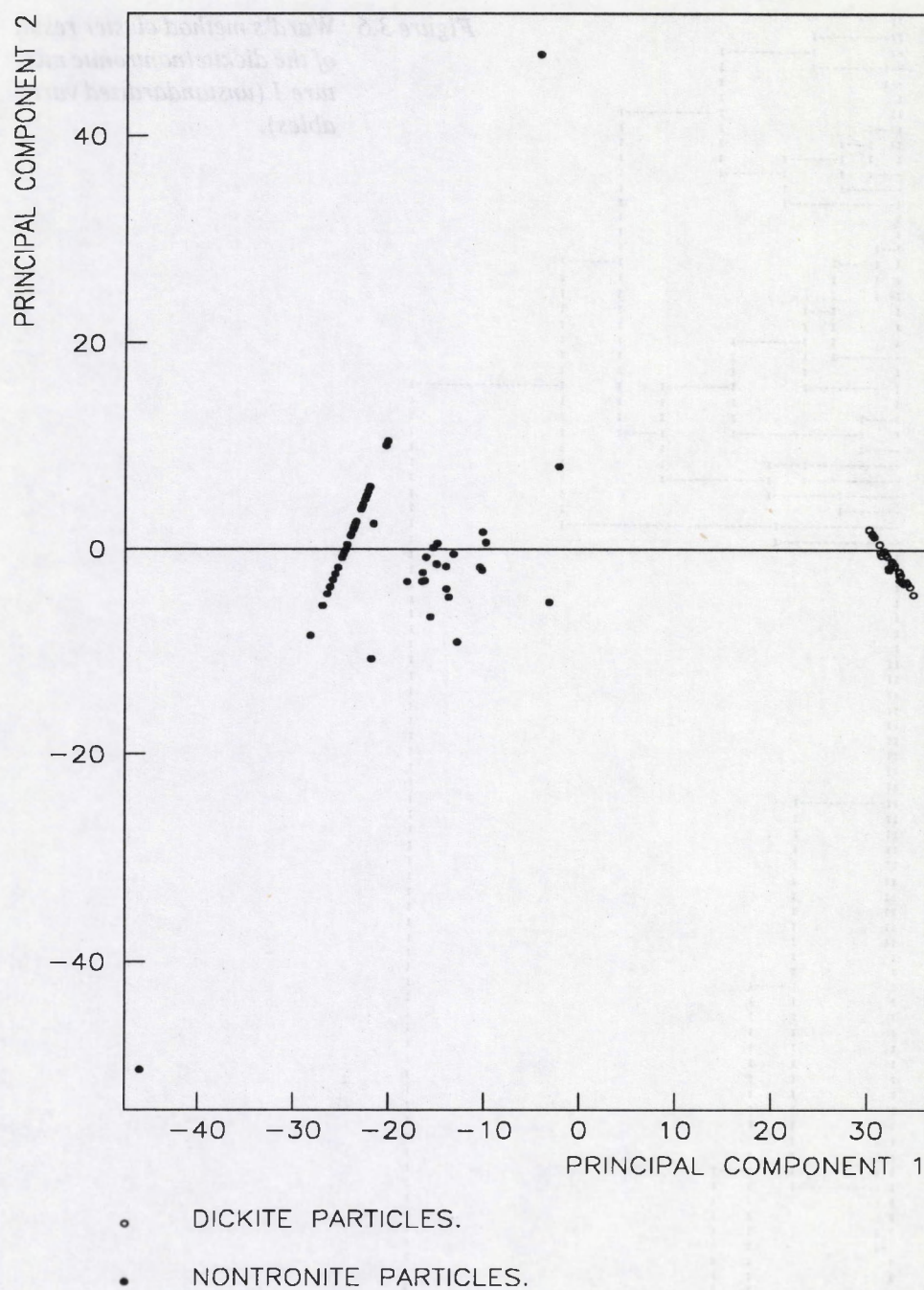
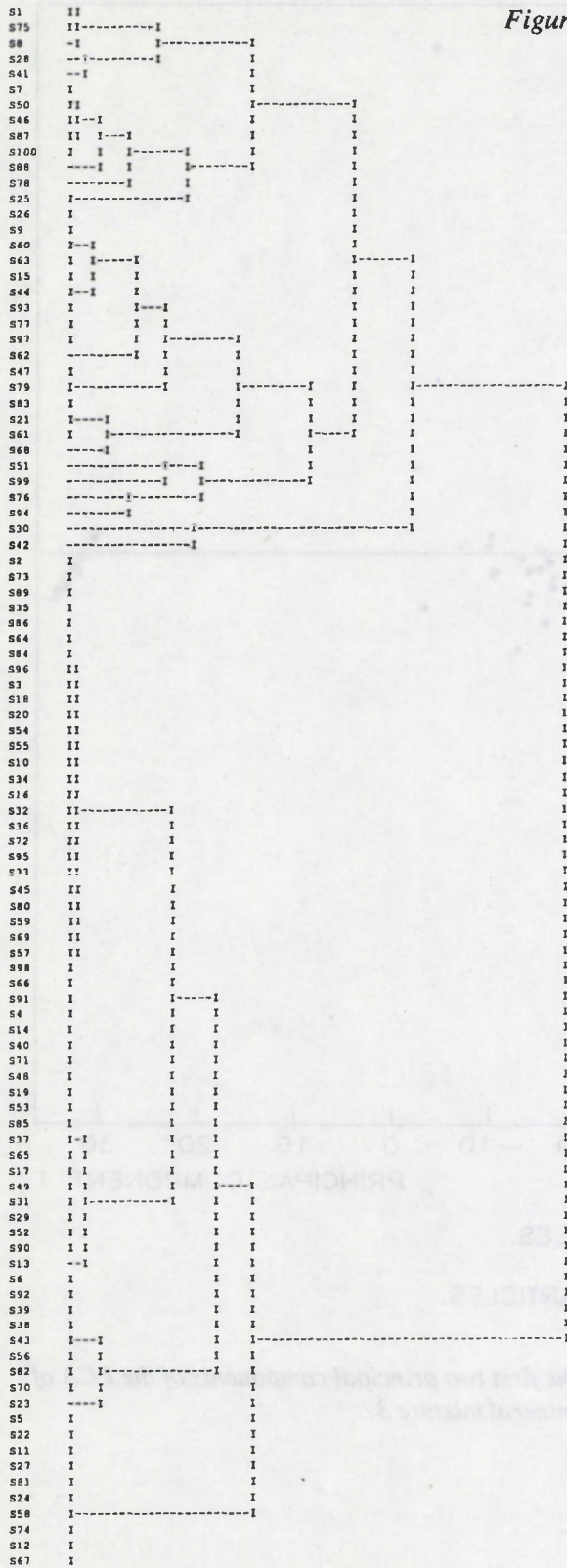


Figure 3.5 : Component scores of the first two principal components of the PCA of the dickite/nontronite mineral mixture 3.

Variables used are : Mg Al Si K Ca Fe (unstandardized)

Strategy : Ward's method

LOG SCALE FOR DISTANCES



Variables used are : Mg Al Si K Ca Fe (unstandardized)

Strategy : Furthest neighbor

LOG SCALE FOR DISTANCES

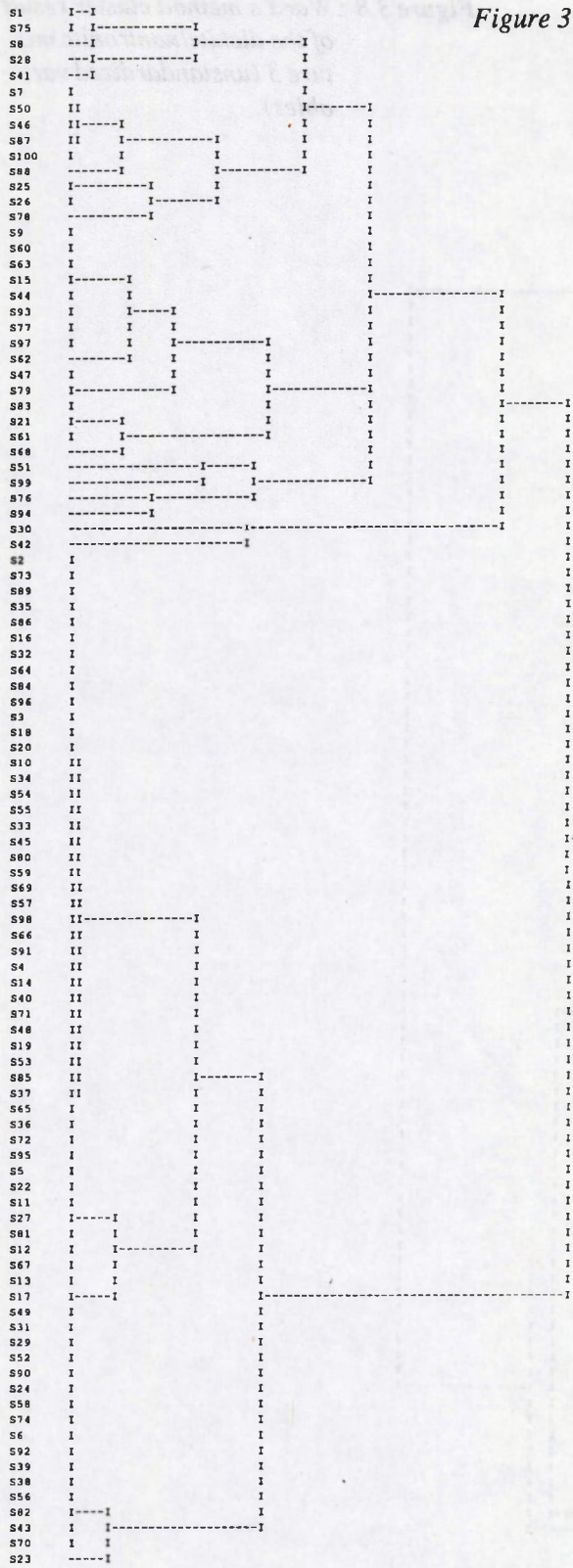


Figure 3.7 : Furthest Neighbor method cluster result of the dic-kite/nontronite mixture 1 (unstandardized variables).

Variables used are : Mg Al Si K Ca Fe (unstandardized)

Strategy : Ward's method

LOG SCALE FOR DISTANCES

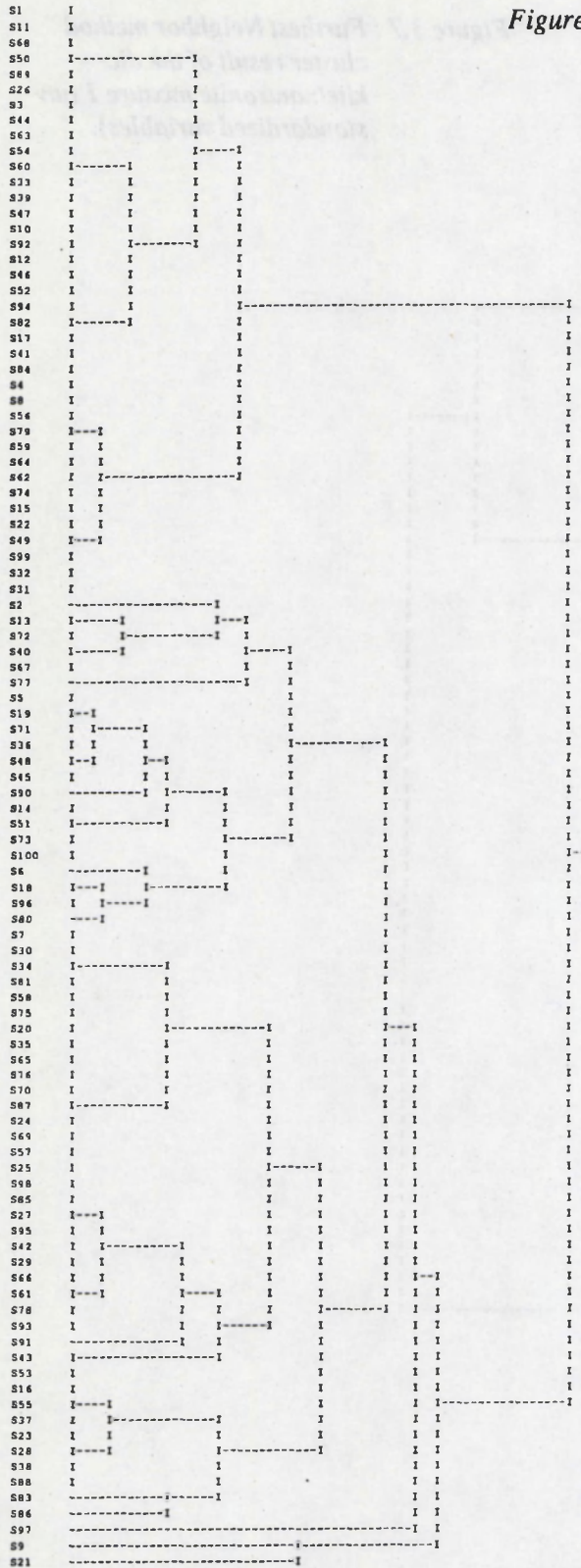


Figure 3.8 : Ward's method cluster result of the dickite/nontronite mixture 3 (unstandardized variables).

Variables used are : Mg Al Si K Ca Fe (unstandardized)

Strategy : Furthest neighbor

LOG SCALE FOR DISTANCES

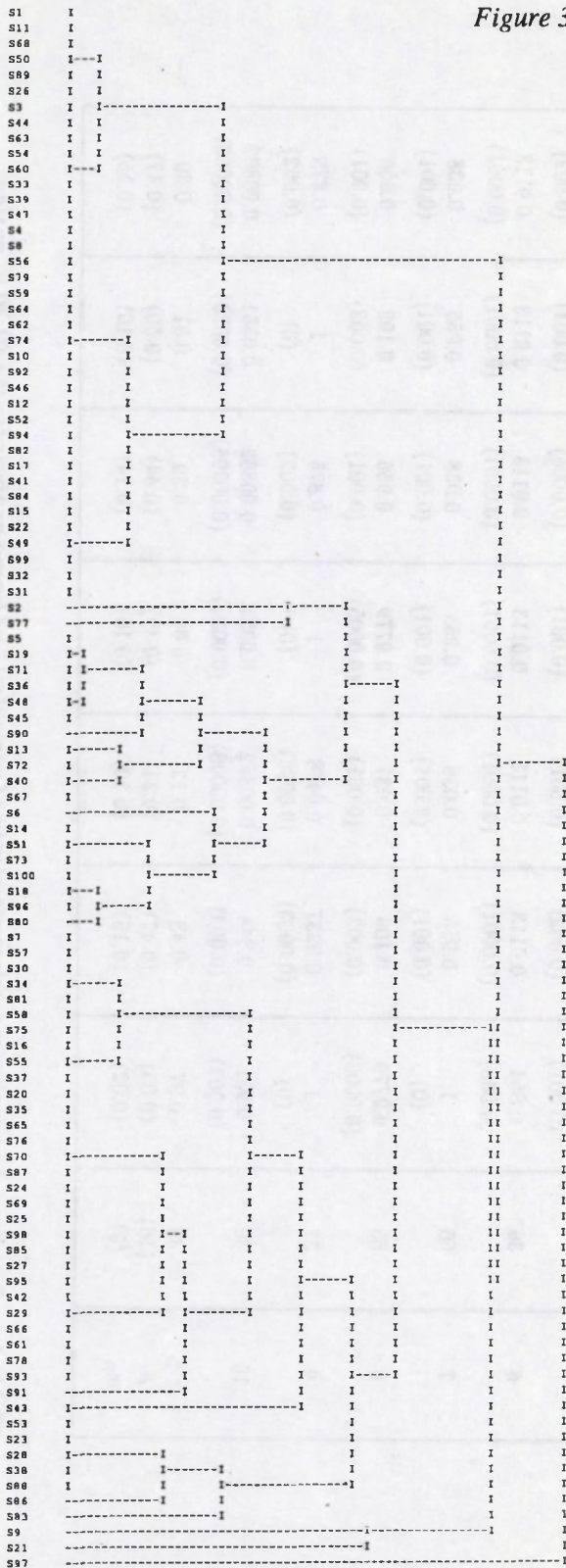


Figure 3.9 : Furthest Neighbor method cluster result of the dic-kite/nontronite mixture 3 (un-standardized variables).

Mixture no.	Mixing ratio (%)	Ward's	Furthest Neighbor	Nearest Neighbor	Group Average	Simple Average	Centroid	Median
1	65	1 (0)	1 (0)	1 (0)	1 (0)	1 (0)	1 (0)	1 (0)
2	31	0.954 (0.001)	0.0274 (0.0003)	0.0274 (0.0003)	0.0274 (0.0003)	0.0274 (0.0003)	0.0274 (0.0003)	0.0274 (0.0003)
3	38	1 (0)	0.0123 (0.0002)	0.0123 (0.0002)	0.0123 (0.0002)	0.0123 (0.0002)	0.0123 (0.0002)	0.0123 (0.0002)
4	68	1 (0)	0.929 (0.002)	0.083 (0.003)	1 (0)	0.083 (0.003)	1 (0)	0.083 (0.003)
5	53	0.940 (0.001)	0.879 (0.002)	0.067 (0.001)	0.940 (0.001)	0.0225 (0.0005)	0.940 (0.001)	0.879 (0.002)
6	36	0.854 (0.003)	0.0113 (0.0001)	0.0113 (0.0001)	0.0113 (0.0001)	0.0113 (0.0001)	0.0113 (0.0001)	0.0113 (0.0001)
7	66	1 (0)	0.955 (0.001)	0.038 (0.001)	0.955 (0.001)	0.038 (0.001)	0.955 (0.001)	0.038 (0.001)
8	65	0.9779 (0.0005)	0.109 (0.003)	0.037 (0.001)	0.9779 (0.0005)	0.956 (0.001)	0.109 (0.003)	0.956 (0.001)
9	37	1 (0)	0.0237 (0.0003)	0.0478 (0.0006)	1 (0)	0.875 (0.002)	1 (0)	0.875 (0.002)
10	30	0.931 (0.001)	0.844 (0.003)	0.00862 (0.00008)	0.0351 (0.0003)	0.00862 (0.00008)	0.0351 (0.0003)	0.00862 (0.00008)
< >	49	0.97	0.48	0.13	0.60	0.30	0.51	0.39
σ	(16)	(0.05)	(0.47)	(0.31)	(0.49)	(0.44)	(0.50)	(0.47)
σ_m	(5)	(0.02)	(0.15)	(0.10)	(0.16)	(0.14)	(0.16)	(0.15)

Table 3.6 : Results of the ten cluster (with unstandardized variables) and kappa analysis for the 30-70 % mixing ratio interval of the dickite/nontronite combination.

Mixture	Ward's	Furthest Neighbor	Nearest Neighbor	Group Average	Simple Average	Centroid	Median
dickite/montmorillonite	1 (0)	0.98 (0.01)	1 (0)	1 (0)	0.98 (0.01)	1 (0)	1 (0)
dickite/nontronite	0.53 (0.10)	0.12 (0.07)	0.0028 (0.0006)	0.20 (0.13)	0.11 (0.07)	0.20 (0.13)	0.12 (0.07)
dickite/illite	0.015 (0.004)	0.005 (0.002)	0.0022 (0.0008)	0.004 (0.002)	0.004 (0.002)	0.04 (0.002)	0.006 (0.002)
dickite/pyrophyllite	0.027 (0.005)	0.028 (0.005)	0.005 (0.004)	0.027 (0.005)	0.031 (0.009)	0.027 (0.005)	0.04 (0.001)
montmorillonite/nontronite	0.38 (0.10)	0.11 (0.07)	0.0026 (0.0006)	0.004 (0.001)	0.06 (0.05)	0.004 (0.001)	0.11 (0.07)
montmorillonite/illite	0.010 (0.003)	0.005 (0.002)	0.0022 (0.0008)	0.004 (0.001)	0.0024 (0.0006)	0.004 (0.002)	0.0024 (0.0006)
montmorillonite/pyrophyllite	0.027 (0.005)	0.027 (0.005)	0.005 (0.004)	0.027 (0.005)	0.021 (0.005)	0.027 (0.005)	0.031 (0.008)
nontronite/illite	0.017 (0.004)	0.11 (0.07)	0.10 (0.10)	0.004 (0.002)	0.005 (0.002)	0.004 (0.002)	0.006 (0.002)
nontronite/pyrophyllite	0.024 (0.005)	0.024 (0.005)	0.47 (0.16)	0.024 (0.005)	0.44 (0.14)	0.024 (0.005)	0.27 (0.13)
illite/pyrophyllite	0.021 (0.008)	0.06 (0.05)	0.08 (0.05)	0.07 (0.05)	0.06 (0.05)	0.07 (0.05)	0.06 (0.05)

Table 3.7a : Results of the cluster (with unstandardized variables) and kappa analysis for the 1-10 % mixing ratio interval of the ten mineral combinations for the different cluster techniques.

Mixture	Ward's	Furthest Neighbor	Nearest Neighbor	Group Average	Simple Average	Centroid	Median
dickite/montmorillonite	1 (0)	0.995 (0.005)	1 (0)	1 (0)	1 (0)	1 (0)	1 (0)
dickite/nontronite	0.94 (0.03)	0.10 (0.09)	0.008 (0.001)	0.20 (0.13)	0.010 (0.001)	0.20 (0.13)	0.010 (0.001)
dickite/illite	0.15 (0.10)	0.03 (0.01)	0.02 (0.01)	0.03 (0.01)	0.03 (0.01)	0.03 (0.01)	0.03 (0.01)
dickite/pyrophyllite	0.13 (0.03)	0.12 (0.02)	0.01 (0.01)	0.10 (0.01)	0.17 (0.05)	0.10 (0.01)	0.12 (0.02)
montmorillonite/nontronite	0.72 (0.09)	0.18 (0.12)	0.008 (0.001)	0.010 (0.001)	0.010 (0.001)	0.010 (0.001)	0.010 (0.001)
montmorillonite/illite	0.04 (0.01)	0.03 (0.01)	0.008 (0.001)	0.03 (0.01)	0.03 (0.01)	0.03 (0.01)	0.03 (0.01)
montmorillonite/pyrophyllite	0.12 (0.02)	0.10 (0.01)	0.02 (0.01)	0.09 (0.01)	0.09 (0.02)	0.09 (0.01)	0.09 (0.01)
nontronite/illite	0.30 (0.13)	0.12 (0.10)	0.04 (0.02)	0.04 (0.02)	0.04 (0.02)	0.04 (0.02)	0.04 (0.02)
nontronite/pyrophyllite	0.32 (0.13)	0.25 (0.12)	0.22 (0.11)	0.07 (0.01)	0.27 (0.11)	0.07 (0.01)	0.25 (0.11)
illite/pyrophyllite	0.06 (0.02)	0.04 (0.02)	0.06 (0.02)	0.06 (0.02)	0.04 (0.02)	0.06 (0.01)	0.04 (0.01)

Table 3.7b : Results of the cluster (with unstandardized variables) and kappa analysis for the 10-30 % mixing ratio interval of the ten mineral combinations for the different cluster techniques.

Mixture	Ward's	Furthest Neighbor	Nearest Neighbor	Group Average	Simple Average	Centroid	Median
dickite/montmorillonite	0.995 (0.002)	1 (0)	0.89 (0.10)	1 (0)	1 (0)	1 (0)	1 (0)
dickite/nontronite	0.97 (0.02)	0.48 (0.15)	0.13 (0.10)	0.60 (0.16)	0.30 (0.14)	0.51 (0.16)	0.39 (0.15)
dickite/illite	0.56 (0.15)	0.040 (0.009)	0.026 (0.004)	0.040 (0.009)	0.040 (0.009)	0.040 (0.009)	0.036 (0.008)
dickite/pyrophyllite	0.34 (0.08)	0.19 (0.03)	0.19 (0.05)	0.19 (0.03)	0.22 (0.04)	0.19 (0.03)	0.19 (0.03)
montmorillonite/nontronite	0.91 (0.02)	0.26 (0.13)	0.036 (0.008)	0.15 (0.10)	0.26 (0.13)	0.15 (0.10)	0.14 (0.10)
montmorillonite/illite	0.27 (0.12)	0.04 (0.01)	0.026 (0.004)	0.040 (0.009)	0.040 (0.009)	0.040 (0.009)	0.040 (0.009)
montmorillonite/pyrophyllite	0.21 (0.03)	0.21 (0.03)	0.19 (0.04)	0.21 (0.03)	0.24 (0.03)	0.17 (0.03)	0.21 (0.03)
nontronite/illite	0.70 (0.11)	0.12 (0.09)	0.030 (0.004)	0.025 (0.005)	0.12 (0.09)	0.027 (0.005)	0.12 (0.09)
nontronite/pyrophyllite	0.89 (0.02)	0.36 (0.13)	0.14 (0.08)	0.10 (0.03)	0.32 (0.12)	0.10 (0.03)	0.32 (0.12)
illite/pyrophyllite	0.15 (0.06)	0.05 (0.01)	0.03 (0.01)	0.04 (0.01)	0.028 (0.007)	0.032 (0.009)	0.028 (0.007)

Table 3.7c : Results of the cluster (with unstandardized variables) and kappa analysis for the 30-70 % mixing ratio interval of the ten mineral combinations for the different cluster techniques.

Mixture	Ward's	Furthest Neighbor	Nearest Neighbor	Group Average	Simple Average	Centroid	Median
dickite/montmorillonite	0.996 (0.004)	1 (0)	0.50 (0.17)	1 (0)	0.75 (0.14)	1 (0)	0.75 (0.14)
dickite/nontronite	0.99 (0.01)	0.64 (0.14)	0.20 (0.09)	0.64 (0.14)	0.48 (0.14)	0.64 (0.14)	0.48 (0.14)
dickite/illite	0.86 (0.10)	0.17 (0.04)	0.15 (0.04)	0.17 (0.04)	0.17 (0.04)	0.17 (0.04)	0.17 (0.04)
dickite/pyrophyllite	0.68 (0.08)	0.40 (0.09)	0.15 (0.05)	0.28 (0.04)	0.34 (0.08)	0.28 (0.04)	0.34 (0.07)
montmorillonite/nontronite	0.95 (0.02)	0.51 (0.14)	0.37 (0.13)	0.37 (0.13)	0.41 (0.13)	0.37 (0.13)	0.41 (0.13)
montmorillonite/illite	0.49 (0.13)	0.16 (0.04)	0.11 (0.02)	0.11 (0.02)	0.16 (0.04)	0.12 (0.02)	0.16 (0.04)
montmorillonite/pyrophyllite	0.40 (0.03)	0.34 (0.03)	0.24 (0.04)	0.29 (0.03)	0.34 (0.02)	0.29 (0.03)	0.34 (0.02)
nontronite/illite	0.71 (0.08)	0.03 (0.01)	0.04 (0.01)	0.03 (0.01)	0.03 (0.01)	0.03 (0.01)	0.03 (0.01)
nontronite/pyrophyllite	0.82 (0.02)	0.08 (0.07)	0.009 (0.003)	0.010 (0.003)	0.08 (0.07)	0.010 (0.003)	0.08 (0.07)
illite/pyrophyllite	0.15 (0.04)	0.02 (0.01)	0.008 (0.001)	0.02 (0.01)	0.010 (0.002)	0.02 (0.01)	0.02 (0.01)

Table 3.7d : Results of the cluster (with unstandardized variables) and kappa analysis for the 70-90 % mixing ratio interval of the ten mineral combinations for the different cluster techniques.

Mixture	Ward's	Furthest Neighbor	Nearest Neighbor	Group Average	Simple Average	Centroid	Median
dickite/montmorinolite	1 (0)	1 (0)	0.60 (0.16)	0.90 (0.10)	0.70 (0.15)	0.90 (0.10)	0.70 (0.15)
dickite/nontronite	0.993 (0.007)	0.84 (0.10)	0.75 (0.12)	0.76 (0.12)	0.76 (0.12)	0.76 (0.12)	0.76 (0.12)
dickite/illite	0.81 (0.08)	0.61 (0.10)	0.32 (0.07)	0.47 (0.08)	0.52 (0.09)	0.37 (0.07)	0.52 (0.09)
dickite/pyrophyllite	0.68 (0.08)	0.56 (0.07)	0.27 (0.06)	0.47 (0.07)	0.41 (0.08)	0.45 (0.06)	0.40 (0.08)
montmorinolite/nontronite	0.983 (0.009)	0.76 (0.12)	0.65 (0.13)	0.65 (0.13)	0.76 (0.12)	0.65 (0.13)	0.76 (0.12)
montmorinolite/illite	0.61 (0.08)	0.51 (0.09)	0.35 (0.05)	0.35 (0.05)	0.40 (0.06)	0.35 (0.05)	0.40 (0.06)
montmorinolite/pyrophyllite	0.60 (0.05)	0.42 (0.07)	0.36 (0.06)	0.39 (0.06)	0.42 (0.07)	0.41 (0.06)	0.41 (0.06)
nontronite/illite	0.48 (0.07)	0.02 (0.02)	0.05 (0.02)	0.09 (0.05)	0.02 (0.02)	0.06 (0.04)	0.02 (0.02)
nontronite/pyrophyllite	0.60 (0.07)	0.07 (0.06)	0.007 (0.005)	0.03 (0.02)	0.07 (0.07)	0.03 (0.02)	0.07 (0.07)
illite/pyrophyllite	0.07 (0.04)	0.0033 (0.0006)	0.0031 (0.0006)	0.0033 (0.0006)	0.0033 (0.0006)	0.0033 (0.0006)	0.0033 (0.0006)

Table 3.7e : Results of the cluster (with unstandardized variables) and kappa analysis for the 90-99 % mixing ratio interval of the ten mineral combinations for the different cluster techniques.

Mixture	Ward's	Furthest Neighbor	Nearest Neighbor	Group Average	Simple Average	Centroid	Median
dickite/montmorillonite	1 (0)	0.86 (0.12)	1 (0)	0.86 (0.12)	1 (0)	0.86 (0.12)	0.86 (0.12)
dickite/nontronite	0.48 (0.12)	0.07 (0.05)	0.0018 (0.0005)	0.0017 (0.0004)	0.0017 (0.0004)	0.0017 (0.0004)	0.0018 (0.0004)
dickite/illite	0.019 (0.005)	0.0024 (0.0006)	0.0015 (0.0004)	0.0017 (0.0004)	0.0016 (0.0004)	0.0018 (0.0005)	0.0019 (0.0004)
dickite/pyrophyllite	0.016 (0.006)	0.02 (0.02)	0.02 (0.02)	0.02 (0.02)	0.04 (0.03)	0.02 (0.02)	0.04 (0.03)
montmorillonite/nontronite	0.32 (0.09)	0.10 (0.05)	0.10 (0.05)	0.10 (0.05)	0.06 (0.04)	0.10 (0.05)	0.09 (0.05)
montmorillonite/illite	0.06 (0.04)	0.0020 (0.0006)	0.0015 (0.0004)	0.0018 (0.0005)	0.0016 (0.0004)	0.0018 (0.0005)	0.0017 (0.0005)
montmorillonite/pyrophyllite	0.016 (0.006)	0.25 (0.12)	0.29 (0.13)	0.19 (0.12)	0.19 (0.12)	0.19 (0.12)	0.26 (0.12)
nontronite/illite	0.19 (0.05)	0.16 (0.08)	0.0015 (0.0004)	0.0015 (0.0004)	0.05 (0.05)	0.0015 (0.0004)	0.0017 (0.0005)
nontronite/pyrophyllite	0.21 (0.10)	0.21 (0.11)	0.28 (0.11)	0.27 (0.11)	0.16 (0.10)	0.27 (0.11)	0.21 (0.11)
illite/pyrophyllite	0.07 (0.03)	0.08 (0.06)	0.10 (0.06)	0.10 (0.06)	0.10 (0.06)	0.08 (0.06)	0.10 (0.06)

Table 3.8a : Results of the cluster (with unstandardized variables) and kappa analysis for the 1-10 % mixing ratio interval of the ten mineral combinations for the different cluster techniques.

Mixture	Ward's	Furthest Neighbor	Nearest Neighbor	Group Average	Simple Average	Centroid	Median
dickite/montmorinolite	1 (0)	0.30 (0.15)	0.44 (0.17)	0.44 (0.17)	0.44 (0.17)	0.44 (0.17)	0.44 (0.17)
dickite/nontronite	0.95 (0.01)	0.03 (0.01)	0.02 (0.01)	0.02 (0.01)	0.02 (0.01)	0.03 (0.01)	0.02 (0.01)
dickite/illite	0.39 (0.15)	0.008 (0.002)	0.007 (0.001)	0.007 (0.001)	0.008 (0.002)	0.008 (0.002)	0.008 (0.002)
dickite/pyrophyllite	0.05 (0.02)	0.03 (0.01)	0.012 (0.006)	0.013 (0.006)	0.02 (0.01)	0.013 (0.006)	0.014 (0.006)
montmorinolite/nontronite	0.79 (0.03)	0.03 (0.01)	0.03 (0.02)	0.03 (0.01)	0.04 (0.02)	0.04 (0.02)	0.03 (0.01)
montmorinolite/illite	0.49 (0.08)	0.008 (0.002)	0.011 (0.004)	0.008 (0.002)	0.008 (0.002)	0.008 (0.002)	0.008 (0.002)
montmorinolite/pyrophyllite	0.16 (0.06)	0.019 (0.008)	0.014 (0.007)	0.020 (0.008)	0.11 (0.08)	0.020 (0.008)	0.11 (0.08)
nontronite/illite	0.62 (0.03)	0.017 (0.007)	0.006 (0.001)	0.017 (0.007)	0.010 (0.004)	0.013 (0.006)	0.010 (0.004)
nontronite/pyrophyllite	0.58 (0.11)	0.13 (0.06)	0.10 (0.06)	0.15 (0.09)	0.15 (0.09)	0.12 (0.06)	0.06 (0.03)
illite/pyrophyllite	0.05 (0.02)	0.06 (0.01)	0.05 (0.01)	0.05 (0.01)	0.06 (0.01)	0.05 (0.02)	0.18 (0.06)

Table 3.8b : Results of the cluster (with unstandardized variables) and kappa analysis for the 10-30 % mixing ratio interval of the ten mineral combinations for the different cluster techniques.

Mixture	Ward's	Furthest Neighbor	Nearest Neighbor	Group Average	Simple Average	Centroid	Median
dickite/montmorinolite	0.995 (0.003)	0.16 (0.10)	0.31 (0.16)	0.31 (0.16)	0.46 (0.16)	0.34 (0.16)	0.46 (0.16)
dickite/nontronite	0.987 (0.006)	0.021 (0.004)	0.023 (0.004)	0.020 (0.004)	0.019 (0.004)	0.019 (0.004)	0.019 (0.004)
dickite/illite	0.90 (0.08)	0.024 (0.004)	0.021 (0.004)	0.024 (0.004)	0.024 (0.004)	0.024 (0.004)	0.024 (0.004)
dickite/pyrophyllite	0.15 (0.04)	0.020 (0.004)	0.020 (0.004)	0.016 (0.003)	0.020 (0.004)	0.016 (0.003)	0.020 (0.004)
montmorinolite/nontronite	0.88 (0.02)	0.04 (0.01)	0.033 (0.009)	0.04 (0.01)	0.03 (0.01)	0.04 (0.01)	0.023 (0.006)
montmorinolite/illite	0.66 (0.08)	0.028 (0.004)	0.026 (0.004)	0.026 (0.004)	0.030 (0.007)	0.026 (0.004)	0.026 (0.004)
montmorinolite/pyrophyllite	0.63 (0.07)	0.09 (0.04)	0.08 (0.04)	0.04 (0.02)	0.05 (0.02)	0.04 (0.02)	0.05 (0.02)
nontronite/illite	0.77 (0.02)	0.026 (0.013)	0.025 (0.004)	0.03 (0.01)	0.04 (0.02)	0.023 (0.005)	0.04 (0.02)
nontronite/pyrophyllite	0.89 (0.01)	0.06 (0.04)	0.024 (0.004)	0.05 (0.02)	0.024 (0.004)	0.029 (0.008)	0.025 (0.004)
illite/pyrophyllite	0.13 (0.04)	0.04 (0.02)	0.04 (0.01)	0.04 (0.01)	0.07 (0.03)	0.04 (0.01)	0.05 (0.01)

Table 3.8c : Results of the cluster (with unstandardized variables) and kappa analysis for the 30-70 % mixing ratio interval of the ten mineral combinations for the different cluster techniques.

Mixture	Ward's	Furthest Neighbor	Nearest Neighbor	Group Average	Simple Average	Centroid	Median
dickite/montmorillonite	0.989 (0.005)	0.19 (0.10)	0.27 (0.14)	0.15 (0.11)	0.25 (0.13)	0.15 (0.11)	0.15 (0.11)
dickite/nontronite	0.89 (0.10)	0.04 (0.02)	0.04 (0.02)	0.04 (0.02)	0.05 (0.02)	0.04 (0.02)	0.05 (0.02)
dickite/illite	0.980 (0.009)	0.08 (0.01)	0.09 (0.02)	0.08 (0.01)	0.09 (0.02)	0.08 (0.01)	0.09 (0.02)
dickite/pyrophyllite	0.38 (0.11)	0.04 (0.03)	0.03 (0.01)	0.03 (0.01)	0.04 (0.03)	0.03 (0.01)	0.03 (0.01)
montmorillonite/nontronite	0.95 (0.02)	0.06 (0.02)	0.06 (0.01)	0.06 (0.02)	0.07 (0.02)	0.06 (0.02)	0.07 (0.02)
montmorillonite/illite	0.63 (0.11)	0.11 (0.02)	0.11 (0.02)	0.11 (0.02)	0.11 (0.02)	0.11 (0.02)	0.11 (0.02)
montmorillonite/pyrophyllite	0.51 (0.07)	0.22 (0.05)	0.13 (0.04)	0.15 (0.04)	0.18 (0.03)	0.15 (0.04)	0.11 (0.03)
nontronite/illite	0.83 (0.02)	0.06 (0.02)	0.05 (0.02)	0.12 (0.03)	0.04 (0.01)	0.10 (0.03)	0.05 (0.01)
nontronite/pyrophyllite	0.83 (0.02)	0.07 (0.02)	0.06 (0.02)	0.12 (0.05)	0.07 (0.02)	0.07 (0.02)	0.07 (0.02)
illite/pyrophyllite	0.15 (0.04)	0.008 (0.001)	0.0073 (0.0008)	0.0071 (0.0009)	0.0073 (0.0008)	0.008 (0.002)	0.0076 (0.0007)

Table 3.8d : Results of the cluster (with unstandardized variables) and kappa analysis for the 70-90 % mixing ratio interval of the ten mineral combinations for the different cluster techniques.

Mixture	Ward's	Furthest Neighbor	Nearest Neighbor	Group Average	Simple Average	Centroid	Median
dickite/montmorillonite	0.96 (0.02)	0.42 (0.16)	0.22 (0.13)	0.22 (0.13)	0.22 (0.13)	0.22 (0.13)	0.22 (0.13)
dickite/nontronite	1 (0)	0.05 (0.03)	0.02 (0.02)	0.05 (0.03)	0.05 (0.03)	0.05 (0.03)	0.05 (0.03)
dickite/illite	0.94 (0.03)	0.24 (0.11)	0.16 (0.07)	0.14 (0.07)	0.16 (0.07)	0.14 (0.07)	0.16 (0.07)
dickite/pyrophyllite	0.56 (0.11)	0.06 (0.05)	0.10 (0.06)	0.07 (0.04)	0.02 (0.02)	0.07 (0.04)	0.02 (0.02)
montmorillonite/nontronite	0.983 (0.009)	0.32 (0.13)	0.48 (0.15)	0.34 (0.14)	0.21 (0.12)	0.21 (0.12)	0.21 (0.12)
montmorillonite/illite	0.62 (0.09)	0.40 (0.06)	0.35 (0.05)	0.35 (0.05)	0.40 (0.06)	0.35 (0.05)	0.40 (0.06)
montmorillonite/pyrophyllite	0.54 (0.06)	0.48 (0.07)	0.33 (0.06)	0.39 (0.06)	0.33 (0.06)	0.33 (0.06)	0.33 (0.06)
nontronite/illite	0.64 (0.05)	0.14 (0.05)	0.07 (0.03)	0.31 (0.07)	0.11 (0.04)	0.30 (0.07)	0.11 (0.04)
nontronite/pyrophyllite	0.63 (0.04)	0.19 (0.06)	0.16 (0.07)	0.19 (0.08)	0.23 (0.08)	0.21 (0.08)	0.19 (0.08)
illite/pyrophyllite	0.09 (0.03)	0.0023 (0.0004)	0.0024 (0.0005)	0.0027 (0.0005)	0.0024 (0.0004)	0.0023 (0.0004)	0.0024 (0.0004)

Table 3.8e : Results of the cluster (with unstandardized variables) and kappa analysis for the 90-99 % mixing ratio interval of the ten mineral combinations for the different cluster techniques.

Mixture	Ward's	Furthest Neighbor	Nearest Neighbor	Group Average	Simple Average	Centroid	Median
Mixture size 200 particles	1 (0)	0.95 (0.02)	1 (0)	1 (0)	0.97 (0.02)	1 (0)	0.995 (0.005)
Different deconvolution techniques							
ROI	0.98 (0.01)	0.98 (0.01)	0.98 (0.01)	0.98 (0.01)	0.98 (0.01)	0.98 (0.01)	0.98 (0.01)
FFA	0.86 (0.11)	0.43 (0.17)	0.43 (0.17)	0.43 (0.17)	0.43 (0.17)	0.43 (0.17)	0.57 (0.17)
AXIL	1 (0)	0.98 (0.01)	1 (0)	1 (0)	0.98 (0.01)	1 (0)	1 (0)
Clustering in the PC space	0.87 (0.11)	0.16 (0.12)	0.43 (0.17)	0.14 (0.12)	0.14 (0.12)	0.14 (0.12)	0.14 (0.12)
Quantification of the data	1 (0)	1 (0)	1 (0)	1 (0)	0.98 (0.01)	1 (0)	1 (0)

Table 3.9a : Results of the cluster (with unstandardized variables) and kappa analysis for the 1-10 % mixing ratio interval of the dickite/montmorillonite mixtures (second series of experiments).

Mixture	Ward's	Furthest Neighbor	Nearest Neighbor	Group Average	Simple Average	Centroid	Median
Mixture size 200 particles	1 (0)	0.994 (0.003)	0.81 (0.13)	1 (0)	0.91 (0.09)	1 (0)	0.91 (0.09)
Different deconvolution techniques							
ROI	1 (0)	0.989 (0.009)	1 (0)	0.989 (0.009)	0.85 (0.11)	0.989 (0.009)	0.989 (0.009)
FFA	1 (0)	0.72 (0.15)	0.57 (0.17)	0.57 (0.17)	0.72 (0.15)	0.58 (0.17)	0.72 (0.15)
AXIL	1 (0)	0.995 (0.005)	1 (0)	1 (0)	1 (0)	1 (0)	1 (0)
Clustering in the PC space	0.60 (0.16)	0.11 (0.05)	0.30 (0.15)	0.02 (0.01)	0.04 (0.01)	0.03 (0.01)	0.16 (0.12)
Quantification of the data	1 (0)	0.995 (0.005)	1 (0)	1 (0)	1 (0)	1 (0)	1 (0)

Table 3.9b : Results of the cluster (with unstandardized variables) and kappa analysis for the 10-30 % mixing ratio interval of the dickite/montmorillonite mixtures (second series of experiments).

Mixture	Ward's	Furthest Neighbor	Nearest Neighbor	Group Average	Simple Average	Centroid	Median
Mixture size 200 particles	1 (0)	0.999 (0.001)	0.41 (0.16)	1 (0)	0.90 (0.10)	1 (0)	1 (0)
Different deconvolution techniques							
ROI	0.995 (0.003)	0.99 (0.01)	0.995 (0.003)	0.995 (0.003)	0.995 (0.003)	0.995 (0.003)	0.995 (0.003)
FFA	1 (0)	0.89 (0.10)	0.89 (0.10)	0.89 (0.10)	0.89 (0.10)	0.89 (0.10)	0.89 (0.10)
AXIL	0.998 (0.002)	1 (0)	0.89 (0.10)	1 (0)	1 (0)	1 (0)	1 (0)
Clustering in the PC space	0.84 (0.10)	0.13 (0.07)	0.020 (0.004)	0.03 (0.01)	0.04 (0.03)	0.019 (0.004)	0.019 (0.004)
Quantification of the data	0.998 (0.002)	0.998 (0.002)	1 (0)	1 (0)	0.998 (0.002)	1 (0)	0.998 (0.002)

Table 3.9c : Results of the cluster (with unstandardized variables) and kappa analysis for the 30-70 % mixing ratio interval of the dickite/montmorillonite mixtures (second series of experiments).

Mixture	Ward's	Furthest Neighbor	Nearest Neighbor	Group Average	Simple Average	Centroid	Median
Mixture size 200 particles	1 (0)	1 (0)	0.20 (0.13)	1 (0)	0.80 (0.13)	1 (0)	0.90 (0.10)
Different deconvolution techniques							
ROI	0.992 (0.005)	0.988 (0.008)	0.28 (0.14)	0.992 (0.005)	0.74 (0.14)	0.992 (0.005)	0.87 (0.10)
FFA	1 (0)	1 (0)	0.40 (0.16)	0.52 (0.16)	0.64 (0.16)	0.40 (0.16)	0.64 (0.16)
AXIL	0.996 (0.004)	1 (0)	0.50 (0.17)	1 (0)	0.75 (0.14)	1 (0)	0.75 (0.14)
Clustering in the PC space	0.58 (0.14)	0.08 (0.03)	0.05 (0.02)	0.06 (0.03)	0.07 (0.03)	0.05 (0.03)	0.05 (0.03)
Quantification of the data	1 (0)	1 (0)	0.63 (0.16)	1 (0)	0.87 (0.11)	1 (0)	0.75 (0.15)

Table 3.9d : Results of the cluster (with unstandardized variables) and kappa analysis for the 70-90 % mixing ratio interval of the dickite/montmorillonite mixtures (second series of experiments).

Mixture	Ward's	Furthest Neighbor	Nearest Neighbor	Group Average	Simple Average	Centroid	Median
Mixture size 200 particles	0.995 (0.005)	1 (0)	0.20 (0.13)	1 (0)	0.90 (0.10)	1 (0)	0.80 (0.13)
Different deconvolution techniques							
ROI	0.994 (0.006)	0.988 (0.008)	0.52 (0.16)	0.994 (0.006)	0.79 (0.13)	0.994 (0.006)	0.79 (0.13)
FFA	1 (0)	1 (0)	0.57 (0.16)	0.87 (0.10)	0.57 (0.16)	0.87 (0.10)	0.57 (0.16)
AXIL	1 (0)	1 (0)	0.60 (0.16)	0.90 (0.10)	0.70 (0.15)	0.90 (0.10)	0.70 (0.15)
Clustering in the PC space	0.20 (0.10)	0.03 (0.02)	0.04 (0.03)	0.02 (0.02)	0.02 (0.02)	0.02 (0.02)	0.02 (0.02)
Quantification of the data	1 (0)	1 (0)	0.80 (0.13)	1 (0)	0.90 (0.10)	0.90 (0.10)	0.90 (0.10)

Table 3.9e : Results of the cluster (with unstandardized variables) and kappa analysis for the 90-99 % mixing ratio interval of the dickite/montmorillonite mixtures (second series of experiments).

3.2.4 Applications.

The hierarchical cluster analysis is used to classify the data generated by the automated analysis of single particles by the use of EPXMA. The particles (objects) were mainly classified on the basis of their elemental composition. A classification based on the size or shape is also possible (Raeymakers et al., 1984).

The choice of which deconvolution technique to use depends on the required accuracy, and the CPU time one wishes to spend to achieve this. In practice, the AXIL deconvolution technique is only used when a high accuracy is required. Otherwise the faster ROI or FFA methods are used.

Generally the cluster analysis is applied to the relative peak intensities. After the particles have been classified into groups, the ZAF-corrections for matrix effects in EPXMA are carried out, taking into account the average composition of the group (Semi Quantitative Method, SQM). The mean composition of the particle types are then in weight percentages, but the listed standard deviations are the standard deviations of the percentile characteristic X-ray ratios, and can only be considered as an estimate of the standard deviations. Performing conventional ZAF-corrections, for bulk samples, or ZAF-corrections specific for particles to the data of every particle would be more rigorous. But this Quantitative Method (QM) requires too much CPU time to be feasible in practice, and is therefore seldomly applied. The effect of the degree of accuracy and quantification on the result of the classification procedure is described in section 3.2.3.3. There it was shown that for the mineral mixture under study no influence on the cluster solution could be measured. For studies of estuarine particles, limited comparisons of these approaches indicate that applying conventional ZAF-corrections to the average data from a particle type is acceptable. This was shown for three samples of the Dordogne estuary. However the differences be-

tween the SQM and the QM were large for low atomic number elements. This was expected, because as these elements have the lowest X-ray energies, important ZAF-corrections are obtained. The QM enlarged the Na/Si, Mg/Si and Al/Si ratio significantly. Cluster analysis resulted, especially, in different quartz and aluminosilicate particle types. As will be shown later on in this section, this is not necessarily a result of these methods, but is a general feature of the cluster analysis applied to this kind of data. For the other particle types, containing particles rich in Ca, Ti and Fe, the abundances of the particle types are the same but the mean compositions of the groups are slightly different. It is assumed that when no accurate average compositions are required, the SQM is sufficient and the abundances of the particle types and the abundance gradients, between samples, can be determined accurately.

The effect of the standardization on the results of the classification procedure was shown in section 3.2.3.3, for different mineral mixtures. Generally, for suspended particulate matter data, no scale conversion (standardization) is carried out in order to reduce the effect of large relative variations in the minor element concentration data.

By studying the dendrogram at a certain similarity level, particle types are obtained. One way, to determine the level at which significant particle types are obtained, is to plot the minimum distance of the similarity matrix as a function of the number of clusters. A schematic presentation of such a plot is represented in Figure 3.10. If similar objects and/or clusters are merged, the minimum distance increases slowly. If, however, two objects and/or clusters, significantly different from each other, are joined, the minimum distance will suddenly increase. From this point only different objects and/or clusters are merged. The relevant number of clusters (K) can practically be determined from tables as Table 3.3 or from figures as Figure 3.6. The practical example of Table 3.3 for an estuarine suspended particulate matter sample shows that the determination

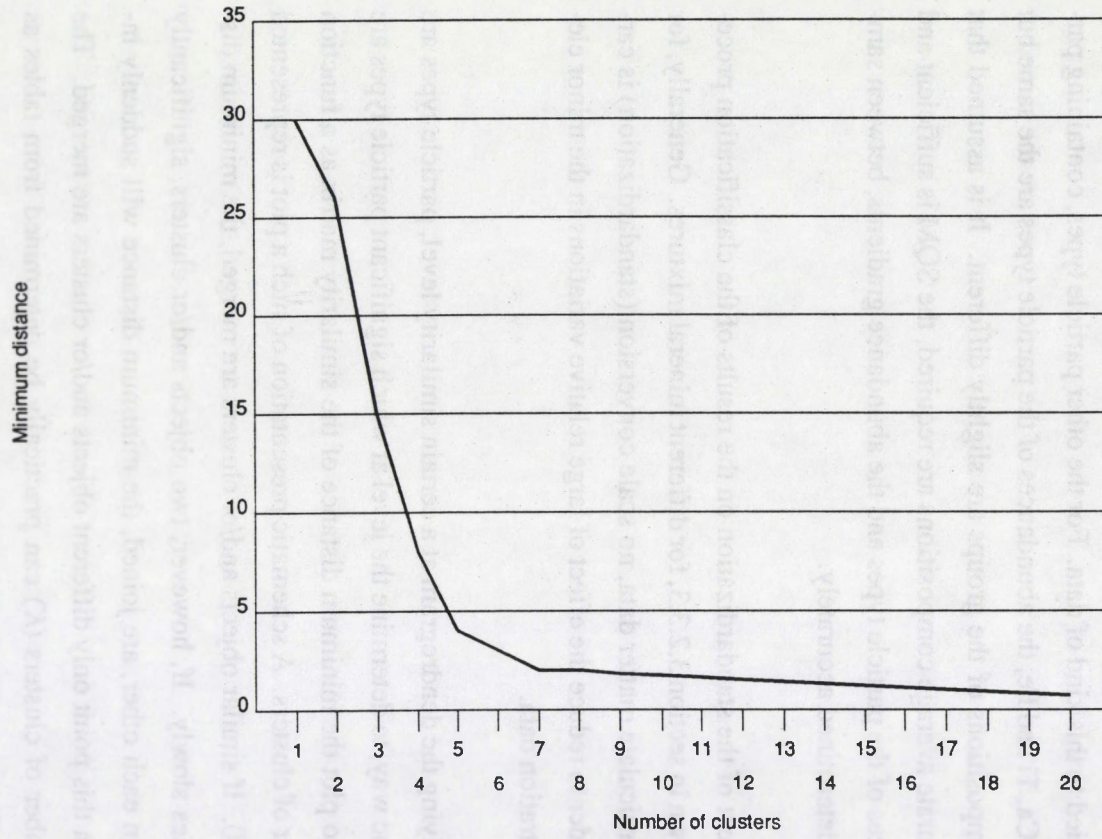


Figure 3.10 : Schematic presentation of the determination of K significant clusters on the hand of the minimum distance versus number of clusters plot. The sudden increase determines the number of significant clusters.

of the number of clusters K , is not always straightforward. In a practical problem the geochemical relevance of the clusters has to be taken into account.

In practice the hierarchical cluster analysis agglomerates the single particle measurements in K relevant clusters. The centroids, which are the average composition and size information of the particle types, are calculated, together with the standard deviation for a single measurement. For each particle type i , the percentile relative abundance is obtained by dividing the number of objects of cluster i by the total number of measured particles multiplied by hundred.

The standard deviation on the percentile relative abundance is given by binomial statistics. The relative abundance of the particle type is the probability (p) that when a single particle is measured, it will belong to the group. The standard deviation of the binomial function is then :

$$\sigma = \sqrt{np(1-p)}$$

where n is the total number of measured particles.

When the standard deviation is expressed in % the formula becomes :

$$\sigma(\%) = \sqrt{\frac{P(100-P)}{n}}$$

where P is the percentile relative abundance.

Van Der Plas and Tobi (1965) presented a chart for different values of P and n which gives the 2σ values, 95 % confidence interval. This chart is given in Figure 3.11 and it is seen that, for a linear decrease of the standard deviation, the number of particles to be measured increases quadratically. As a result a compromise must be found between the measurement time and the necessary ac-

curacy of the percentile relative abundances. In most practical applications ca. 300 particles were measured, which results in percentile standard deviations between 2-6 % on a 95 % confidence interval.

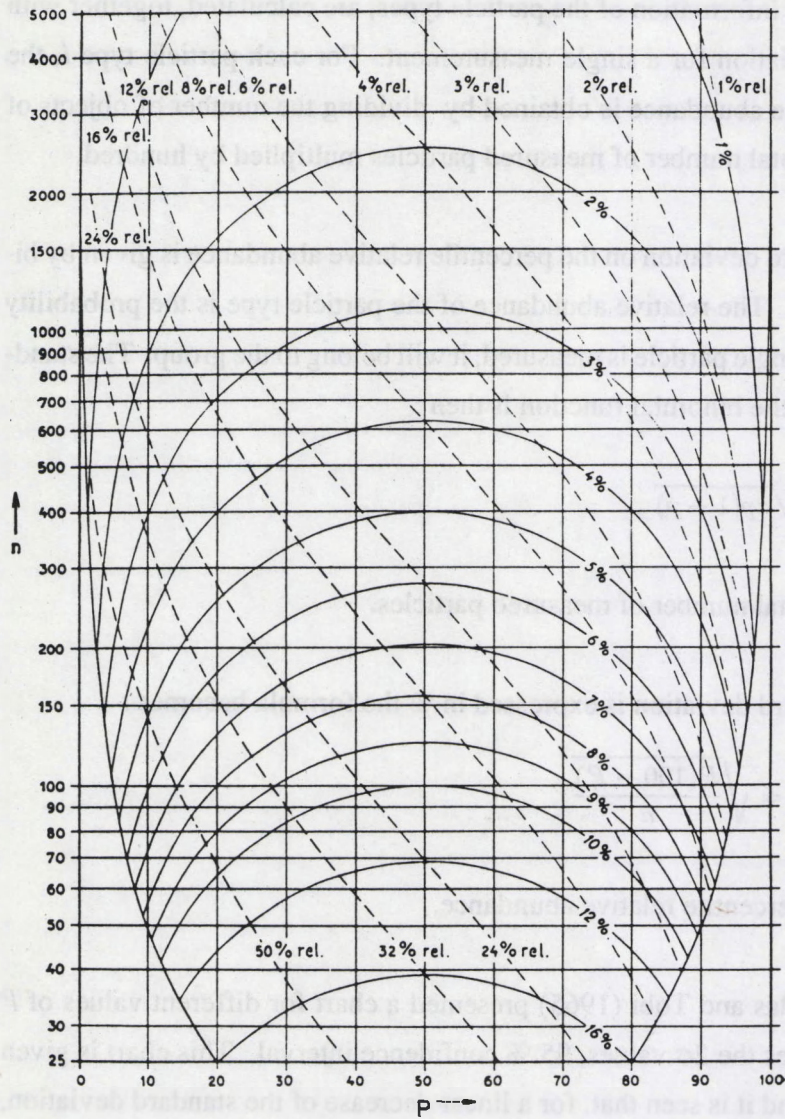


Figure 3.11 : A chart for the determination of the standard deviation on the results of point-counting results (after Van Der Plas and Tobi, 1965).

The final result of a hierarchical cluster analysis of an estuarine suspended particulate matter sample is given in Table 3.10a. The sample is characterized by the abundance of its geochemical particle types.

The objective of recognizing particle types in a sample and following their behavior through the whole study area is however not served by classification per individual sample. Indeed, due to statistical fluctuations, the groups identified by the cluster algorithm can differ in average composition from sample to sample or even for successive measurements of a finite number of particles in one sample. This is seen by comparing Table 3.10a with Table 3.10b, where the cluster results are presented for two river suspension samples taken simultaneously at the same location. As far as major elements are concerned, the overall composition calculated as the weighted average of the compositions of the different groups is the same for both samples, confirming the representativeness of the sampling and validity of the chemical analysis. Of course, mainly due to counting statistics the relative differences are up to a factor of 3 for the minor elements, but since no normalization was carried out for the calculation of the dissimilarity matrix, low abundance elements have less influence on the cluster analysis results. In both samples corresponding groups with an identical composition (e.g. groups 1, 2, 6 and 8 in sample 1 and groups 1, 2, 7 and 8 in sample 2, respectively), albeit sometimes with a different abundance, can easily be recognized. Yet some groups that are separated in one sample are seen to merge in the other sample (e.g. groups 1 and 2 in sample 2 correspond with group 7 in sample 1). Also groups 4 and 5 in sample 1 seem to correspond with groups 5 and 6 in sample 2. Therefore the classification should consider simultaneously all examined particles in all samples of the study area. This simultaneous classification should not be done by a hierarchical cluster analysis. Indeed, when the number of particles analyzed is large, e.g. 3000 (about 10 samples) as many as 4,500,000 Euclidean distance coefficients have to be calculated and processed in every cycle. Therefore the nonhierarchical centroid sorting method of Forgy

group no.	% Abun.	Na %	Mg %	Al %	Si %	P %	S %	Cl %	K %	Ca %	Ti %	Fe %
1	13	— ^b	0.1 (0.3)	1 (1)	95 (3)	0.03 (0.17)	0.06 (0.24)	0.06 (0.24)	0.2 (0.4)	0.1 (0.4)	—	0.3 (0.8)
2	12	0.6 (0.9)	0.2 (0.5)	12 (5)	72 (8)	—	0.3 (0.8)	0.3 (0.6)	6 (8)	2 (2)	0.4 (0.7)	2.3 (2.2)
3	57	0.1 (0.2)	0.6 (0.8)	22 (4)	54 (4)	0.3 (0.8)	1 (1)	0.3 (0.7)	7 (4)	3 (3)	1 (2)	7 (4)
4	8	0.1 (0.3)	3.0 (2.5)	19 (4)	39 (6)	0.5 (0.7)	1 (1)	0.2 (0.5)	4.4 (3.4)	2.2 (2.2)	1.5 (1.8)	26 (7)
5	2	—	0.3 (0.5)	3 (3)	9 (6)	—	0.7 (1.2)	1.0 (2.4)	0.2 (0.4)	7 (9)	3 (3)	73 (10)
6	5	—	3 (6)	1.9 (1.6)	6 (4)	0.1 (0.4)	0.6 (0.6)	—	0.3 (0.5)	83 (7)	0.2 (0.6)	1.7 (1.5)
7	1	—	4 (4)	5.3 (2.3)	24 (8)	0.7 (1.2)	0.7 (0.6)	0.3 (0.6)	1.7 (0.6)	49 (6)	—	9 (12)
8	0.4 ^a	—	—	7	23	—	1	—	3	—	60	3
av ^c		0.1 (0.4)	0.8 (2.0)	16 (9)	56 (22)	0.3 (0.7)	0.5 (0.9)	0.3 (0.7)	1 (4)	7 (19)	1 (4)	9 (12)

^a This group corresponds to one particle only. ^b Not detectable. ^c Weighted average.

Table 3.10a : Results of the hierarchical cluster analysis of an estuarine suspended particulate matter sample, for which the abundance and the average composition (centroids) is represented for each particle type. Sample 1.

group no.	% Abun.	Na %	Mg %	Al %	Si %	P %	S %	Cl %	K %	Ca %	Ti %	Fe %
1	14	0.2 (0.3)	0.2 (0.3)	1.8 (2.3)	94 (4)	0.1 (0.3)	1 (1)	0.1 (0.2)	1.0 (1.1)	0.7 (0.8)	0.6 (0.9)	0.9 (1.2)
2	5	0.9 (0.9)	0.4 (0.5)	13 (5)	74 (3)	0.1 (0.3)	0.8 (1.2)	0.4 (0.7)	2.6 (1.7)	1.7 (1.5)	2 (5)	4 (3)
3	39	0.3 (0.6)	1.1 (1.2)	21 (4)	55 (4)	0.4 (0.8)	1 (2)	0.8 (1.2)	5.5 (2.7)	3 (2)	1.1 (1.4)	9 (3)
4	23	0.3 (0.4)	0.6 (0.8)	22 (6)	53 (5)	1 (1)	2 (2)	1 (1)	14 (5)	1.9 (1.7)	1 (1)	4.5 (2.5)
5	10	0.3 (0.5)	2 (2)	18 (5)	45 (6)	1.3 (1.8)	1.5 (2.5)	1.0 (1.3)	4 (2)	8 (9)	2 (2)	17 (6)
6	2	0.02 (0.05)	2.5 (2.7)	11 (5)	28 (12)	2 (2)	2.4 (2.2)	1 (1)	4 (4)	4 (8)	2.1 (2.2)	44 (14)
7	5	0.3 (0.3)	0.4 (0.5)	2.8 (1.5)	8 (5)	0.2 (0.4)	1 (1)	0.6 (0.6)	1.4 (1.6)	83 (9)	0.6 (0.9)	2 (2)
8	1	0.2 (0.2)	0.7 (0.8)	1.9 (1.5)	7 (4)	— ^b	0.4 (0.5)	0.3 (0.3)	0.5 (0.3)	0.9 (0.8)	87 (7)	1.5 (0.7)
av ^c		0.3 (0.5)	0.9 (1.3)	17 (9)	57 (21)	0.5 (1.0)	1.3 (1.8)	0.6 (1.1)	6 (5)	7 (18)	2 (9)	9 (8)

^b Not detectable. ^c Weighted average.

Table 3.10b : Results of a hierarchical cluster analysis of the duplicate estuarine suspended particulate matter sample. Sample 2.

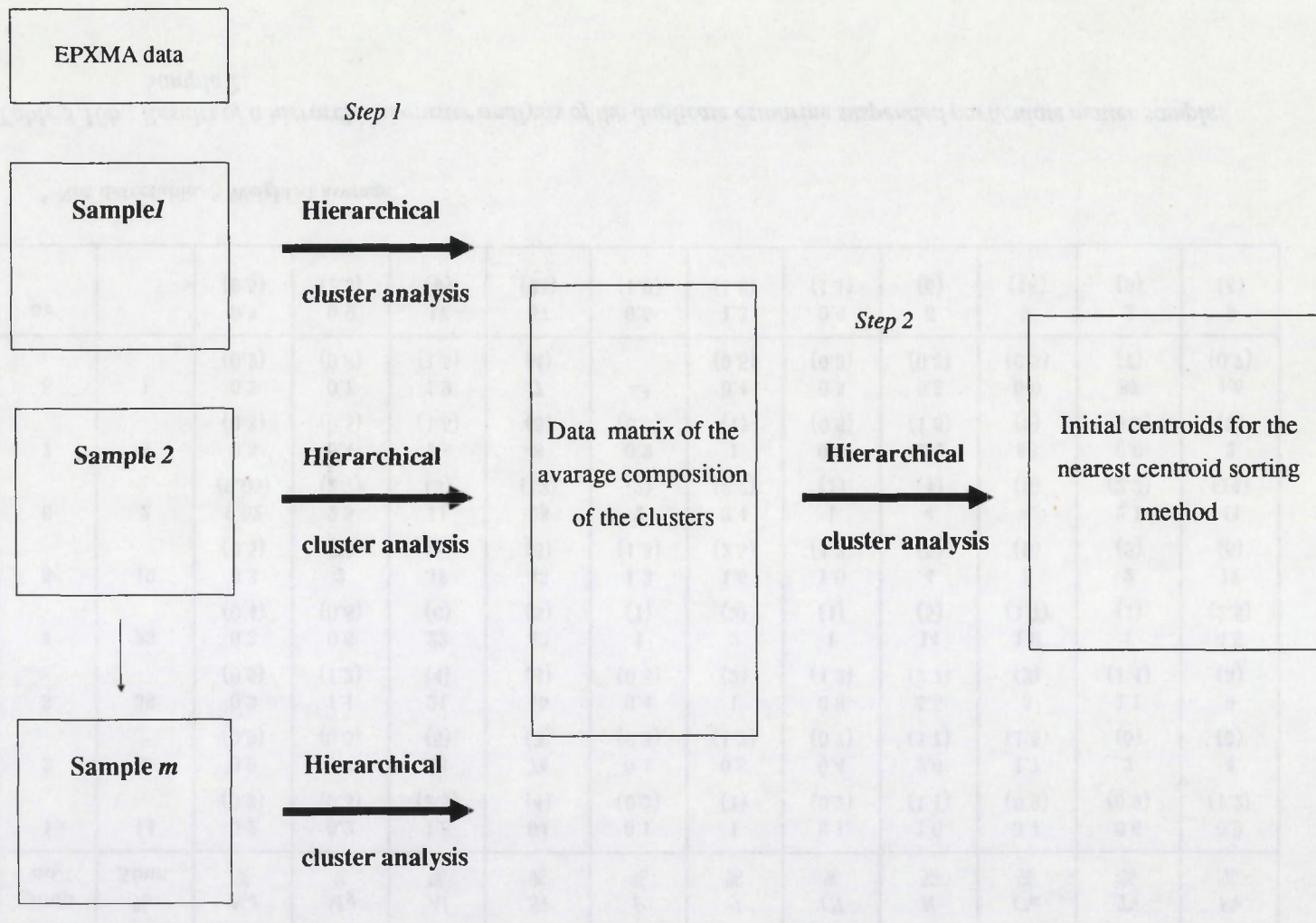


Figure 3.12 : The selection of a well-balanced initial set of centroids by the use of a sequence of hierarchical cluster analyses.

is used. The selection of a well-balanced initial set of centroids is essential for a successful classification. This is achieved by a sequence of hierarchical cluster analyses as follows (Figure 3.12):

1. cluster analysis of the composition data of the particles for each individual sample.
2. subsequent cluster analysis of the average composition data of all the groups obtained via step 1. Hence, groups representative for the whole study area are obtained ; their average composition are taken as the initial centroids.

In this way geochemical relevant particle types are obtained by the method of Forgy. The Forgy program was written in such a way that the abundance of the particle types per individual sample is determined. The abundance of the particle types can then be followed throughout the study area, and the changes provide information about processes that influence the abundance of the particle types. Recently a more or less similar approach has also been used by Shattuck et al. (1985) for the classification of individual atmospheric aerosol EPXMA data. These authors compared a number of methods for the determination of seedpoints (initial centroids). These methods were however only applied to a small part, 70 objects, of the original data set. Our proposed method, the sequence of hierarchical cluster analysis, is more rigorous, but requires also more CPU time.

3.3 REFERENCES

- Anderberg, M. R., 1973. Cluster Analysis for Applications, Academic Press, New York, 359 pp.
- Bernard, P. C., Van Grieken, R. E., and Eisma, D., 1986. Classification of estuarine particles using automated electron microprobe analysis and multivariate techniques. *Environ. Sci. Technol.*, 20 : 467-473.
- Blashfield, R. K., 1976. Mixture model tests of cluster analysis : accuracy of four agglomerative hierarchical methods. *Psychological Bulletin*, 83 : 377-388.
- Cohen, J., 1960. A coefficient of agreement for nominal scales. *Educational and Psychological Measurement*, 20 : 37-46.
- Cunningham, K. M., and Ogilvie, J. C., 1971. Evaluation of hierarchical grouping techniques : a preliminary study. *The Computer Model*, 15 : 209-213.
- Everitt, B. S., 1979. Unresolved problems in cluster analysis. *Biometrics*, 35 : 169-181.
- Fisher, L., and Van Ness, J. W., 1971. Admissible clustering procedures. *Biometrika*, 58 : 91-104.
- Fleiss, J. L., Cohen, J., and Everitt, B. S., 1969. Large sample standard errors of kappa and weighted kappa. *Psychological Bulletin*, 72 : 323-327.
- Forgy, E. W., 1965. Cluster analysis of multivariate data : efficiency versus interpretability of classifications. *Biometrics*, 21 : 768
- Gross, A. J., 1972. A Monte Carlo study of the accuracy of a hierarchical grouping procedure. *Multivariate Behavioral Research*, 7 : 379-389.
- Jardine, N., and Sibson, R., 1968. The construction of hierarchic and non-hierarchic classifications. *The Computer Journal*, 177-184.
- Kuiper, F. K., and Fisher, L., 1975. A Monte Carlo comparison of six clustering procedures. *Biometrics*, 31 : 777-783.
- Lance, G. N., and Williams, W. T., 1967. Mixed-data classificatory programs : I. Agglomerative systems. *The Australian Computer Journal*, 15-20.

- Landis, J. R., and Koch, G. G., 1977. An application of hierarchical kappa-type statistics in the assessment of majority agreement among multiple observers. *Biometrics*, 33 : 363-374.
- Massart, D. L., Dykstra, A., and Kaufman, L., 1978. *Evaluation and Optimization of Laboratory Results and Analytical Procedures*, Elsevier, Amsterdam, 596 pp.
- Massart, D. L., and Kaufman, L., 1983. *The Interpretation of Analytical Data by the Use of Cluster Analysis*. John Wiley & Sons, New York, 237 pp.
- Mather, P., 1976. *Computational Methods of Multivariate Analysis in Physical Geography*, John Wiley & Sons, London, 532 pp.
- Rand, W. M., 1971. Objective criteria for the evaluation of clustering methods. *Journal of the American Statistical Association*, 66 : 846-850.
- Raeymakers, B., Van Espen, P., and Adams, F., 1984. The morphological characterization of particles by automated scanning electron microscopy. *Mikrochimica Acta*, II/5-6 : 437-454.
- Shattuck, T. W., Germani, M. S., and Buseck, P. R., 1985. Cluster analysis of chemical compositions of individual atmospheric particle data. In : J. J. Breen and P. E. Robinson (Editors), *Environmental Applications of Chemometrics*, ACS Symposium Series 292, American Chemical Society, Washington D. C., 1985, pp. 118-129.
- Van Der Plass, L., and Tobi, A.C., 1965. A chart for judging the reliability of point counting results. *American Journal of Science*, 263 : 87-90.
- Van Espen, P., 1984. A program for the processing of analytical data (DPP). *Anal. Chim. Acta*, 165 : 31-49.
- Wishart, D., 1969. Mode analysis in numerical taxonomy. In : A. J. Cole (Editor), *Numerical taxonomy : Proceedings of the Colloquium in Numerical Taxonomy held in the University of St. Andrews, September 1968*, Academic Press, London, pp. 282-311.
- Wolfe, J. H., 1970. Pattern clustering by multivariate mixture analysis. *Multivariate Behavioral Research*, 5 : 329-350.

Chapter 4

Geochemistry of individual suspension particles

Suspended particulate matter from estuarine and marine environments is being investigated extensively in order to assess sediment processes, the interactions between sediments and the water column, and the physicochemical reactions that particles undergo. Most of the analytical techniques, as for instance X-ray fluorescence, instrumental neutron activation analysis, atomic absorption spectrometry and X-ray diffraction, used in this context hitherto, provide the bulk composition or mineralogy of the samples. Associations between, e.g., chemical elements, mineral phases, and morphology must then be made on a statistical basis. For the differentiation of metals in various organic and inorganic phases, sequential extraction procedures were developed. However none of these techniques elaborate the occurrence of certain individual particles. Alternatively, single particle analysis methods such as Scanning Electron Microscopy (SEM) combined with X-ray analysis or electron microprobe analysis were invoked by Dehairs et al. (1980), Jedwab (1980), Skei and Melson (1982) and Sundby et al. (1984) for the confirmation of the presence of certain expected particles. These studies had in common that the particles were searched and analyzed for their chemical and morphological characteristics manually, which is time-consuming and hardly feasible for large number of samples. It is clear that the use of the automated probe X-ray microanalysis, which allows the chemical and morphological analysis of a large number of particles within a relatively short time, has great perspectives for these research topics.

The first results of automated EPXMA of marine suspended particulate matter was reported by Bishop and Biscaye (1982). A part of the data was also described by Lambert et al. (1984). Bishop and Biscaye applied this technique to individual particles from the nepheloid layer in the Atlantic Ocean, and classified the analyzed particles on the basis of their Si/Al ratio.

In the present work the practical applicability of the automated EPXMA technique in combination with multivariate analysis techniques was shown for

suspended particulate matter from different aquatic environments. For the collection of the samples and the geochemical interpretation of the results, cooperation with a number of scientists working in the estuarine and marine field was accomplished. Because a major part of the work deals with estuarine research some typical features of estuaries will briefly be discussed in the theoretical part of this chapter. This theoretical part contains information on the definition and the classification of estuaries and some aspects of estuarine processes will be outlined. In the experimental part of this chapter the geochemical studies on some estuaries (namely the Ems, Gironde and Scheldt) and the Baltic Sea will be discussed.

The study of the Ems and Gironde estuary were performed in cooperation with Dr. D. Eisma attached to the Netherlands Institute for Sea Research (NIOZ), Texel, The Netherlands. He coordinated the sampling campaigns and the work of a number of scientists involved with the analysis of the particulate inorganic and organic material in these estuaries. By this approach it was tried to characterize the particulate material and to study its fate throughout these estuaries.

The study of the Scheldt estuary was conducted in cooperation with Dr. F. Dehairs from the Free University of Brussels (VUB), Brussels, Belgium. This study aimed to characterize the most typical particles in the Scheldt, and their behavior throughout the estuary. Because the highly polluted estuary also contains an anoxic region, it is believed that in such an environment rare anthropogenic particles can be formed. Because these particles consist mostly of higher atomic number elements, relative to the common aluminosilicate minerals, it is possible to search selectively for these particles. This approach has been used for a specific sample.

The Baltic Sea, a sea with an estuarine character and a strong stratification, was studied in cooperation with Dr. L. Brüggemann, Institute of Marine Research,

Rostock-Warnemünde, German Democratic Republic. The aim of the study was to identify the individual inorganic particles of the suspended particulate matter with the aid of EPXMA. Furthermore the suspended particulate matter was also analyzed by a sequential extraction method. The elemental fractions were determined by atomic absorption analysis. Comparison of the single particle and bulk analytical data gave additional information about the types and sources of the suspended matter in the Baltic Sea.

4.1 ESTUARINE PROCESSES

An estuary is defined as a semi-enclosed coastal body of water which has a free connection with the sea and within sea water is measurably diluted with fresh water derived from land drainage (Pritchard, 1967). This definition takes the basic features of the salinity and density distributions into account, as well as the circulation pattern and the mixing processes. It also points out the importance of the boundaries which control the distribution of properties and the movement and mixing of waters.

In general, estuaries are subclassified on the basis of their geomorphological characteristics. There are primarily four subdivisions of estuaries, namely 1) drowned river valleys, 2) fjord-type estuaries, 3) bar built estuaries and 4) estuaries produced by tectonic processes. Also with regard to the dominant physical processes associated with movement and mixing in the estuary, four types of estuaries were distinguished by Postma (1980). The schematic representation of the four types of estuaries is given in Figure 4.1, with respect to their salinity distribution and their sediment transport characteristics :

- a) salt wedge estuary : most or all suspended material is fluvial and is carried to the sea in the low salinity surface layer and does not enter the estuarine cycle proper.
- b) partially mixed estuary : the landward bottom flow is sufficiently strong to move suspended sediments up the estuary until the head of the salt intrusion is reached. This sediment may be fluvial material that has settled from the upper into the lower layer, but it may also be of marine origin, depending on the concentration of suspended matter in the river and in the sea and their fluxes toward the estuary.
- c) fully mixed estuary : the suspended matter is concentrated nearshore. This occurs also for estuaries without appreciable river flow that are tidally dominated.

d) negative estuary : having a net inflow at the surface and the outward flow near the bottom. These may form in areas where excess evaporation (arid regions) causes high salinities in the inner section of the estuary; material is transported by the bottom current.

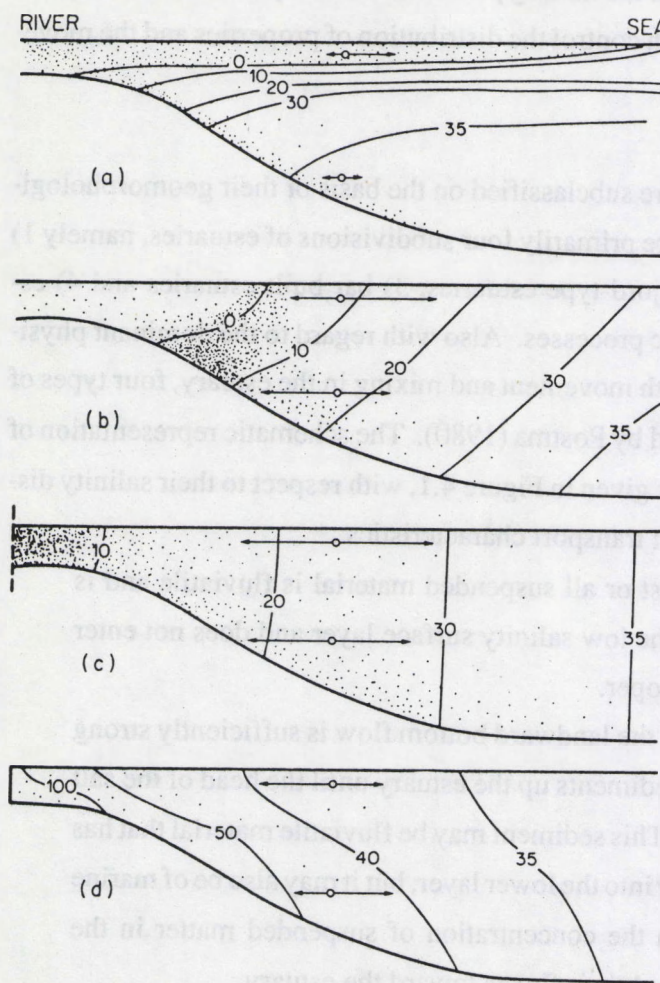


Figure 4.1 : Schematic representation of the four types of estuaries, after Postma (1980).

These estuarine circulations are especially important in understanding the fate of fluvial and marine suspended matter and sediments in the estuary. Because the estuaries studied in this work are all stratified the main features of water and sediment movements will be outlined in detail for this kind of estuary; as is shown in Figure 4.2. The freshwater discharge generates a residual seaward flow in the upper layer. The seawater which is entrained from the lower layer by this flow is provided by a residual landward flow along the bottom. The particles transported by the river are subjected to gravitational settling and settle during horizontal transport. Here they are taken up by the residual landward flow along the bottom. The suspended matter concentration near the bottom is generally greater than near the surface and this causes a residual sediment transport in the transition region between salt and freshwater. Accumulation of sediments occurs until a state of (dynamic) equilibrium is reached between sediment supply along the bottom, removal of suspended matter from the lower to the upper layer

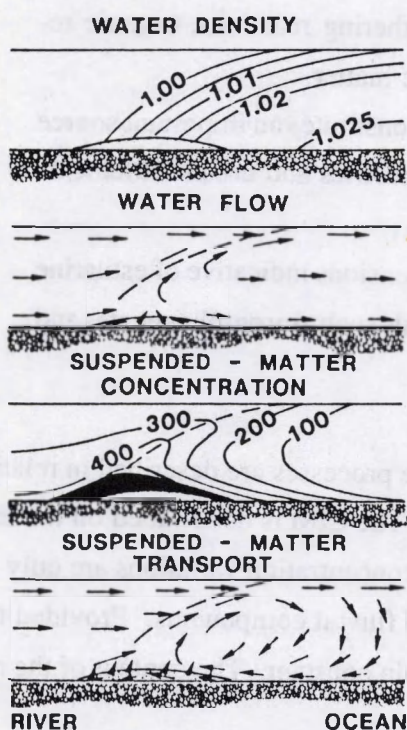


Figure 4.2 : The mean features of water and sediment movements for a stratified estuary.

by mixing, seaward transport in the upper layer and sinking of suspended matter from the upper layer back to the lower layer. The maximum concentration of suspended matter in the water, the so-called turbidity maximum, appears to occur at the tip of the saltwater wedge in the estuary. The recirculation of mud gives rise to longer particulate residence times for the suspended matter than for the water. River water, with its dissolved components, actually flows through the turbidity maximum whereas some proportion of the particles are returned within the maximum.

Particulate material in estuaries originates from numerous sources (Goldberg, 1978) :

- the oceanic source of particulate matter is characterized by biogenic skeletons of diatoms, coccoliths and foraminifera as well as by the clay minerals having specific properties of material originating from coastal sources due to marine erosion.
- the fluvial source includes materials eroded from the catchment area, oxyhydrates and clay minerals from weathering reactions, organic remains from vascular plants or as humic matter.
- airborne anthropogenic particulate matter constitutes an important source locally because of the proximity of industries and urban settlements to most of the world's major estuaries.
- organic and inorganic flocculations in suspensions indicative of estuarine sources as are certain authigenic minerals such as iron-phosphates and manganese hydroxides.

In most estuarine studies, the estuarine processes are described in relation to a Conservative Index of Mixing (CIM). The CIM is determined on the base of a "conservative" element, for which the concentration variations are only the result of the mixing ratio of the marine and fluvial components. Provided that the concentration of the end-members remain constant. The content of the ele-

ment under study is placed relatively to the CIM, and deviations from the theoretical linear mixing curve point to processes other than simple mixing (Figure 4.3). In general, the salinity or chlorinity is used as a CIM in the case dissolved element concentrations are considered. For the determination of the mixing ratio of the marine to fluvial material in suspended matter natural tracers are used in most cases. To be useful as a CIM there has to exist a natural difference in composition between two or more sediment sources, and the tracer has to behave conservatively throughout the estuary. Differences in mineralogy, in chemical composition, and in isotopic composition have been used in the past for a number of estuaries. A review of these studies was made by Salomons and Förstner (1984).

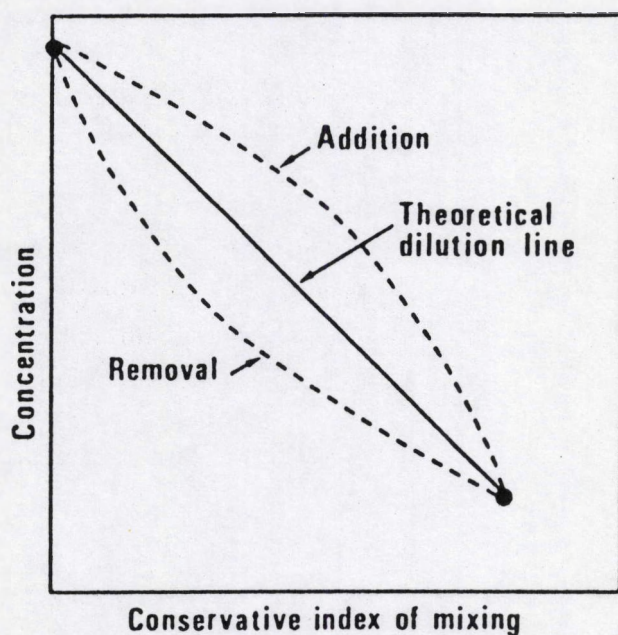


Figure 4.3 : Schematic representation of conservative and non-conservative behavior in an estuary.

3.2 THE EMS ESTUARY

The study of the Ems estuary was conducted in cooperation with Dr. D. Eisma, Netherlands Institute for Sea Research (NIOZ), Texel, Netherlands. The main objective of the study was to characterize the particulate organic and inorganic matter in the estuary and to describe their behavior throughout the estuary, e.g. river and sea samples, and several samples in the transition zone were taken. The Ems estuary is situated at the Dutch - German border, and is part of the Wadden Sea, characterized by channels and extensive tidal flats. Sampling was performed during high and low run-off discharge, in November-December 1982 and May 1984, respectively. In Figure 4.4 the full circles represent the sample stations during high run-off and the open circles these of low run-off. The salinity and turbidity profiles in the Ems estuary are shown for the two sampling campaigns in Figures 4.5 and 4.6, respectively.

For the analysis of the composition of the particulate organic matter, pyrolysis gas chromatography mass spectrometry (PyGMS) was performed by J. J. Boon, Institute for Atomic and Molecular Physics, Amsterdam. Because this technique is rather elaborate and not suitable for large series of samples, Curie-point flash pyrolysis mass spectrometry (PyMS), a semi-quantitative method, was also used. Additionally, determinations of $^{13}\text{C}/^{12}\text{C}$ were carried out by W. G. Mook, Laboratory of Isotope Physics, Groningen. In this way the particulate organic matter was characterized. The characterization of the particulate inorganic matter was accomplished by automated EPXMA analysis. For this analysis small aliquots of water, one drop to a few milliliters, were filtered over a 47 mm diameter 0.4 μm pore-size Nuclepore membrane filter. Care was taken to obtain a sufficient loading for efficient analysis while maintaining a low percentage (less than 5 %) of overlapping particles (Kelly et al., 1980); generally the sample loading was between 1-150 ng/mm^2 . After washing with Milli-Q-water and air drying in a laminar flow box, the filters were coated with carbon.

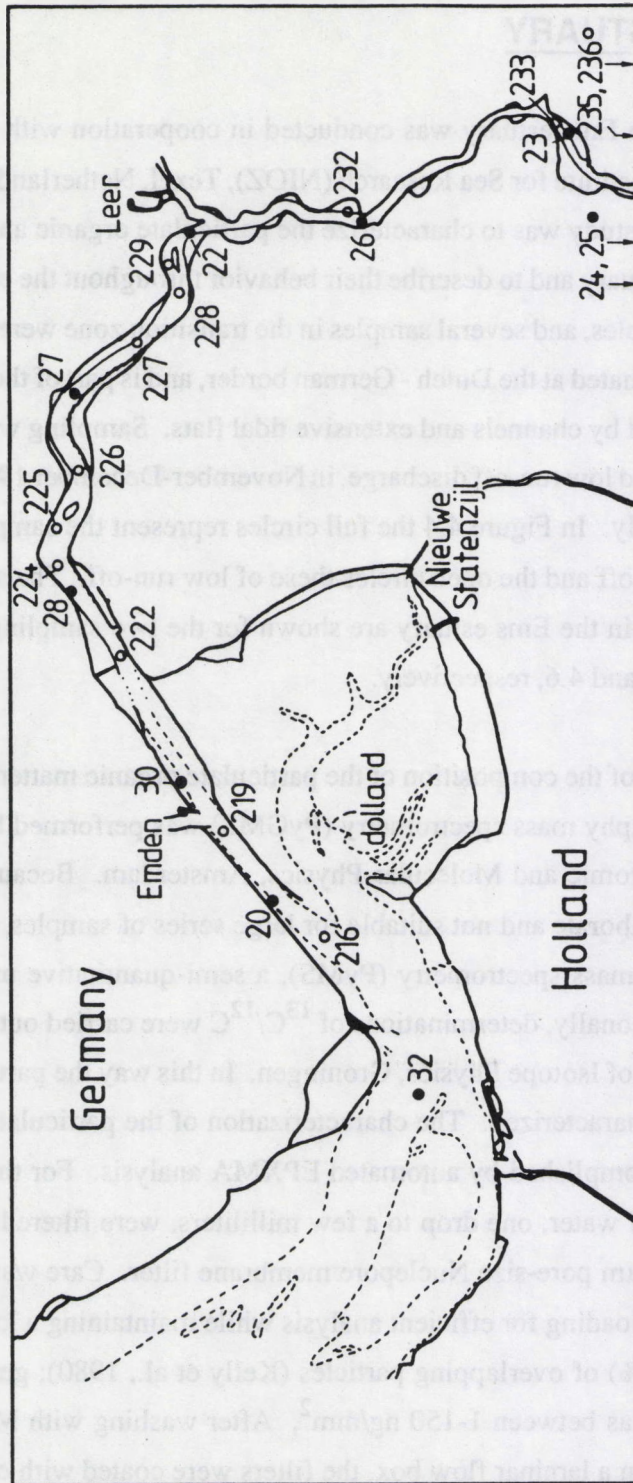


Figure 4.4 : Ems estuary. Sample stations during : high run-off. ● low run-off. ○

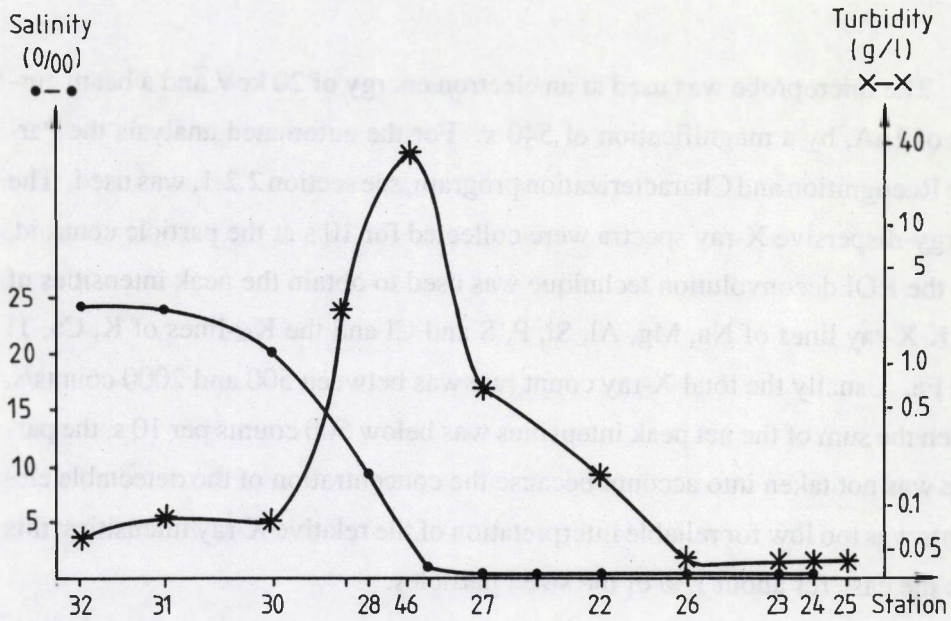


Figure 4.5 : Salinity and turbidity during high run-off at the sampling stations of the Ems estuary.

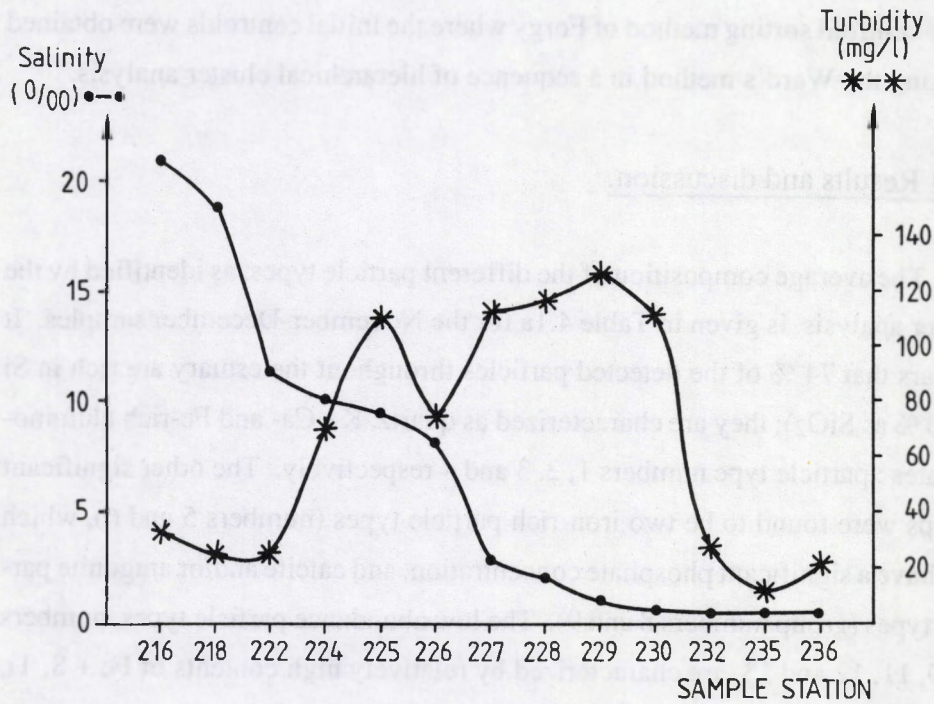


Figure 4.6 : Salinity and turbidity during low run-off at the sampling stations of the Ems estuary.

The microprobe was used at an electron energy of 20 keV and a beam current of 1nA, by a magnification of 540 x. For the automated analysis the Particle Recognition and Characterization program, see section 2.2.1, was used. The energy-dispersive X-ray spectra were collected for 10 s at the particle centroid, and the ROI deconvolution technique was used to obtain the peak intensities of the K X-ray lines of Na, Mg, Al, Si, P, S and Cl and the K_{α} -lines of K, Ca, Ti and Fe. Usually the total X-ray count rate was between 500 and 2000 counts/s. When the sum of the net peak intensities was below 500 counts per 10 s, the particle was not taken into account because the concentration of the detectable elements was too low for reliable interpretation of the relative X-ray intensities; this was the case for about 1 % of the sized particles.

For each of the samples, approximately 300 particles were analyzed. The particles were classified by the method outlined in section 3.2.4, i.e. by the use of the centroid sorting method of Forgy where the initial centroids were obtained by using the Ward's method in a sequence of hierarchical cluster analysis.

4.2.1 Results and discussion.

The average composition of the different particle types, as identified by the cluster analysis, is given in Table 4.1a for the November-December samples. It appears that 74 % of the detected particles throughout the estuary are rich in Si (> 40 % as SiO_2); they are characterized as quartz, K-, Ca- and Fe-rich aluminosilicates : particle type numbers 1, 2, 3 and 4 respectively. The other significant groups were found to be two iron-rich particle types (numbers 5 and 6), which also have a significant phosphate concentration, and calcite and/or aragonite particle types (group numbers 8 and 9). The low abundance particle types, numbers 7, 10, 11, 12 and 13, are characterized by relatively high contents of Fe + S, Ti, Ti + S, Al, and S + P, respectively.

The relative abundance of each particle type in every individual sample is given in Table 4.1b. Except for the low abundance particle types, significant abundance variations exist throughout the Ems estuary. At the most upriver stations, the iron-rich particle types and the Fe-aluminosilicate are predominant. They represent 67 % of all the measured particles at sample station 25, and their abundance decreases sharply toward the turbidity maximum and the salt intrusion region (Figure 4.5); this suggests a fluvial origin. These particles probably have their origin in the peatbog areas that are drained by the Ems river. These areas supply the Ems river with an excess of iron, and it is assumed that at least a part of it is concentrated in single particles. The marine suspended particulate matter is mainly characterized by the K-aluminosilicate and, to a lesser extent, the quartz and calcite and/or aragonite particle type. At sample station 32, the most marine station, 81 % of the measured particles belong to one of these groups. The chemical inorganic composition of the suspended particulate matter of the end-members of the Ems estuary are significantly different. If it is assumed that in the transition zone these end-members behave conservatively, or nearly conservatively, the abundance variations of these particle types can be used as a Conservative Index of Mixing (CIM).

Figure 4.7 shows the particle frequency distribution, and the salinity profile, with location throughout the Ems estuary for the two iron-rich, the K-aluminosilicate and the calcite/aragonite particle types. Note in this figure the complementary abundance distribution of the fluvial and marine characteristic particle types. If the distribution of the iron particle types is taken as an indicator of the conservative mixing of fluvial with marine suspended particulate matter, it is seen that mixing of riverborne with marine suspended matter occurs entirely in the freshwater tidal area, between sample station 27 and 25. Downstream sample station 27, which is near to the contact with saline water, the relative abundance of the iron-rich particle types are negligible. These results confirm earlier data for this area from Salomons (1975) who came to the same con-

clusion but used the isotopic composition of carbonates as a tracer for the origin of the sediment.

Table 4.1b and Figure 4.7 further elaborate the accumulation of the K-aluminosilicate particle type in the turbidity maximum region. This can be a consequence of the preferential accumulation of the smectite type mineral in the turbidity maximum, or may indicate a smaller third (local ?) source (supply from the nearby Dollard, erosion ?) of particulate matter.

The PyMS and the $\delta^{13}\text{C}$ results (Figure 4.8, Eisma et al., 1985) also show a marked change in composition upstream of the salinity contact, as was shown already by Eisma et al. (1984a). Comparison of the results on inorganic and organic material indicates that the mixing of both components goes parallel, even in such detail, that for all characteristics suspended matter collected at sample station 26 contains somewhat more river-derived material than suspended matter collected at stations 22 and 23. It follows that during the sampling period, particulate organic matter coming from the river behaved conservatively, while compositional changes are caused by tidal mixing. The good correlation of the inorganic and organic analysis also points out that, for both methods, representative sampling and analyses were performed.

During low run-off, approximately the same particle types, with a significant abundance throughout the estuary, were identified by the multivariate analysis as for high run-off conditions (Table 4.2a). The abundance distributions throughout the estuary are given in Table 4.2b and represented in Figure 4.9 for the important quartz, K-aluminosilicate, iron-rich and the calcite and/or aragonite particle types, which are particle type numbers 1, 2, 5 and 7, respectively.

Again mixing of riverborne material with marine suspended particulate matter appears to occur in the freshwater region, now owing to low river run-off

further upriver (Figure 4.7 and 4.9) in the estuary. The higher concentration of the K-aluminosilicate particle type at the turbidity maximum is still observed but the enrichment, from the marine environment to the turbidity maximum, is smoother than for high run-off. This enrichment seems to be a general feature in the Ems estuary. The shape of the distribution profiles of the calcite and/or aragonite group during high and low run-off differ significantly. During high run-off, the abundance increase from the turbidity maximum toward the marine environment is more gradual than for the K-aluminosilicate, while, at low run-off, the shape of the distribution profile approaches the one of the K-aluminosilicate particle type. The quartz particle type shows a remarkable behavior in the freshwater region, where its abundance increases from 25 ± 4 % in the more saline environment to a maximum value of 61 % at sample station 233. At the upriver sample station 235 the abundance decreases again. The quartz maximum at sample stations 233 and 235 is probably due to a high diatom content in that area. This implies that the quartz particle type does not only contain detrital quartz particles but also biogenic features rich on Si. The mean morphological information of the quartz particle type suggests, by its relatively low shape factor increase, that broken frustules would be present. However, manual search of the samples shows the presence of intact diatom skeletons (Figure 4.10). It is seen that the PRC program is not able to size these features accurately, which leads to reanalysis, overestimating the abundance of the particle type, and to smaller mean diameters and shape factors. Probably, the use of the 733b program, with the more advanced sizing routine, avoids these problems.

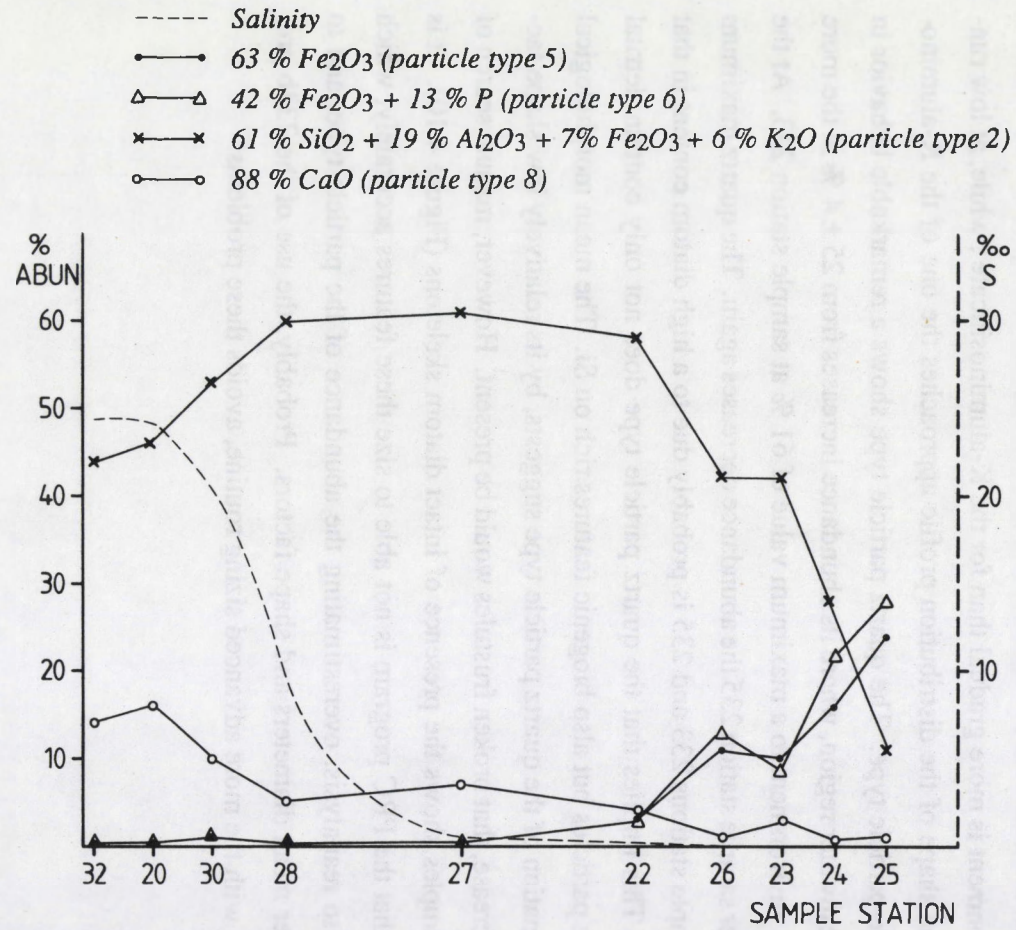


Figure 4.7 : Abundance during high run-off of the K-aluminosilicate, the two iron rich and the calcium carbonate particle type and the salinity at the sampling stations of the Ems estuary.

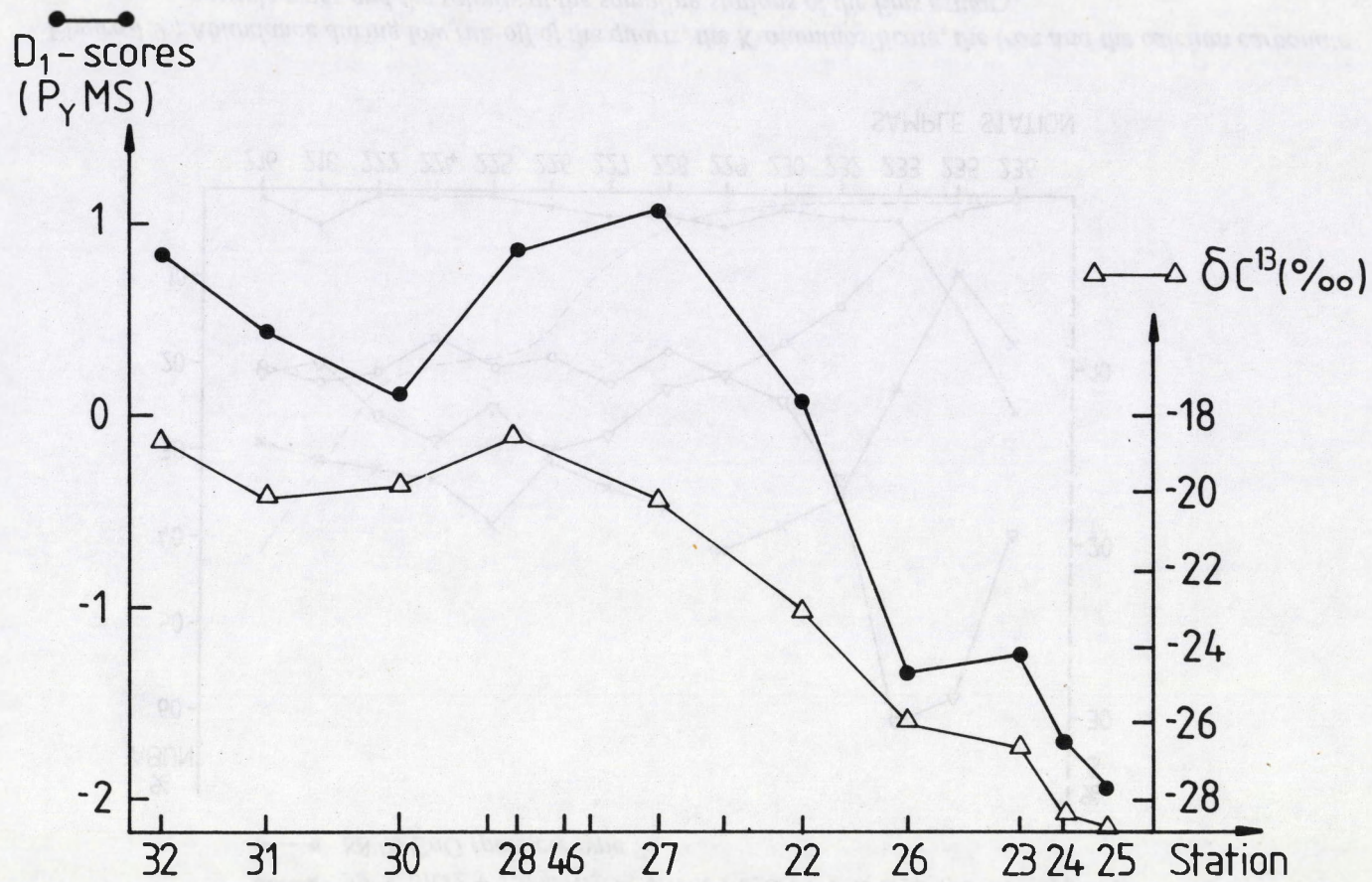


Figure 4.8 : Results of the PyMS and organic $\delta^{13}\text{C}$ analysis of the suspended matter of the Ems estuary during high run-off.

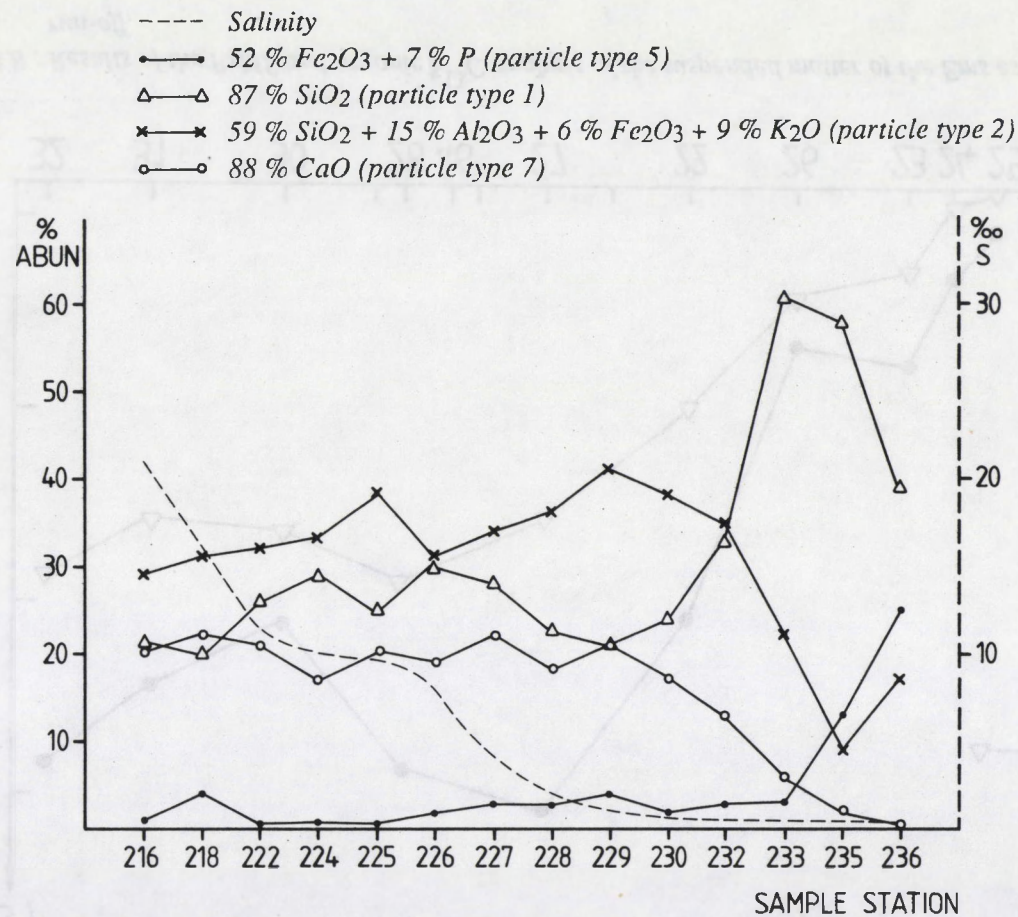


Figure 4.9 : Abundance during low run-off of the quartz, the K-aluminosilicate, the iron and the calcium carbonate particle types and the salinity at the sampling stations of the Ems estuary.

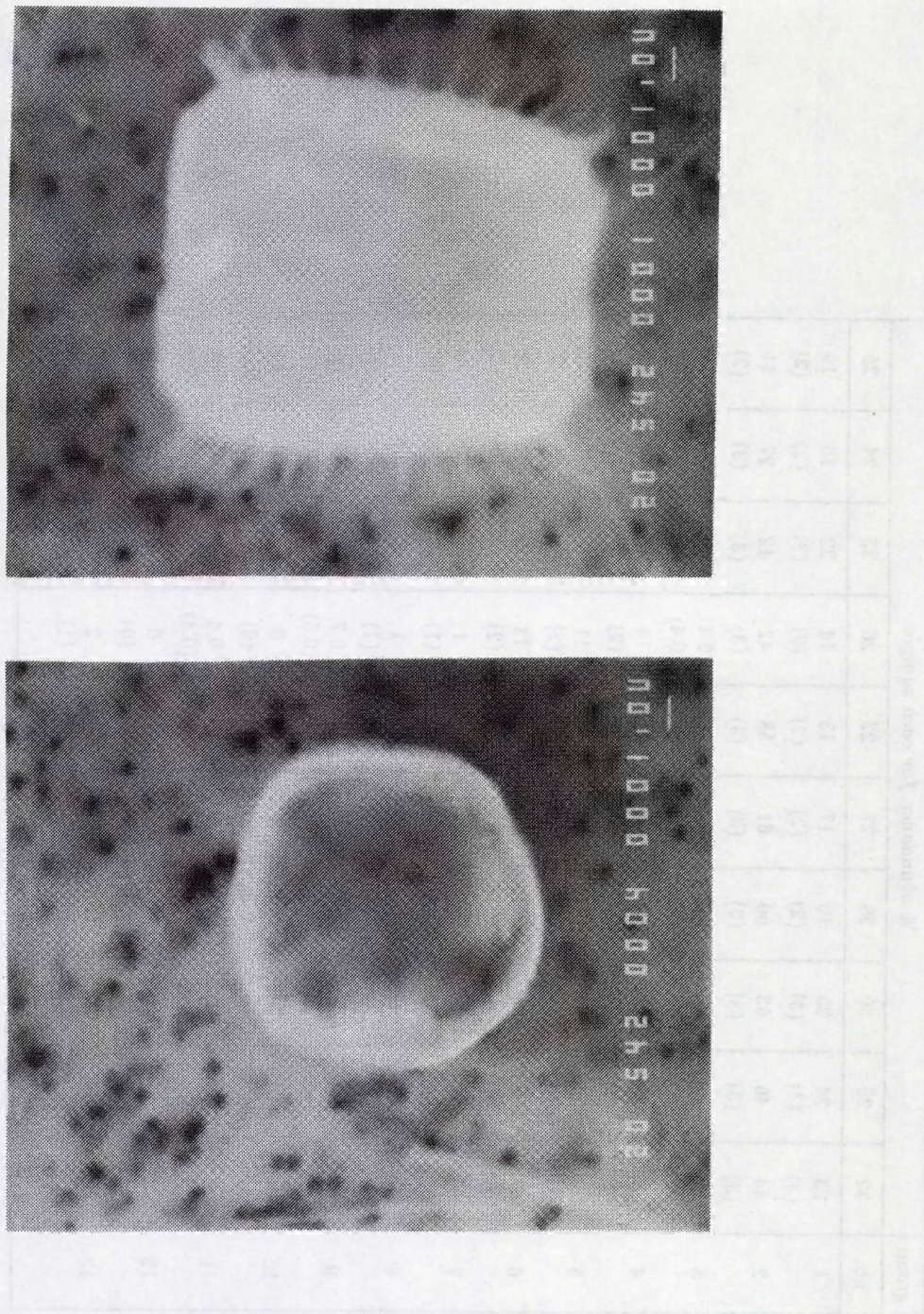


Figure 4.10 : Secondary electron image of some diatom frustules found at sample station 233. The solid bar represents 1 μ m.

group	% abundance for each sample									
	no.	32	20	30	28	27	22	26	23	24
1	23 (3)	24 (3)	25 (3)	19 (2)	17 (2)	15 (2)	14 (2)	22 (3)	16 (2)	19 (2)
2	44 (3)	46 (3)	53 (3)	60 (3)	61 (3)	58 (3)	42 (3)	42 (3)	27 (3)	11 (2)
3	6 (2)	4 (1)	2 (1)	2 (1)	4 (1)	1 (1)	0.4 (0.4)	0.4 (0.4)	0.8 (0.6)	0.4 (0.4)
4	5 (1)	4 (1)	5 (1)	5 (1)	8 (2)	10 (2)	14 (2)	12 (2)	15 (2)	15 (2)
5	0.4 (0.4)	0.3 (0.3)	0.8 (0.6)	0.3 (0.3)	0.4 (0.4)	3 (1)	11 (2)	10 (2)	16 (2)	24 (3)
6	0 (0)	0 (0)	0.8 (0.6)	0.3 (0.3)	0.4 (0.4)	3 (1)	13 (2)	9 (2)	22 (3)	28 (3)
7	0.8 (0.6)	1 (1)	0 (0)	0.3 (0.3)	0.4 (0.4)	0 (0)	1 (1)	0 (0)	0.8 (0.6)	0.4 (0.4)
8	14 (2)	16 (2)	10 (2)	5 (1)	7 (2)	4 (1)	1 (1)	3 (1)	0.4 (0.4)	1 (1)
9	6 (2)	4 (1)	3 (1)	2 (1)	2 (1)	2 (1)	0.7 (0.5)	0.4 (0.4)	1 (1)	0.4 (0.4)
10	0.4 (0.4)	1 (1)	0 (0)	0.3 (0.3)	0 (0)	2 (1)	0 (0)	1 (1)	0 (0)	0.8 (0.5)
11	0 (0)	0.3 (0.3)	0.4 (0.4)	0 (0)	0 (0)	0 (0)	0.4 (0.4)	0 (0)	0 (0)	0 (0)
12	0 (0)	0 (0)	0 (0)	2 (1)	0 (0)	0.3 (0.3)	0 (0)	0 (0)	0 (0)	0 (0)
13	0.4 (0.4)	0.3 (0.3)	1 (1)	4 (1)	0.7 (0.5)	1 (1)	2 (1)	2 (1)	1 (1)	1 (1)

Table 4.1b : Abundance of the particle types at each sample station for the Ems estuary during high run-off (1982).

group no.	% Abun.	SiO ₂ %	Al ₂ O ₃ %	CaO %	Fe ₂ O ₃ %	MgO %	Na ₂ O %	K ₂ O %	TiO ₂ %	Cl %	S %	P %	MAD μm	MID μm	AVD μm	SF
1	20	90 (8)	5 (4)	1 (2)	1.6 (2.4)	0.1 (0.8)	0.2 (0.4)	1.0 (1.5)	0.4 (0.9)	0.3 (0.7)	0.5 (0.8)	0.2 (0.5)	4 (4)	2.0 (1.7)	2.8 (2.2)	1.7 (0.8)
2	45	61 (6)	19 (6)	2.4 (2.5)	7 (4)	0.8 (1.2)	0.0 (0.3)	6 (5)	1 (2)	0.7 (1.2)	0.9 (1.4)	1 (1)	5 (4)	2.1 (1.6)	3.0 (2.2)	1.6 (0.7)
3	2	49 (7)	13 (4)	24 (9)	6.8 (4.5)	1 (2)	0.0 (0.2)	3.4 (2.6)	0.3 (0.7)	0.9 (1.1)	1.3 (2.4)	1 (1)	6 (5)	2.8 (2.6)	4.2 (3.4)	1.8 (0.7)
4	9	46 (7)	16 (5)	4 (4)	20 (6)	2.1 (2.3)	0.1 (0.3)	3 (3)	0.6 (1.8)	0.9 (1.5)	4 (3)	3 (3)	4.6 (3.4)	2.1 (1.6)	3.1 (2.2)	1.6 (0.7)
5	6	11 (5)	5.6 (2.3)	7 (4)	63 (8)	0.9 (0.7)	0.3 (0.3)	0.6 (1.2)	0.5 (1.1)	1 (2)	1.3 (1.7)	9 (5)	3.2 (2.3)	1 (1)	2.1 (1.2)	1.7 (0.8)
6	7	21 (8)	9 (3)	9 (4)	42 (6)	1 (1)	0.2 (0.4)	1.2 (1.6)	1 (1)	1.2 (1.6)	2 (2)	13 (6)	4.5 (3.5)	1.9 (1.6)	3 (2)	1.8 (0.8)
7	0.5	13 (9)	4.0 (2.5)	1 (1)	26 (9)	0.5 (0.8)	0.2 (0.5)	0.6 (0.7)	0.4 (0.8)	0.3 (0.4)	55 (9)	0.0 (0.3)	3.6 (2.2)	2 (1)	2.5 (1.3)	1.8 (1.2)
8	7	7 (4)	2.4 (1.3)	88 (6)	0.7 (0.9)	0.5 (1.4)	0.00 (0.17)	0.2 (0.6)	0.2 (0.5)	0.2 (0.4)	0.3 (0.6)	0.2 (0.4)	4.4 (3.6)	2.1 (1.5)	3 (2)	1.5 (0.7)
9	2	22 (8)	7.2 (3.4)	57 (10)	4 (5)	3 (4)	0.2 (0.3)	1 (2)	0.3 (0.7)	0.5 (1.3)	0.9 (1.4)	3 (7)	5 (4)	1.9 (1.3)	3 (2)	1.6 (0.8)
10	0.5	16 (9)	6 (4)	1.7 (2.7)	4 (5)	0.3 (0.4)	0.10 (0.24)	0.8 (1.2)	69 (20)	0.2 (0.6)	0.5 (0.9)	0.4 (0.7)	3 (3)	1.8 (1.3)	2.4 (1.5)	1.3 (0.5)
11	0.1	11 (9)	3.0 (2.5)	0.4 (0.6)	0.8 (1.5)	0 (0)	0.7 (0.5)	1.3 (1.5)	45 (8)	0 (0)	37 (7)	0.3 (0.5)	4 (2)	1.7 (0.6)	2.3 (1.1)	1.5 (0.3)
12	0.2	13 (10)	47 (20)	7 (11)	2 (6)	3 (7)	7 (10)	2 (5)	8 (10)	7 (10)	0 (1)	3 (4)	2.1 (0.4)	0.9 (0.3)	1.36 (0.26)	2.0 (0.7)
13	1	27 (9)	16 (7)	10 (9)	12 (10)	1.3 (1.5)	0.3 (0.5)	4.7 (3.5)	5 (9)	5 (7)	9 (11)	8 (9)	3 (2)	1.4 (0.7)	2 (1)	1.7 (0.8)

Table 4.1a : Average composition of the particle types (normalized to 100 weight %) for the Ems estuary during high run-off (1982).

MAD = maximum diameter; MID = minimum diameter; AVD = average diameter; SF = shape factor

group	% abundance for each sample													
no.	216	219	222	224	225	226	227	228	229	230	232	233	235	236
1	21 (2)	20 (2)	26 (2)	29 (3)	25 (3)	30 (3)	28 (3)	23 (3)	21 (2)	24 (3)	33 (3)	61 (3)	58 (3)	39 (3)
2	29 (3)	31 (3)	32 (3)	33 (3)	37 (3)	31 (3)	34 (3)	36 (3)	41 (3)	37 (3)	35 (3)	22 (3)	9 (2)	17 (2)
3	4 (1)	8 (2)	8 (1)	4 (1)	4 (1)	9 (2)	5 (1)	8 (2)	4 (1)	9 (2)	6 (1)	2 (1)	13 (2)	13 (2)
4	7 (2)	4 (1)	2 (1)	4 (1)	2 (1)	3 (1)	2 (1)	4 (1)	2 (1)	2 (1)	2 (1)	1 (1)	0.4 (0.4)	0 (0)
5	1 (1)	4 (1)	1 (1)	0.7 (0.5)	0.4 (0.4)	2 (1)	3 (1)	3 (1)	4 (1)	2 (1)	3 (1)	3 (1)	13 (2)	25 (3)
6	1 (1)	1 (1)	0.7 (0.4)	0.7 (0.5)	2 (1)	0.8 (0.5)	0.8 (0.6)	1 (1)	1 (1)	0.7 (0.5)	2 (1)	0 (0)	0.8 (0.6)	0.5 (0.4)
7	20 (2)	22 (2)	21 (2)	17 (2)	20 (2)	19 (2)	22 (3)	18 (2)	21 (2)	17 (2)	13 (2)	6 (1)	2 (1)	0.5 (0.4)
8	9 (2)	6 (1)	6 (1)	4 (1)	4 (1)	9 (2)	4 (1)	4 (1)	4 (1)	6 (1)	4 (1)	3 (1)	2 (1)	0.5 (0.4)
9	3 (1)	2 (1)	0 (0)	6 (1)	0.8 (0.5)	0 (0)	0.4 (0.4)	0.7 (0.5)	0.4 (0.4)	0 (0)	0.3 (0.3)	0.4 (0.4)	0.8 (0.6)	4 (1)
10	4 (1)	0.4 (0.4)	1 (1)	0.3 (0.3)	0.8 (0.5)	1 (1)	0.4 (0.4)	1 (1)	0 (0)	1 (1)	0.3 (0.3)	0.7 (0.5)	0 (0)	0.5 (0.4)
11	0.9 (0.6)	0 (0)	0.7 (0.4)	0.7 (0.5)	1 (1)	0.3 (0.3)	0.4 (0.4)	0.7 (0.5)	0.7 (0.5)	0.4 (0.4)	1 (1)	0 (0)	0 (0)	0 (0)

Table 4.2b : Abundance of the particle types at each sample station for the Ems estuary during low run-off (1984).

group no.	% Abun.	SiO ₂ %	Al ₂ O ₃ %	CaO %	Fe ₂ O ₃ %	MgO %	Na ₂ O %	K ₂ O %	TiO ₂ %	Cl %	S %	P %	MAD μm	MID μm	AVD μm	SF
1	29	87 (9)	2 (3)	1.8 (2.5)	1.0 (1.7)	0.3 (0.7)	0.7 (0.9)	1 (2)	0.8 (1.4)	3 (3)	1.2 (1.7)	0.8 (1.3)	4 (3)	1.3 (1.4)	2 (2)	2.1 (2.1)
2	28	59 (7)	15 (6)	3 (3)	6 (5)	1.4 (1.4)	0.4 (0.6)	9 (6)	1.0 (2.3)	3 (4)	1 (2)	0.7 (1.2)	3.0 (2.6)	1.4 (1.3)	2.0 (1.7)	1.7 (0.8)
3	6	43 (8)	12 (7)	3 (4)	23 (8)	4 (3)	0.7 (0.7)	2.9 (3.4)	1 (3)	4 (5)	2.4 (3.6)	3.0 (3.8)	3.0 (2.7)	1.4 (1.4)	2 (2)	1.7 (0.7)
4	2	40 (8)	11 (7)	31 (10)	5 (4)	1 (1)	0.1 (0.4)	3 (3)	2 (6)	3 (5)	2 (4)	1.5 (3.4)	2.8 (2.5)	1.3 (1.4)	1.9 (1.8)	1.7 (0.7)
5	4	14 (7)	3.5 (2.6)	6 (6)	52 (14)	2.4 (1.5)	1.5 (0.8)	1 (2)	1.6 (3.5)	8 (7)	2.0 (3.6)	7 (5)	2.3 (1.8)	1.1 (0.7)	2 (1)	1.6 (0.5)
6	1	8 (6)	1.8 (1.6)	1.6 (2.4)	32 (4)	0.3 (0.4)	0.2 (0.3)	1.0 (1.8)	0.2 (0.6)	2 (2)	54 (8)	0.2 (0.5)	1.9 (1.4)	1.1 (0.8)	1.4 (0.9)	1.3 (0.3)
7	15	5 (3)	2 (1)	88 (5)	0.9 (1.2)	0.9 (1.5)	0.2 (0.3)	1 (1)	0.5 (0.9)	0.8 (1.5)	0.7 (1.2)	0.4 (0.9)	3 (2)	1 (1)	1.8 (1.3)	1.5 (0.5)
8	4	16 (7)	3.7 (2.3)	65 (8)	3 (4)	3 (4)	0.4 (0.5)	1.2 (1.4)	0.8 (1.1)	3 (5)	1 (2)	2 (5)	2.3 (2.3)	1.1 (0.9)	1.5 (1.3)	1.5 (0.5)
9	1	19 (10)	3 (4)	25 (9)	7 (8)	2.6 (2.4)	1.5 (3.3)	3.3 (2.5)	1.0 (1.5)	5 (5)	26 (10)	5 (16)	3 (2)	1.3 (0.8)	1.9 (1.3)	1.5 (0.5)
10	0.7	8 (4)	2.0 (1.5)	0.9 (1.3)	2.1 (2.4)	0.6 (0.7)	0.20 (0.25)	1 (1)	83 (9)	0.8 (1.2)	0.8 (1.2)	0.4 (0.7)	1.9 (1.2)	1.1 (0.7)	1.3 (0.8)	1.38 (0.34)
11	0.5	19 (15)	5 (5)	3 (6)	4 (4)	1 (1)	0.8 (0.6)	1.6 (2.3)	40 (10)	1 (2)	24 (20)	0.3 (0.6)	1.7 (1.2)	0.9 (0.6)	1.3 (0.9)	1.4 (0.6)

Table 4.2a : Average composition of the particle types (normalized to 100 weight %) for the Ems estuary during low run-off (1984).

MAD = maximum diameter; MID = minimum diameter; AVD = average diameter; SF = shape factor

4.3 THE GIRONDE ESTUARY

The study of the Gironde estuary was conducted in cooperation with Dr. D. Eisma, NIOZ, Texel, Netherlands, as part of the GRECO-ICO program of the C.N.R.S., France. The main objective of this study is, as in the case of the Ems estuary, the characterization of the particulate organic and inorganic matter and to study its behavior throughout the estuary. For this purpose the same analytical techniques were used.

The Gironde, the largest estuary in France, is located on the south west coast of France (Figure 4.11). The estuary is formed by junction of the Garrone and Dordogne rivers, which drain respectively the Western Pyrenees and the Massif Central. Sediment transport between the North and South channel of the Gironde and toward the sea, in response to varying river discharge, were studied in detail using hydrological and tracer techniques by Allen et al.(1977).

The North and South channel of the Gironde estuary and the Garrone and Dordogne rivers were sampled, 19 samples, during May 1983, in a period of rather high river discharge conditions. The results of the salinity and turbidity measurements are shown in Figure 4.12. Because of the mixing of the two river end-members in the estuary, and the geographical barrier between the North and South channel a complex system is present, in which the composition of the suspended particulate matter in the estuary is determined by the mixing ratio between the Garrone, Dordogne and marine suspended matter. In the first instance it is required to study the river end-members and their mixing in the estuary.

The sampling and the experimental conditions for the EPXMA were identical as for the Ems study (see section 4.2). The results should therefore be comparable.

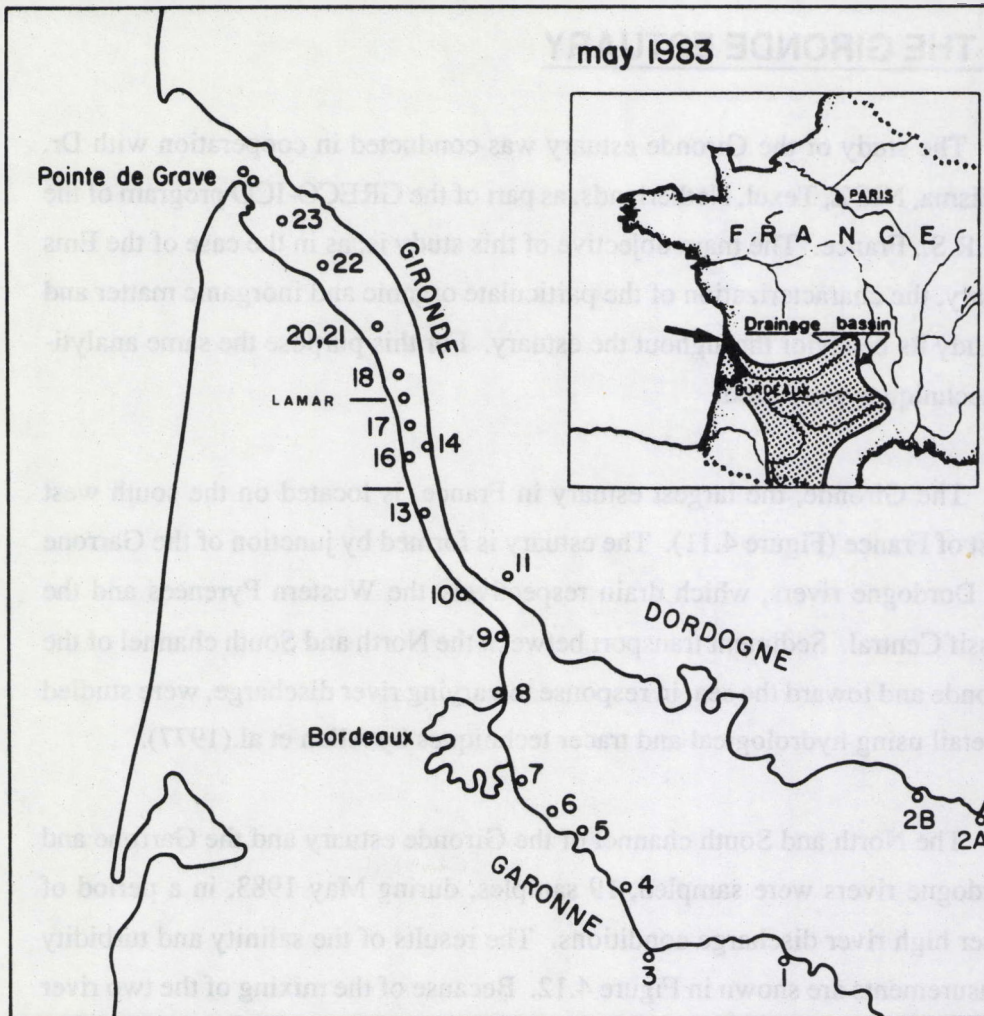


Figure 4.11 : Location of the Gironde estuary and of the sample stations.

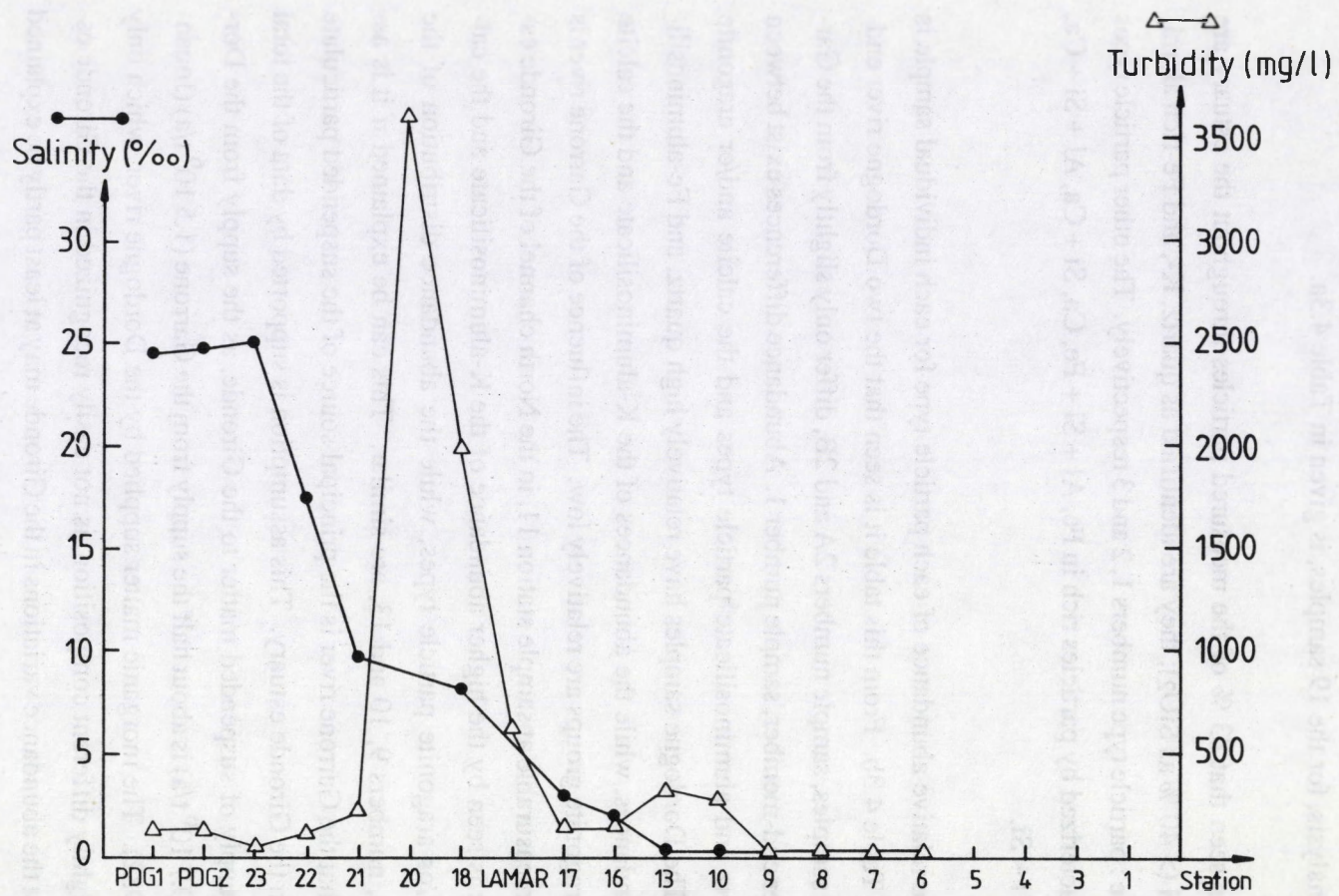


Figure 4.12 : Salinity and turbidity profile throughout the Gironde estuary and Garonne river.

4.3.1 Results and discussion.

The average composition of the different particle types, as identified by the cluster analysis, for the 19 samples, is given in Table 4.3a.

It is seen that 83 % of the measured particles throughout the estuary are rich in Si (> 40 % as SiO₂); they are identified as quartz, K-, and Fe-rich aluminosilicate : particle type numbers 1, 2 and 3 respectively. The other particle types are characterized by particles rich in Fe, Al + Si + Fe, Ca, Si + Ca, Al + Si + Ca, Ti and Ti + Si.

The relative abundance of each particle type for each individual sample is given in Table 4.3b. From this table it is seen that the two Dordogne river end-member samples, sample numbers 2A and 2B, differ only slightly from the Garrone river end-member, sample number 1. Abundance differences exist between the quartz and aluminosilicate particle types and the calcite and/or aragonite group. The Dordogne samples have relatively high quartz, and Fe-aluminosilicate abundances, while the abundances of the K-aluminosilicate and the calcite and/or aragonite groups are relatively low. The influence of the Garrone river is already measurable at sample station 11, in the North channel of the Gironde estuary, as is seen by the higher abundance of the K-aluminosilicate and the calcite and/or aragonite particle types, while the abundance distribution of the samples, numbers 9, 10 and 13, are similar. This can be explained if it is assumed that the Garrone river is the principal source of the suspended particulate matter in the Gironde estuary. This assumption is supported by data of the total yearly supply of suspended matter to the Gironde, as the supply from the Dordogne ($0.7 \cdot 10^6$ t/a) is about half the supply from the Garrone ($1.5 \cdot 10^6$ t/a) (Jouanneau, 1982). The inorganic matter supplied by the Dordogne river, which only has a slightly different composition, is not easily recognized in the Gironde estuary but the abundance variations in the Gironde may at least partly be explained

by an admixture of Dordogne material in different proportions. On the other hand it is seen that the composition of the sample representing North channel suspended matter; sample number 14, has a distinct composition. The admixture of North and South channel suspended particulate matter can also lead to fluctuations in the abundance of some of the particle types.

The abundance distribution of the Si-rich particle types and the calcite and/or aragonite particle types are represented in Figure 4.13, for the Garonne and Gironde (South channel) samples. This figure shows that despite some exceptions no significant or systematic abundance variations between the samples are encountered throughout the whole estuary. No evidence is found for a net flux of marine suspended particulate matter into the estuary; even the abundance of the calcite and/or aragonite particle type is constant throughout the estuary.

If however the composition of the particulate organic matter is regarded (Eisma et al., 1985), no uniform composition is found (Figure 4.14). The EPXMA of the particulate inorganic suspended matter indicates that this is not, as in the case of the Ems study, caused by mixing of estuarine with marine suspended matter, unless the suspended matter that comes in from the sea has the same composition as the Garonne suspended matter. Therefore probably an admixture of older estuarine suspended material or resuspended sediments with a lower organic content and different composition occurs. Or there is a process of transformation of organic matter in the estuary, resulting in a different organic composition and a higher $\delta^{13}\text{C}$ value.

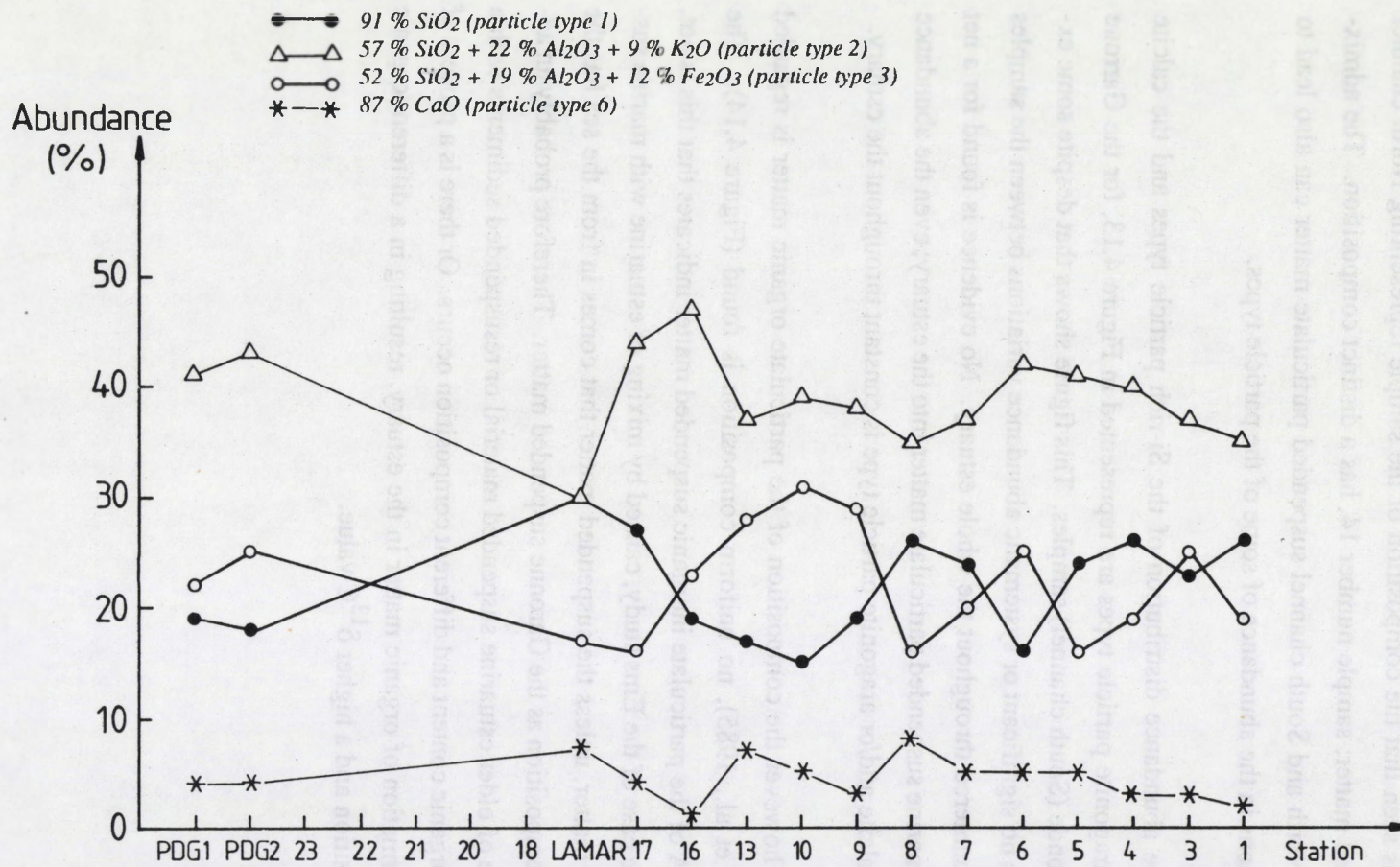


Figure 4.13 : Abundance of the quartz, the K- and Fe-aluminosilicate particle types and the calcite and/or aragonite particle type throughout the garrone river and Gironde estuary.

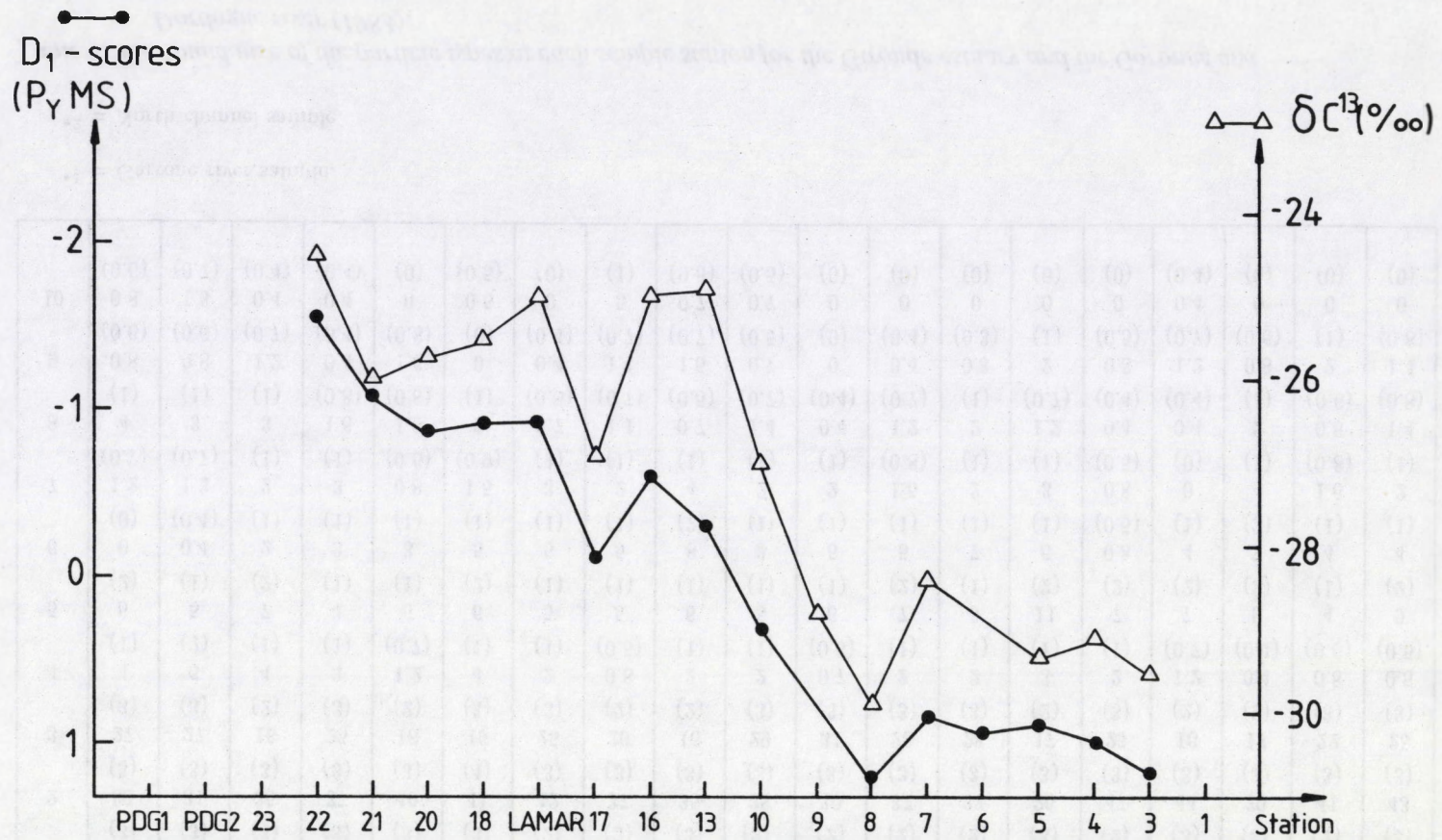


Figure 4.14 : Results of the PyMS and organic $\delta^{13}C$ analysis of the suspended matter of the Garrone river and the Gironde estuary.

group	% abundance for each sample																		
no.	2A* ¹	2B* ¹	1	3	4	5	6	7	8	9	10	11* ²	13	14* ²	16	17	Lamar	PDG1	PDG2
1	27 (3)	23 (3)	27 (3)	23 (3)	27 (3)	24 (3)	16 (2)	24 (3)	26 (3)	19 (2)	15 (2)	18 (2)	17 (2)	30 (3)	19 (2)	27 (3)	30 (3)	19 (2)	18 (3)
2	30 (3)	31 (3)	35 (3)	37 (3)	40 (3)	41 (4)	42 (3)	37 (3)	35 (3)	38 (3)	39 (3)	37 (3)	37 (3)	26 (3)	47 (3)	44 (3)	30 (3)	41 (3)	43 (3)
3	27 (3)	27 (3)	18 (2)	25 (3)	18 (2)	16 (3)	25 (3)	20 (2)	16 (2)	29 (3)	31 (3)	28 (3)	28 (3)	17 (2)	23 (3)	16 (2)	17 (2)	22 (3)	25 (3)
4	4 (1)	6 (2)	4 (1)	3 (1)	1.2 (0.7)	4 (1)	2 (1)	0.8 (0.5)	2 (1)	2 (1)	0.7 (0.5)	2 (1)	2 (1)	3 (1)	2 (1)	1.2 (0.7)	0.4 (0.4)	0.8 (0.6)	0.5 (0.5)
5	6 (2)	5 (1)	7 (2)	4 (1)	6 (1)	6 (2)	5 (1)	5 (1)	6 (1)	5 (1)	6 (1)	7 (2)	5 (1)	11 (2)	7 (2)	7 (2)	9 (2)	4 (1)	9 (2)
6	0 (0)	0.4 (0.4)	2 (1)	3 (1)	3 (1)	5 (1)	5 (1)	5 (1)	8 (2)	3 (1)	5 (1)	5 (1)	7 (1)	6 (1)	0.8 (0.5)	4 (1)	7 (2)	4 (1)	4 (1)
7	1.2 (0.7)	1.3 (0.7)	2 (1)	3 (1)	0.8 (0.6)	1.5 (0.9)	3 (1)	2 (1)	4 (1)	2 (1)	2 (1)	1.5 (0.8)	2 (1)	3 (1)	0.8 (0.5)	0 (0)	4 (1)	1.6 (0.8)	2 (1)
8	4 (1)	3 (1)	3 (1)	1.6 (0.8)	1.6 (0.8)	2 (1)	0.7 (0.5)	1.1 (0.7)	0.7 (0.5)	1.4 (0.7)	0.4 (0.4)	1.2 (0.7)	2 (1)	1.2 (0.7)	0.4 (0.4)	0.4 (0.4)	2 (1)	0.8 (0.6)	1.4 (0.8)
9	0.8 (0.6)	0.8 (0.6)	1.2 (0.7)	0.4 (0.4)	1.6 (0.8)	0 (0)	0.4 (0.4)	1.1 (0.7)	1.5 (0.7)	0.7 (0.5)	0 (0)	0.4 (0.4)	0.3 (0.3)	2 (1)	0.8 (0.5)	1.2 (0.7)	0.8 (0.6)	2 (1)	1.4 (0.8)
10	0.8 (0.6)	1.3 (0.7)	0.4 (0.4)	0.4 (0.4)	0 (0)	0.5 (0.5)	0 (0)	5 (1)	0.7 (0.5)	0.7 (0.5)	0 (0)	0 (0)	0 (0)	0 (0)	0 (0)	0.4 (0.4)	0 (0)	0 (0)	0 (0)

*¹ = Garrone river sample.

*² = North channel sample.

Table 4.3b : Abundance of the particle types at each sample station for the Gironde estuary and the Garonne and Dordogne river (1983).

group no.	% Abun.	SiO ₂ %	Al ₂ O ₃ %	CaO %	Fe ₂ O ₃ %	MgO %	Na ₂ O %	K ₂ O %	TiO ₂ %	Cl %	S %	P %	MAD μm	MID μm	AVD μm	SF
1	23	91 (7)	3 (4)	0.6 (1.5)	0.8 (1.4)	0.1 (0.4)	0.1 (0.5)	1 (1)	0.3 (0.9)	0.2 (0.5)	0.3 (0.8)	0.1 (0.8)	4 (3)	2 (2)	3 (2)	1.5 (0.8)
2	37	57 (6)	22 (6)	2 (2)	4 (3)	0.4 (0.7)	0.1 (0.3)	9 (6)	1 (1)	0.3 (0.7)	1 (1)	0.2 (0.9)	4 (4)	2 (2)	3 (2)	1.5 (0.6)
3	23	52 (5)	19 (4)	3 (3)	12 (4)	1 (2)	0.1 (0.4)	5 (3)	2 (3)	1 (1)	1 (1)	1 (3)	4 (3)	2 (2)	3 (2)	1.6 (0.7)
4	2	11 (7)	4 (4)	3 (4)	72 (13)	0.3 (0.7)	0.1 (0.3)	1 (1)	2 (5)	1 (1)	1 (1)	1 (2)	3 (3)	2 (1)	2 (2)	1.3 (0.5)
5	6	39 (6)	17 (5)	2 (2)	29 (8)	3 (3)	0.1 (0.3)	3 (3)	1 (4)	1 (1)	1 (2)	1 (2)	4 (4)	2 (2)	3 (3)	1.4 (0.4)
6	4	5 (3)	1 (1)	87 (6)	1 (1)	2 (4)	0.1 (0.2)	0.3 (0.7)	0.2 (0.5)	0.1 (0.4)	0.4 (0.7)	0.2 (0.5)	4 (3)	1 (1)	3 (2)	1.3 (0.4)
7	2	14 (7)	4 (3)	63 (8)	4 (5)	4 (5)	0.1 (0.3)	2 (2)	1 (2)	0.4 (0.8)	1 (1)	3 (7)	4 (3)	2 (1)	3 (2)	1.5 (0.6)
8	2	35 (11)	10 (6)	31 (9)	9 (7)	2 (3)	0.1 (0.5)	2 (2)	2 (4)	1 (4)	2 (3)	2 (6)	5 (4)	2 (1)	3 (2)	1.7 (0.9)
9	0.9	12 (8)	4 (3)	1 (1)	6 (10)	0.2 (0.6)	0.1 (0.1)	1 (1)	72 (16)	0.2 (0.5)	0.4 (1.0)	0.3 (0.7)	3 (2)	1.4 (0.8)	2 (1)	1.5 (0.5)
10	0.5	8 (7)	2 (4)	3 (7)	4 (7)	2 (4)	1 (2)	3 (5)	25 (20)	3 (6)	35 (16)	11 (22)	3 (2)	1.4 (0.8)	2 (1)	1.5 (0.5)

Table 4.3a : Average composition of the particle types (normalized to 100 weight %) for the Gironde estuary and the Garonne and Dordogne river (1983).

MAD = maximum diameter; MID = minimum diameter; AVD = average diameter; SF = shape factor

4.4 THE SCHELDT ESTUARY

The sampling of the Scheldt longitudinal profile was performed in November 1985. The Scheldt a highly polluted estuary, owing to industrial and municipal waste, has anoxic conditions at the lower salinity region. The sample locations at the Scheldt estuary are given in Figure 4.15. A total of 17 samples were taken from 16 sample stations. Sample station 1 was sampled twice with a 50 minutes time difference : samples 1 and 1b respectively. The longitudinal profile was taken from Vlissingen till a few miles upstream of Rupelmonde. The salinity and turbidity profile is shown in Figure 4.16. The sampling procedure and the experimental parameters for the EPXMA are identical to those of the study of the Ems estuary.

4.4.1 Results and discussion.

The results of the automated EPXMA are given in Table 4.4a, which lists the average composition of the different particle types identified by the cluster analysis, and in Table 4.4b which gives the relative abundance of each of the particle types in every sample.

As seen from Table 4.4a, thirteen particle types were retained. The silicon rich particle types ($\text{SiO}_2 > 40\%$), particle types 1 to 6, account for 81 % of the measured particles. They consist of quartz, and a number of aluminosilicate groups. The last four aluminosilicate groups are rich in K, Fe + K, Fe and Ca, respectively. Besides these silicon rich particle types Fe-, Fe + S-, Ca + Fe + P-, Ca- and Ti-rich particle types were identified.

The abundances of the K- and Fe + K-aluminosilicate particle types and the calcite and/or aragonite group are represented for each sample station in Figure 4.17, together with the salinity profile throughout the estuary. None of

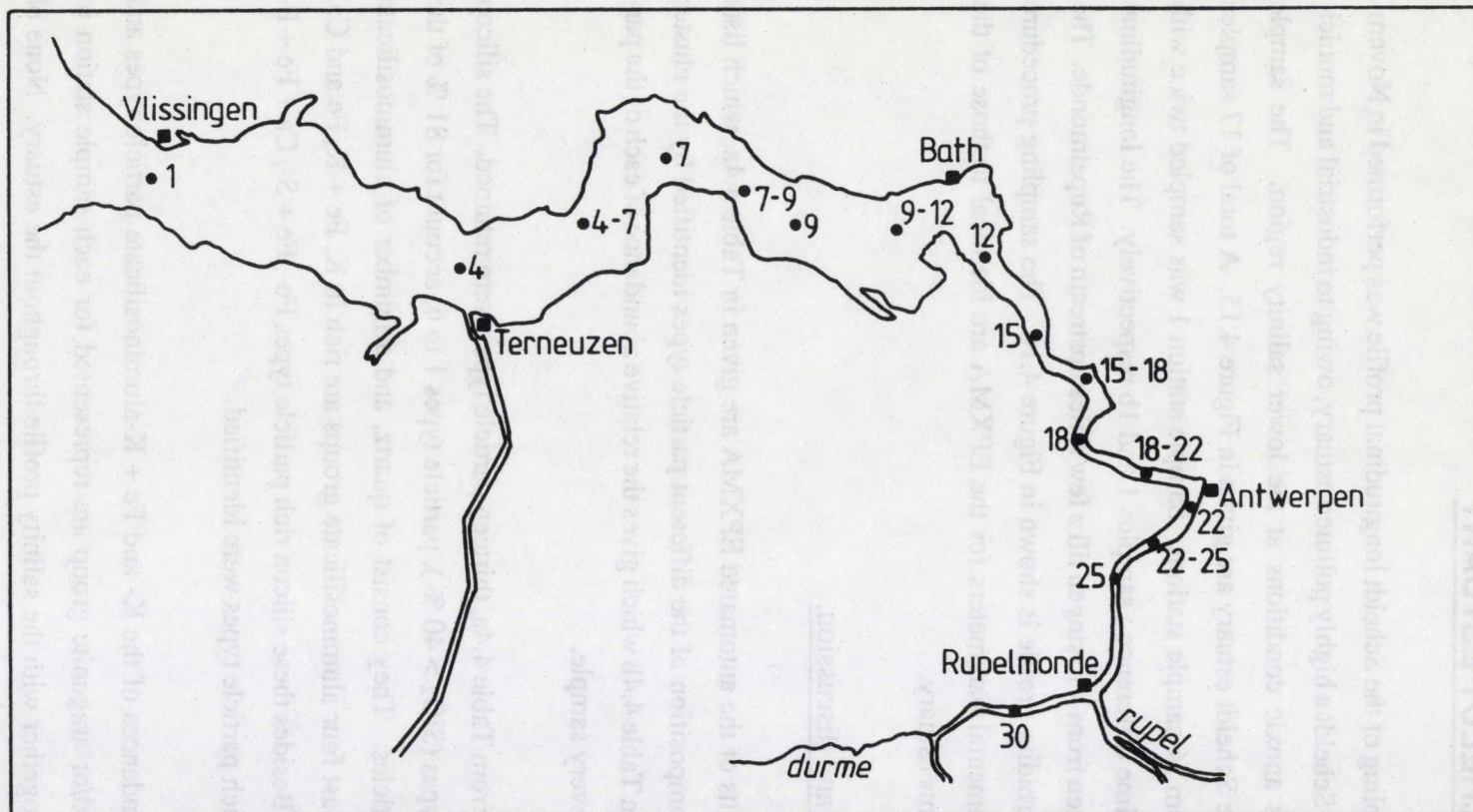


Figure 4.15 : Sampling locations throughout the Scheldt estuary (Belgium, The Netherlands) November 1985.

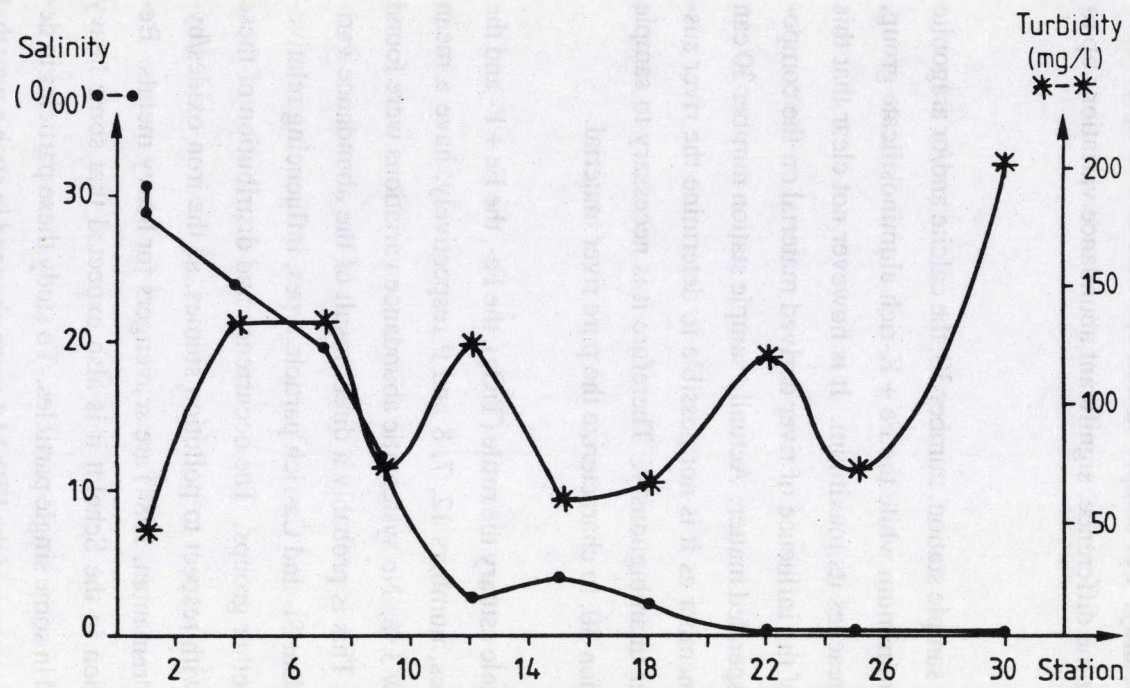


Figure 4.16 : Salinity and turbidity profile throughout the Scheldt estuary.

the identified groups showed systematic abundance variations throughout the estuary, except for the calcite and/or aragonite particle type of which the abundance increases gradually seaward, a phenomena which was also found in the Ems estuary. But while the abundance of the CaCO_3 group at the Ems downstream stations increased steadily to 15 % in November-December 1982, and was nearly constant at 20 % in May 1984, the abundance of the CaCO_3 particle type in the Scheldt fluctuates significantly. For sample station 1, where two samples were taken with a 50 minutes time difference, significant abundance variations up to 10 % were measured.

At the most upriver sample station, number 30, the calcite and/or aragonite particle type reaches its minimum while the Fe + K-rich aluminosilicate group, particle type number 4, reaches its maximum. It is however not clear that this would be an indication of the influence of river derived material on the composition of the estuarine suspended matter. Actually sample station number 30 can not be taken as an end-member as it is not possible to determine the river suspended particulate matter unambiguously. Therefore it is necessary to sample further upriver from station 30, to characterize the pure river material.

Throughout the whole estuary the rutile (TiO_2), the Fe-, the Fe + P- and the Fe + S-rich particle types, numbers 12, 7, 8 and 9 respectively, have a mean relative abundance below 3 %. No systematic abundance variations were found for these particle types. This is probably a direct result of the abundance variations of the more abundant Si- and Ca-rich particle types, influencing relatively the abundance of the other groups. The occurrence and distribution of these particles are important with respect to pollution studies, as the iron oxides/hydroxides (Singh and Subramanian, 1984) are scavengers for heavy metals. Because of the anoxic region in the Scheldt it is also expected that some heavy metals could be enriched in some single particles. To study these particles in detail the experimental parameters of the EPXMA were changed in such a way that

only particles with a relatively high atomic number were measured. This was achieved by measuring with a high threshold-to-background ratio for the detection of the particles during the EPXMA. A centrifuge sample collected at a salinity of 2.5 ppt nearby Antwerp, was resuspended in Milli-Q-Water and filtered on a 25 mm diameter 0.4 μm pore-size Nuclepore filter. For analysis the microprobe was used at an accelerating voltage of 20kV and a beam current of 1nA. The X-ray acquisition time was 20 s, and the threshold/background ratio was 2 during the analysis, while under normal measurement conditions this is approximately around 1.1.

In this way a variety of particles were measured. A number of Ca-rich particles enriched in Fe, P, Ti + Fe were detected. Probably a number of these particles are anthropogenic or authigenically formed. A possible source could be the fertilizer industry.

The iron-rich particles were divided into particles rich in Fe, Fe + S, Fe + P and Fe + Ca. Enrichment of Mn was found with the Fe + P and Fe + Ca particles, while the abundance of the individual Mn-rich particles is low. Only one Mn-rich particle was measured. It is therefore thought that probably the major part of the excess Mn is associated with, coprecipitated and/or adsorbed to, the iron-rich particles. It was also seen that particles rich in Zn were measured of which some Zn-rich aluminosilicates, one of these contained a few percent Pb, and Zn + S particles. No evidence for the occurrence of ZnCO_3 particles was found.

Generally, it is seen that the use of automated EPXMA allows the identification of a variety of particles with a relatively high atomic number. At least a part of these particles are formed in the anoxic region of the Scheldt estuary, or have an anthropogenic origin.

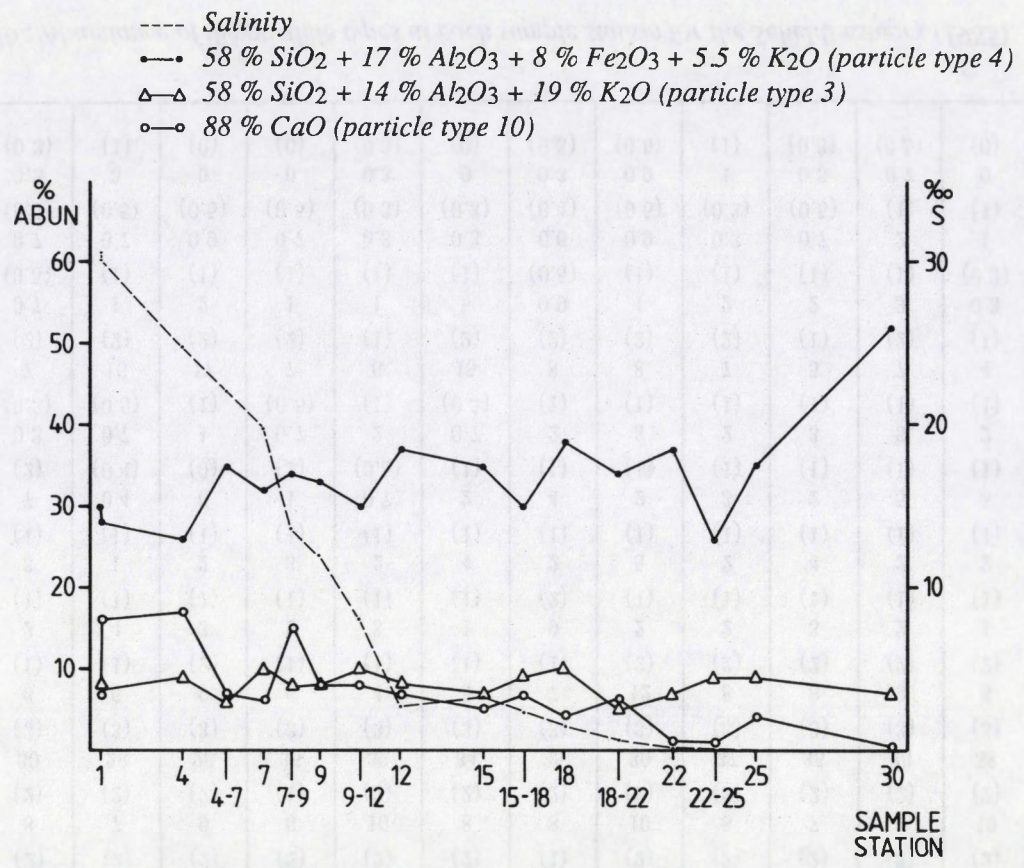


Figure 4.17 : Salinity and the abundance of the K- and Fe + K- rich aluminosilicate particle types and the calcite and/or aragonite particle type for each sample station at the Scheldt estuary (November 1984).

group	% abundance for each sample																
	no.	1	1b	4	4-7	7	7-9	9	9-12	12	15	15-18	18	18-22	22	22-25	25
1	20 (2)	19 (2)	18 (2)	20 (2)	21 (2)	13 (2)	15 (2)	16 (2)	16 (2)	18 (2)	17 (2)	16 (2)	15 (2)	18 (2)	29 (3)	19 (2)	18 (2)
2	13 (2)	13 (2)	12 (2)	16 (2)	16 (2)	11 (2)	5 (1)	9 (2)	11 (2)	11 (2)	8 (2)	11 (2)	15 (2)	11 (2)	14 (2)	10 (2)	7 (2)
3	8 (2)	7 (2)	9 (2)	6 (1)	10 (2)	8 (2)	8 (2)	10 (2)	8 (2)	7 (2)	9 (2)	10 (2)	5 (2)	7 (1)	9 (2)	9 (2)	7 (2)
4	30 (3)	28 (3)	26 (3)	35 (3)	32 (3)	34 (3)	35 (3)	30 (3)	37 (3)	35 (3)	30 (3)	38 (3)	34 (3)	37 (3)	26 (3)	35 (3)	49 (3)
5	6 (1)	6 (1)	9 (2)	6 (1)	4 (1)	5 (1)	7 (1)	12 (2)	8 (2)	8 (2)	9 (2)	8 (2)	11 (2)	11 (2)	10 (2)	10 (2)	11 (2)
6	2 (1)	4 (1)	3 (1)	2 (1)	3 (1)	1 (1)	9 (2)	2 (1)	2 (1)	3 (1)	2 (1)	1 (1)	2 (1)	4 (1)	2 (1)	4 (1)	1 (1)
7	3 (1)	1 (1)	2 (1)	3 (1)	2 (1)	4 (1)	2 (1)	5 (1)	2 (1)	4 (1)	2 (1)	2 (1)	2 (1)	3 (1)	2 (1)	3 (1)	2 (1)
8	7 (2)	0.4 (0.4)	0 (0)	1 (1)	0.7 (0.5)	2 (1)	4 (1)	2 (1)	3 (1)	2 (1)	5 (1)	5 (1)	3 (1)	1 (1)	0.8 (0.6)	1 (1)	2 (1)
9	0.3 (0.3)	0.7 (0.5)	1 (1)	0.7 (0.5)	2 (1)	0.7 (0.5)	2 (1)	3 (1)	2 (1)	3 (1)	5 (1)	2 (1)	0.3 (0.3)	2 (1)	1 (1)	0.7 (0.5)	0.7 (0.5)
10	7 (2)	16 (2)	17 (2)	7 (2)	6 (1)	15 (2)	8 (2)	8 (2)	7 (2)	5 (1)	7 (2)	4 (1)	6 (1)	1 (1)	0.8 (0.6)	4 (1)	0.3 (0.3)
11	0.7 (0.5)	1 (1)	2 (1)	1 (1)	1 (1)	5 (1)	0.9 (0.5)	1 (1)	2 (1)	2 (1)	3 (1)	0.3 (0.3)	1 (1)	0.7 (0.5)	2 (1)	0.3 (0.3)	0.7 (0.5)
12	0.7 (0.5)	0.7 (0.5)	0.9 (0.5)	0.7 (0.5)	0.3 (0.3)	0.3 (0.3)	0.6 (0.4)	0.9 (0.5)	0.3 (0.3)	0.7 (0.5)	2 (1)	1 (1)	2 (1)	1 (1)	3 (1)	0.7 (0.5)	0.3 (0.3)
13	0.3 (0.3)	3 (1)	0 (0)	0 (0)	0.3 (0.3)	0 (0)	0.3 (0.3)	0.9 (0.5)	1 (1)	0.3 (0.3)	0.7 (0.5)	0 (0)	2 (1)	0.3 (0.3)	0 (0)	0.7 (0.5)	0.3 (0.3)

Table 4.4b : Abundance of the particle types at each sample station for the Scheldt estuary (1985).

group no.	% Abun.	SiO ₂ %	Al ₂ O ₃ %	CaO %	Fe ₂ O ₃ %	MgO %	Na ₂ O %	K ₂ O %	TiO ₂ %	Cl %	S %	P %	MAD μm	MID μm	AVD μm	SF
1	18	92 (5)	1 (2)	0.8 (1.1)	1.0 (1.3)	0.2 (0.5)	0.1 (0.3)	0.9 (1.2)	1 (1)	2 (1)	1.1 (1.2)	0.2 (0.5)	2 (2)	1.2 (1.3)	1.5 (1.6)	1.5 (0.8)
2	11	72 (6)	11 (5)	2.4 (2.6)	5 (4)	0.8 (1.1)	0.5 (0.7)	4 (3)	1 (2)	1 (2)	1 (2)	1.0 (1.2)	3 (2)	1.2 (1.1)	1.7 (1.5)	1.8 (0.8)
3	8	58 (6)	14 (6)	2 (2)	2 (2)	1 (1)	0.1 (0.4)	19 (5)	1 (2)	0.9 (1.7)	1.1 (1.7)	0.6 (0.9)	2.4 (2.3)	1.3 (1.3)	1.7 (1.6)	1.5 (0.6)
4	33	58 (5)	17 (6)	3 (3)	8 (4)	1.3 (1.6)	0.4 (0.6)	5.5 (3.5)	1.3 (2.2)	2 (3)	1.9 (2.4)	1.5 (1.7)	2.8 (2.5)	1.3 (1.2)	1.9 (1.7)	1.7 (0.7)
5	8	47 (7)	13 (5)	4 (4)	21 (7)	3 (2)	0.5 (0.8)	5 (4)	1 (3)	2 (3)	2 (3)	3 (2)	2 (2)	1 (1)	1.6 (1.4)	1.6 (0.6)
6	3	42 (7)	12 (5)	14 (10)	8 (5)	1.5 (1.6)	2 (1)	4 (3)	3 (4)	7 (9)	3 (4)	4 (4)	3.4 (3.4)	1.5 (1.7)	2.3 (2.4)	1.8 (0.9)
7	3	12 (6)	4.1 (2.7)	9 (6)	65 (10)	2 (1)	0.3 (0.2)	1 (2)	1 (2)	1 (2)	1 (3)	3 (3)	2.0 (1.5)	1 (1)	1.5 (1.2)	1.3 (0.3)
8	2	14 (9)	4 (3)	16 (7)	35 (8)	1.5 (1.3)	1.2 (0.9)	2 (3)	1.7 (2.4)	3 (4)	2 (4)	19 (9)	2.0 (1.6)	0.9 (0.9)	1.3 (1.1)	1.8 (0.8)
9	2	3 (4)	0.8 (1.1)	1 (2)	33 (4)	0.1 (0.4)	0.2 (0.5)	0.2 (0.8)	0.3 (0.7)	0.1 (0.7)	61 (5)	0.3 (0.7)	1.3 (1.1)	0.9 (0.7)	1.1 (0.9)	1.2 (0.2)
10	7	4 (3)	2 (1)	88 (5)	0.8 (1.2)	2 (1)	0.2 (0.2)	1 (1)	0.7 (1.1)	0.4 (0.9)	0.9 (1.4)	0.7 (1.3)	3.2 (2.4)	1.7 (1.4)	2.3 (1.7)	1.4 (0.5)
11	1	15 (8)	4 (3)	58 (11)	4 (5)	5 (5)	0.4 (0.5)	1.8 (2.7)	1 (2)	2 (3)	3 (5)	6 (8)	3 (2)	1.3 (1.1)	1.8 (1.5)	1.5 (0.4)
12	1	8 (5)	3 (2)	1.0 (1.5)	3 (4)	0.6 (0.6)	0.3 (0.3)	0.8 (1.3)	81 (9)	0.5 (0.9)	0.7 (1.5)	0.6 (1.1)	1.6 (1.2)	0.9 (0.7)	1.1 (0.8)	1.4 (0.5)
13	0.7	21 (11)	6 (5)	7 (9)	9 (10)	1 (2)	1.3 (1.4)	3 (4)	4 (9)	7 (8)	38 (9)	2 (3)	4 (3)	1 (1)	2.1 (1.6)	1.9 (0.9)

Table 4.4a : Average composition of the particle types (normalized to 100 weight %) for the Scheldt estuary (1985).
MAD = maximum diameter; MID = minimum diameter; AVD = average diameter; SF = shape factor

4.5 THE BALTIC SEA

The abundance, composition and distribution pattern of dispersed matter in the Baltic Sea is governed by the geography, topography and hydrography of this brackish water body. Major influences are expected to be caused by the estuarine character with the main fresh water inflow in the North and steady intrusions or episodic swells of sea water from the Southwest and by a mean depth of only 55 m. Strong and relatively stable thermohaline stratification causing oxygen depletion and even hydrogen sulphide formation in the central deep basins, is also of importance. The uplift of the sea bottom in the North (up to 10 mm/a) and submergence of 1 to 2 mm/a in the transition zone to the North Sea is expected to have an influence. The relatively long residence time of the water masses in the order of 25 to 40 years, a high primary productivity (up to about 150 g C/m²/a) and the high anthropogenic load through the atmosphere, by rivers and with direct discharges of industrial and municipal waste waters (Melvasalo et al., 1981; Voipio, 1981) also influence the distribution pattern of dispersed matter. Therefore, the load of particulate matter in the Baltic Sea must be mainly a mixture of material that is introduced with inflowing fresh and saline waters or from the atmosphere, re-suspended/eroded from the sea bottom and from the shore, derived from the organic life in the sea (living cells, fecal pellets, organic detritus, etc.), precipitated in the water column, e.g. oxides/hydroxides, carbonates, sulphides, phosphates and/or flocculated from colloidal dispersed macromolecules (e.g. humic acids) or clay minerals. The chemical composition of this material should reflect the relative importance of these different sources and may therefore act as an indicator for the origin of the water masses and their properties. Hitherto, the available information was restricted to the geochemistry of the bulk of particulate matter (Andrulewicz et al., 1979; Boström et al., 1981; Brüggmann, 1986; Brzezinska et al., 1984; Eisma et al., 1984b; Emelyanov, 1974; Emelyanov and Pustelnikov, 1975; Gordeev et al., 1984; Gustavsson and Notter, 1978; Gustavsson, 1981; Oreshkin et al., 1980;

Pustelnikov, 1977; Weigel, 1976, 1977; Yurkovsky and Pinkule, 1980). Studies on the composition of individual particles have not been performed. The pool of bulk data is still limited with respect to the number of investigated samples and elements and the areal and seasonal coverage. In addition, the results from different authors cannot be compared straightforwardly. This is mainly due to the different methods and materials used for the sampling, pre-treatment and final analysis.

Sampling was performed during a biologically less productive period of the year on a transect between the Bothnian Bay and the North Sea. This avoided that the collected material was composed mainly of organic particles which will not be very site-specific in their composition (Sigg, 1984) and could therefore "dilute" the information gained from the characterization of the inorganic constituents. The selected locations and depths were assumed to be representative for the corresponding water bodies.

The studies were aimed to identify the most typical particles in Baltic waters with the aid of electron microprobe analysis and multivariate statistical techniques. The results of the individual particle analyses were supplemented by measurements on the bulk composition of material collected in parallel. The study of the Baltic was conducted in cooperation with Dr. L. Brüggmann, Institute of Marine Research, Rostock-Warnemünde, German Democratic Republic, who performed the sampling and bulk analysis.

4.5.1 Experimental.

4.5.1.1 Sampling.

Sampling was performed from 18 November to 17 December 1984 from the GDR R/V "A.v. Humboldt" during the expedition POLEX'84 between the Bothnian Bay and the North Sea. The station grid corresponded mainly to that of the Baltic Monitoring Programme (BMP) of the HELCOM (1982). We collected surface water samples at 0.2 m depth into 2 l silica bottles from a rubber boat, wearing arm-length plastic gloves. Sub-surface sampling was performed using home-made 2 l PTFE samplers of type "WATES" (Brügmann et al., 1987).

For the present studies 50 samples were collected at 18 stations (Figure 4.18), either at the "surface" (0.2 or 10 m depth), from medium depths above the permanent halocline and from the bottom layer (Table 4.6b).

For the individual particle analyses immediately after sampling sub-samples of 50 to 100 ml were pressure filtered in a clean bench through 0.4 μm pore-size Nuclepore filters (diameter 25 mm) using a 50 ml Millipore syringe connected to a suitable filter holder. The loaded filters were flushed two times with 10 ml de-ionized "Milli Q" water (MQW), air-dried and stored unfolded, and wrapped in plastic bags in a deep freeze.

For the bulk analyses the suspended matter was separated by pressure filtration of 0.5 l water through 0.4 μm pore-size Nuclepore filters (diameter 47 mm) held in a Sartorius filtering device "SM 16511". The filters had been cleaned previously by leaching them for several weeks in 2M HCl and rinsing with MQW. Before use, the filters were dried and pre-weighed. The loaded filters were flushed two times with 25 ml MQW, double folded with the loaded surface inside and stored in a deep-freeze.

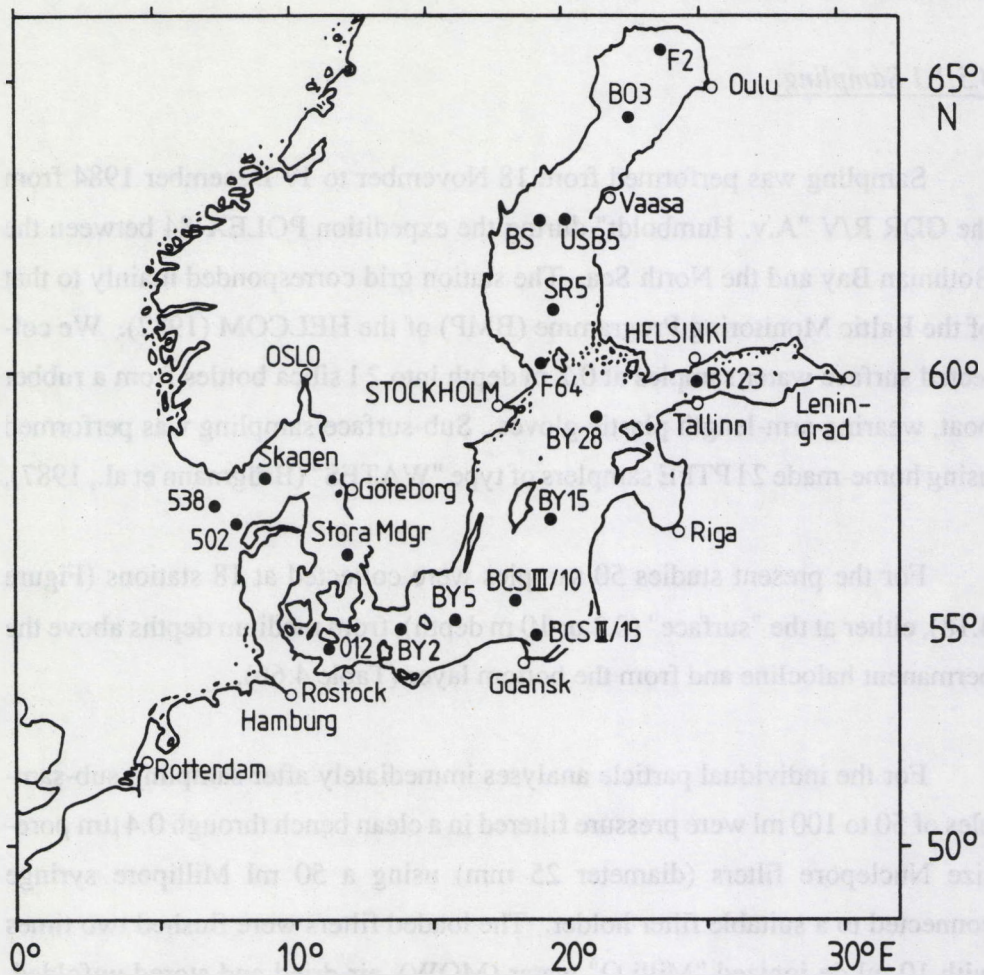


Figure 4.18 : Sampling grid of the 18 stations at which parallel samples of particulate matter were collected in November/December 1984, for individual and bulk analyses.

4.5.1.2 Individual particle analysis.

For analysis the microprobe was used at an electron energy of 20 keV, a beam current of 1 nA and a magnification of 1000 x.

The "Particle Recognition and Characterizations (PRC)" program (see section 2.2.1) was used for the analysis of the individual suspended particles. The peak intensities of the K X-ray lines of Na, Mg, Al, Si, P, S and Cl, the K_{α} -lines of K, Ca, Ti, Mn and Fe and the L-lines of Ba are integrated after subtracting linearly interpolated background contributions from the total counts in the spectrum regions of interest. Due to overlap of the Ti- K_{α} X-ray with the Ba $L_{\alpha 1}$ X-ray, it is necessary to search for the Ba $L_{\beta 1}$ and $L_{\beta 2}$ X-ray to distinguish between Ti and Ba.

In this way for every sample approximately 300 particles are measured in ca. 1.4 h. The total number of particles from the Baltic Sea analyzed for their chemical composition and morphology was around 15,000.

To make the interpretation of this large amount of information possible, hierarchical and non-hierarchical cluster analyses are used to classify the particles (see section 3.2.4) into various particle types or groups on the basis of their elemental composition. The relative frequency distribution of the particle types can be followed through the study area, and the changes provide information about geochemical and physical processes which influence the abundance of certain groups.

After the particles have been classified into groups, corrections for matrix effects in EPXMA, the so-called ZAF-corrections, are carried out, taking into account the average composition of the particle type.

4.5.1.3 Bulk analysis.

The exsiccated filters loaded with the particulate matter were re-weighed. Their pre-treatment for subsequent analyses by atomic absorption spectroscopy (AAS) included the following two steps :

- a) leaching with 0.5 N HCl to release the weakly bound metal fraction and
- b) "total" decomposition of the collected material with a mixture of HCl, HNO₃ and HF in a PTFE pressure bomb (Eggiman and Betzer, 1976).

The AAS measurements of both extracts have been carried out in the flameless mode using the STPF (stabilized-temperature-platform-furnace) concept (Bettinelli et al., 1986; Desaulniers et al., 1985) and by the flame injection techniques. For the investigated elements the total blanks were always below 10 % of the metal quantities contributed by the collected material. The r.s.d. of the determinations did not exceed 15 %. The entire procedure of the bulk analyses of suspended matter on 0.4 µm pore-size Nuclepore filters has been tested before in the course of an ICES intercalibration exercise (Yeats and Dalziel, 1985).

4.5.2 Results and discussion.

4.5.2.1 Hydrographical/hydrochemical background conditions during the sampling period.

The whole data set from the expedition was used for the characterization of the background conditions in the investigated area (Table 4.5). The 140 samples from 36 stations which represent both true "Baltic Sea sites" (Bothnian Bay to Kattegat) and "North Sea samples" (Skagerrak and NE North Sea, 4 stations/16 samples) were divided into 3 categories for further interpretation, namely the surface, medium and bottom water samples.

	"Surface" (0.2 to 10 m) n = 64	"Medium" (20 to 400 m) n = 38	"Bottom" (10 to 550 m) n = 38
Temperature (°C)	6 ± 2 (2.1 - 8.4)	6 ± 2 (2.5 - 9.9)	7 ± 2 (2.8 - 12.2)
Salinity (ppt)	13 ± 8 (3.4 - 33.6)	15 ± 12 (3.6 - 35.2)	17 ± 11 (4.1 - 35.2)
Oxygen saturation (%)	95 ± 2 (93 - 99)	77 ± 30 (<0.01 - 97)	71 ± 30 (0.01 - 97)
Phosphate (μmol/l)	0.5 ± 0.3 (0.02 - 1.1)	0.8 ± 0.7 (0.04 - 3.1)	1.1 ± 0.7 (0.1 - 3.6)
Nitrite (μmol/l)	0.5 ± 0.6 (0.05 - 3.0)	0.3 ± 0.4 (0.01 - 2.1)	0.3 ± 0.2 (<0.01 - 0.8)
Suspended matter (mg/l)	0.4 ± 0.2 (0.1 - 1.2)	0.4 ± 0.2 (<0.01 - 0.9)	0.7 ± 0.5 (0.1 - 2.6)

Table 4.5 : Hydrographical/hydrochemical background data for the investigated area in the Baltic Sea during the sampling period.

Our data reflect a typical late autumn/winter situation for the Baltic Sea (Grasshoff, 1975; Melvasalo et al., 1981; Voipio, 1981). From the STD profiles no sign of a thermocline was visible. The medium and bottom water layers are more saline, enriched in phosphate and partly in nitrate, and depleted in oxygen with respect to the surface waters. This is partly the result of the permanent halocline which exists throughout the whole Baltic Sea except in those parts of the Gulfs of Bothnia and Finland where convective overturn of the water column occurs during winter time. The halocline is a barrier for the exchange between deep waters and the surface layer, allowing only slow mixing. The high phosphate concentrations in the deep water are the combined result of the mineralization of suspended organic material and the release of dissolved phosphate out

of the sediments, especially when anoxic conditions prevail. The mineralization of organic material is also responsible for the higher nitrate concentrations found in the medium depth water. In the bottom water of deep basins with very low oxygen levels or with anoxic conditions, the nitrate is consumed as oxidizing agent and finally removed by de-nitrification. The measured nitrite concentrations were low throughout the whole Baltic Sea; only slightly higher levels were found in the surface waters.

The primary productivity during the sampling period is generally low, less than $0.1 \text{ g C/m}^2/\text{d}$. This is about one fifth of the annual mean or only 2 % of the primary productivity observed during blooms in spring and summer (Schulz, 1985). In the Northern parts of the Baltic Sea the productivity drops to nearly zero in winter time.

The suspended particulate matter concentrations measured during the sampling period were lower than all previously published data. Pustelnikov (1977) found a mean value of 3 mg/l (0.2 - 12.4 mg/l) for the suspended matter content (0.5 μm , membrane filter, about 1500 samples). Boström et al. (1981) reported 1 mg/l as a mean value for 39 samples using 0.45 μm pore-size Millipore filters under pressure filtration but without filter washing. Later on they suggested a four times higher value (4 mg/l) to be more representative (Boström et al., 1983). A level of 0.94 mg/l (0.05 - 15 mg/l) was found by Brüggmann (1986) as the mean of 233 samples which were pressure filtered through 0.4 μm pore-size Nuclepore filters, and finally washed with MQW. The average obtained by Eisma et al. (1984b) (0.4 μm pore-size Nuclepore filters, 9 samples) for the Kattegat waters outflowing into the Skagerrak was 1.2 mg/l. Our mean values for the surface, medium and bottom water samples (0.4, 0.4 and 0.7 mg/l, respectively, Table 4.5) result from a period with low biological productivity. However, they may be not representative for the whole winter season. There is a lack of information on seasonal differences of the suspended matter load in

Baltic waters. For instance, Jonasz (1983) found that the size distribution and number of particles per volume vary greatly in the Baltic Sea depending on season, depth and location. Particles $> 2 \mu\text{m}$ show maximum numbers of $35,000/\text{cm}^3$ in the summer mixing layer (0 to 20 or 30 m) and minima above the halocline (60 - 70 m) with 1000 to $1500/\text{cm}^3$ in winter time (Jonasz, 1983).

4.5.2.2 Individual particle analysis.

The classification which was based on the elemental composition of 15,000 particles taken from different parts of the Baltic Sea identifies 10 particle types of geochemical relevance. The average composition - converted to oxides when relevant - of the different particle types is listed in Table 4.6a.

It can be seen that the prevailing groups in the overall study area are the Si-rich particle types ($\text{SiO}_2 > 40\%$). They account for 80 % of all investigated particles and consist of a quartz (type number 1), a K-rich (type number 2) and a Fe-rich aluminosilicate particle group (type number 3). The mineralogical composition of the Si-rich particle types cannot be elaborated by EPXMA, but X-ray diffraction data from recent Baltic Sea sediments, e.g. the Arkona Basin (Brügmann and Niemistö, 1987) reveal the presence of up to 30 % quartz, about 10 % of each feldspars (plagioclase, K-feldspar) and chlorites, up to 30 % of clay minerals (mainly illite, some kaolinite, traces of montmorillonite and un-identified "mixed layers"). In addition, different proportions of dolomite, pyrite and only occasionally calcite were identified (Emelyanov and Trimonis, 1981).

The less abundant particle types, group numbers 4 to 10, were identified as Ba + S-, Fe-, Mn-, Ca-, P + S-, Ti- and Al-rich particles, respectively.

The relative abundance of each particle type at every individual sample is given in Table 4.6b. Except for the Ti-rich (possibly rutile) and the Al-rich par-

ticle type, significant abundance variations exist throughout the Baltic Sea. The relative abundance variations and the nature of the particles classified in the Ba + S-, Fe-, Mn-, Ca-, P + S-rich particle types will be discussed in more detail.

The Ba + S-rich particle type

Particle type 4 reveals the occurrence of Ba + S-rich particles with a mean relative abundance of 5 % in the Baltic Sea. An electron micrograph and EPXMA-spectrum of a typical particle are given in Figure 4.19A and Figure 4.20A, respectively. Electron diffraction of the Ba-rich phase of the Atlantic and Pacific suspended matter showed the diffraction pattern of barite (Klossa, 1977). This allowed Dehairs et al. (1980) to conclude that barite is a genuine component of natural marine suspensions and in most cases the main particulate Ba carrier in the marine environment. If it is assumed that Ba + S-rich particles found in the Baltic Sea are also barite mineral grains, the distribution of particle type number 4 can be used to derive information on its origin and transport.

It is shown in Table 4.6b that the relative abundance of the barite particle type ranges between 0 and 44 %. The relative contents in the Gulf of Bothnia and at station BY 23 in the Gulf of Finland are low and do not exceed 2 % (only at the medium depth sample of station SR5 a high barite content of 25 % is found). Most of the other samples in the Baltic Sea have higher relative abundances than 2 %. This is a direct evidence for the ubiquitous character of this mineral in the Baltic Sea. In some cases barite is even the predominant particle type, as e.g. at the medium depth of station BCSIII/15 where a relative abundance of 44 % was observed. For the two North Sea samples (stations 538 and 502), the relative barite content is 2 %. It seems that the central Baltic Sea at medium depths (50 m samples) is enriched in barite in relation to other areas and layers.

No data are available on the origin of suspended barite in the Baltic Sea. Four possible processes exist for the input or formation of barite in the aquatic environment :

- Authigenic formation (precipitation) is possible in waters saturated with respect to barite. Dissolved Ba can be delivered by input of fresh water, hydrothermal solutions and/or interstitial water. Boström et al. (1971) showed the precipitation of barite from hydrothermal exhalations on the East Pacific Rise.
- Biogenic production of barite has been shown for many marine organisms (Lowenstam, 1974). Barium accumulation in deep sea sediments is observed to extend under Atlantic surface waters characterized by a high organic productivity and a high dissolved phosphate concentration (Turekian and Taush, 1964).
- Anthropogenic input of barite as a constituent of oil-drilling muds. This has already been observed in Southern California waters, where a significant increase in dissolved Ba was measured in the vicinity of some drilling areas (Chow, 1976). Holmes (1982) even used the higher particulate barite concentrations to tag the sediment movements from areas of hydrocarbon exploration.
- Atmospheric fall- and wash-out of barite is another possible source. A Ba-based organo-metallic compound is used as an additive for diesel fuels. Combustion of these fuels releases BaSO₄ aerosols. The presence of Ba + S-rich particles in aerosols sampled over the Northern North Sea has been proven directly by the use of automated EPXMA (F. Bruynseels, pers. comm.). Frequently, particle abundances of 1 to 2 % have been found for the Ba + S type in contaminated marine aerosols.

Due to the lack of data on the barium content of different compartments of the Baltic environment, it is not possible at this moment to estimate the relative

contributions of the above listed four different sources to the particulate Ba load of the water body. The relatively low Ba content of Baltic sediments which is in the order of 1000 to 3000 $\mu\text{g/g}$ for mud sediments of central areas (Emelyanov, 1986) and the low particulate Ba content of the bottom water layer seem to exclude the sediments as a source. An extra-ordinarily high Ba input from the atmosphere would probably be reflected by an enrichment in the surface water layer. This was not observed. The low productivity during the sampling period would not favour biogenic sources. Two explanations are left, one authigenic and one anthropogenic :

- a) BaSO_4 could precipitate where the dissolved Ba input from river waters meets higher salinities (with higher sulfate concentrations) for the first time.
- b) drilling activities increased during the last 10 years in the Baltic Sea and could therefore significantly contribute to the particulate Ba load.

At present with the available data no final conclusions about the source can be drawn. However, the automated individual particle analysis showed that barite is a significant compound of the suspended particulate matter in some parts of the Baltic Sea.

The Fe-rich particle type

All particles classified into type number 5 are characterized by their high contents of Fe. Probably, the predominant types of Fe which cannot be distinguished by their X-ray spectra are the oxides/hydroxides and, of lesser importance, the carbonates. Besides the high Fe contents, significant amounts of Si, Mn and P can be present in single particles. Most of the investigated Fe-rich particles are authigenic, as seen from micrographs such as Figure 4.19B. The most probable condensation nuclei for the precipitation of iron are the aluminosilicates in view of their high abundance. This could explain the sometimes high Si-con-

tent of some particles. The high contents of Mn frequently found suggest the coprecipitation and/or adsorption of Mn oxides/hydroxides and of Mn(II) (Ingri and Ponter, 1986). The observed iron-phosphorus association could mainly be due to the surface adsorption of phosphorus onto the Fe oxides/hydroxides (Upchurch et al., 1974; Williams et al., 1976; Filipek and Owen, 1981) whereas the detrital apatite fraction will be low.

The abundance of the Fe-rich suspended phase is highly variable as seen in Table 4.6b. At most stations the relative abundance is below 7%. However, in the Skagerrak deep water samples and especially at station BY5 in the Bornholm Basin, much higher values are observed. At station Skagen there is a significant increase of the relative abundance toward the bottom. An excess of Fe relative to adjacent waters was already mentioned by Eisma et al. (1984b) for the deep Skagerrak waters. They found particulate Fe concentrations of 27-66 $\mu\text{g/l}$ (6-7% of the particulates) in the deep water, whereas only 3-7 $\mu\text{g/l}$ were present in the surface layer. By individual particle analysis it is now shown that this "Fe excess" documented by bulk analysis is concentrated in individual Fe oxides/hydroxide particles. In the Norwegian Trench, iron excesses were measured in quaternary clays (Roaldset, 1978) of the same order of magnitude as in the Skagerrak. The formation of Fe-enriched layers may be due to the different settling velocities of the aluminosilicates in relation to the more finely dispersed Fe oxides/hydroxides (Price and Skei, 1975). Another important process which could contribute to the Fe excess in the deep water could be the resuspension of the sediment top layer enriched in Fe by diagenetic activities. The diffusion of Fe-rich pore waters into the bottom water could be another important source.

The maximum concentration of the Fe-rich particle type was measured at station BY5. Nearly anoxic conditions are reached here at the bottom. Under these conditions high concentrations of ferrous Fe and phosphate (7.5 $\mu\text{mol/l}$) are present. Authigenic formation of the Fe phosphates and Fe oxides/hydrox-

ides at or near the oxic/anoxic boundary will then take place (Davison et al., 1980). The morphology of the investigated particles supports this.

Furthermore, a slightly higher relative abundance of the iron-rich particles (ca. 5 %) is found in the Northern Bothnian Bay at station F2 and at the surface sample of station BO3. Ingri (1985) showed that the Northern Swedish rivers transport excessive amounts of Fe, of which most is present in a non-detrital suspended phase. Probably, these are the particles, measured with the electron microprobe.

The Mn-rich particle type

The identified Mn-rich particles (Figures 4.19C and 4.20C), classified in particle type number 6, are assumed to consist of Mn oxides/hydroxides and/or carbonates. In some particles also significant contents of Si and Fe are present. As for the Fe-rich particle type the relative abundance of the Mn-rich suspended phase is controlled by the redox conditions.

For Skagen 2 an increase of particulate Mn is shown for the bottom water sample as with Fe before. The Mn-rich particles detected with the electron microprobe seem to represent the excess Mn measured by bulk analytical techniques in this area (this work; Eisma et al., 1984b). Again, this excess may be due to selective settling, to resuspension of bottom sediments and/or to diffusion of Mn(II) out of the sediment followed by precipitation of Mn in the more oxygenated bottom water layers. The escape of Mn from sediments by resuspension, diffusion and/or compaction causing the formation of Mn-enriched fine grained particles, was studied in detail by Sundby et al. (1984) for the sediments of the Laurentian Trough, Gulf of St. Lawrence and by Skei and Melson (1982) in a Norwegian fjord. These authors suggested that this phenomenon is likely in many mud sediments of coastal areas.

The highest relative concentrations of the Mn-rich suspended phase, 41 % and 88 %, are measured at 100 m depth at station BY15 and at the bottom of station BY28, respectively. In both cases, reducing conditions in the water phase are reached. At station BY15 hydrogen sulphide was present from the bottom (240 m) up to about 150 m. Consequently, above the redoxcline a pronounced maximum of re-oxidized Mn oxides/hydroxides was detected by both the bulk and individual particle analyses. The "bottom" water at station BY28 (170 m) has a low oxygen content (0.3 % saturation). It covered an anoxic water layer and reducing sediments. The Mn(II), migrating out from the sediment and adjacent bottom layer, is oxidized under oxic conditions to particulate Mn phases.

Less extreme but still significantly elevated relative concentrations are found in the bottom waters of stations BCSIII/10, BCSIII/15 and BY5. The oxygen saturation for these samples is 43.4 %, 52.1 % and 3.3 %, respectively. Again it is assumed that redistribution of Mn occurs in this area leading to higher particulate Mn concentrations.

In the Northern Bothnian Bay a similar situation is found as for Fe. The Swedish rivers supply the non-detrital suspended Mn phase (Ingri et al., 1984). This input increases the abundance of the Mn-rich particle type at station F2 (surface and medium depth samples) and for the surface sample at station BO3. No increase is measured at the bottom water samples.

The Ca-rich particle type

The particles classified in particle type number 7 are assumed to be calcium carbonates, probably calcite and/or aragonite. It is seen from Table 4.6b that their concentrations are low throughout the whole Baltic Sea. Only in the zone where mixing between the North Sea suspended particulate matter with suspensions from the Baltic Sea occurs, significant relative concentrations were de-

tected. For the surface samples the relative concentration of the calcium particle type is given in Figure 4.21. It is seen that high relative concentrations (ca. 20 %) of this type number 7 is representative for the marine suspended matter. A positive correlation between the relative abundance of the carbonate particle type and the salinity was seen in the estuarine studies of the Ems and the Scheldt (respectively, sections 4.2 and 4.4). The North Sea acts as a source of calcium carbonate in the Baltic Sea. Therefore, an inflow of particulate Ca is measurable down to station BY2 in the Arkona Basin. However, this study cannot define quantitatively how much of this CaCO_3 is authigenically formed in the Baltic Sea and which fraction is imported from the North Sea.

The carbonate content of the sediments shows a similar decline between the Skagerrak/Kattegat (mean : about 10 %) and the Northern Baltic Sea (Gulf of Bothnia mean : about 0.8 %). But in between, in very fine grained mud sediments of the northern deep basins (e.g. stations BY15, BY28), elevated carbonate contents are observed (Brügmann, unpubl. rep., 1986), which are diagenetically formed in the sediments and not derived from the water column.

The S + P-rich particle type

Several elements are present in considerable relative amounts in particles classified into particle type number 8, namely P, Si, S and Ca. This group could consist partly of organic particles. Normally, in the automated EPXMA particle recognition procedure, organic particles are not detected because their backscattered electron signal, which depends on the atomic number, is close to that of the filter backing. When, however, because of statistical fluctuations or a significant inorganic content, such particles are detected occasionally, the concentrations of the elements yielding measurable X-rays will be normalized to 100 % and the data in Table 4.6a will be rather irrelevant.

Frequently, in the Baltic Sea the amount of organic matter can make up to 62 % of the total suspended particulate matter in biologically more productive periods (Eisma et al., 1984b; Boström et al., 1981, 1983; Pustelnikov, 1977). In those cases, the fraction analyzed by EPXMA can become significant and must be taken into account due to its influence on the relative abundance of the inorganic particle types.

4.5.2.3 Principal component analysis.

A Principal Component Analysis (PCA) was performed on a data matrix which includes the hydrographical data and the relative abundances of the particle types. The used variables are the "depth" (percentage of total depth), the temperature, the salinity, the oxygen saturation, the phosphate, nitrate and suspension concentrations and the particle type numbers 1 to 7. Particle type numbers 8, 9 and 10 were omitted for the analysis, as their occurrence was not assumed to be significant or relevant in respect of the inorganic single particle analysis. Furthermore, the medium depth sample of station BO3 was excluded because of its high content of the not clearly identified particle type 8. The correlation matrix is used for the calculation of the principal components. The first four principal components represent 70 % of the total variance present in the original data set, and 80 % is reached with six components. The loadings of the first six principal components are listed in Table 4.7.

The first principal component could elaborate the difference between oxygenated surface samples, relatively rich in aluminosilicates, and the oxygen depleted deep water samples with higher phosphate, Fe- and Mn-particle concentrations.

The second component has high loadings on salinity, Ca-rich particle type abundance and temperature. This component is assumed to describe the vari-

ation which occurs in the mixing area between the North Sea and the Baltic Sea water. Samples having a high score are representative for the North Sea. Above a positive correlation between the calcite content and the salinity was already discussed (Figure 4.21). PCA shows that to a minor extent this is also true for the temperature.

The third component has a positive loading on the barite particle type and temperature and a negative loading on the depth, suspension content, nitrate concentration and on the Fe-rich aluminosilicate particle type. This component probably discriminates between oxygenated surface water and oxygenated deep water samples.

The fourth component is mainly characterized by negative loadings on the Fe particle type and the Fe-rich aluminosilicate abundances while it has a positive loading on the quartz particle type. This component probably describes the sometimes high concentrations of these variables found in selected areas of the Baltic Sea. The high relative concentrations of the Fe-particle type will be found in samples with a reduced quartz abundance, while the Fe-rich aluminosilicate group becomes relatively more important in these areas.

While the fourth component describes the variation in the Baltic Sea suspended matter owing to the occurrence of high concentrations of Fe-rich particles, the fifth principal component does the same for the Mn-rich particles. These particles are found in regions with low total contents of suspended matter and low relative concentrations of Fe-rich particles.

The sixth component has a high loading on the barite particle type. Samples with a high score on the sixth component have high relative abundances of the barite particle type. None of the measured hydrographical parameters is related with high barite concentrations.

Summarizing, the first six principal components, representing 83 % of the total variance, seem to describe the differences between oxygenated surface and oxygen-poor deep water samples, the mixing processes between the North Sea and the Baltic Sea and the variation due to the occurrence of high quantities of particles enriched with Fe, Mn or barite.

4.5.2.4 Bulk analysis.

Preliminary results from the bulk analyses which can be compared directly with the individual particle analyses are given in Figure 4.22. The "leachable fraction" is related to that which could be extracted by 0.5 N HCl. The "detrital fraction" became available after decomposition by HNO₃/HCl/HF. "Total" is the sum of the leachable plus detrital fraction.

The "excess" content of the elements is relative to the mean abundance in the continental crust (Taylor, 1964). Since most of the Al is present in the more resistant aluminosilicates and is not leached by a weak acid attack, Al is used as reference element for the calculation of metal excesses according to

$$\text{Me}_{\text{excess}} = \text{Me}_{\text{total}} - (\text{Al}_{\text{total}} \cdot (\text{Me}/\text{Al})_{\text{crust}})$$

The major fraction of the total Mn is leachable. Only for the medium-depth samples a noteworthy detrital fraction was observed. This leads to the conclusion, that nearly all particulate manganese is present as authigenically formed phases, e.g. oxides/hydroxides or resuspended carbonates.

No positive Fe excess contents were observed in the water column. However, high positive excess contents for some single samples are observed. In those samples the leachable fraction always prevails.

The leachable Zn fraction represents the major part of this element. This fraction seems to be responsible for the observed excess contents. For the 200 m sample from station BY15 a bulk Zn content as high as 0.64 % was measured by AAS. The presence of ZnCO₃ enriched particles is expected at stations with these extremely high contents. A manual electron microprobe search led to the identification of a single Zn rich particle (Figures 4.19D and 4.20D), and gave direct evidence that Zn is partially concentrated in specific particles in the Baltic Sea. However, the X-ray spectrum does not allow final conclusions about a Zn/carbonate association.

For Ba the mean excess content is always positive. The enrichment of Ba in marine suspensions relative to the earth's crust is a general feature. In the Baltic Sea, the particulate matter is enriched with Ba even with respect to the underlying sediments.

4.5.2.5 Comparison of the individual particle and bulk analysis.

For all samples analyzed by EPXMA, bulk analytical data by AAS exist. To elaborate the relationship between the abundance of the identified particle types, the elemental bulk concentrations (leachable, detrital, total and excess contents) and the hydrographical data, correlation coefficients were calculated. These coefficients are given in Table 4.8a-b. The boldface typed numbers are significant at a confidence level 0.5 % (50 samples) i.e. all higher than 0.36.

As previously mentioned, the major Al fraction is detrital and the leachable fraction is low. This is reflected by significant correlation between the detrital and total aluminium contents and the K-rich and Fe-rich aluminosilicate particle types, whereas no significant correlation was found for the leachable Al fraction. The negative correlation of the Al with the barite particle type is in accordance with the third principal component discussed above. There the relative abun-

dance decrease of the Fe-aluminosilicate was owing to the increase of the barite particle type. Furthermore, the total Al content is found to be correlated with the nitrate and the suspended matter concentrations.

On the basis of the correlation factors the geochemical distinction between the leachable and detrital Ca fraction is seen clearly. The leachable fraction correlates with the relative abundance of the calcite particle type whereas the detrital fraction does so with the aluminosilicate particle type. The aluminosilicate particle types have indeed a significant Ca content as shown in Table 4.6a. In the mixing area between the Baltic Sea and the North Sea the same behavior for the temperature, salinity, nitrite and the relative abundance of the calcium carbonate particle type was found for this sampling period. The correlation between the bulk Ca contents (leachable and total) further support this.

From Table 4.8a it is seen further that high amounts of leachable Mn are expected to be found in areas with depleted oxygen and increased phosphate concentrations. In these areas the formation of authigenic Mn particles can occur. Furthermore, the individual particle analysis shows significant negative correlations between the leachable Mn and the silicate particle types, whereas this Mn fraction is highly significantly correlated ($r = 0.93$) with the abundance of the manganese oxide/hydroxide particles. No significant correlations were found for the detrital Mn fraction, and the total and excess contents are only correlated with the phosphate concentration and the presence of the Mn oxide/hydroxides particle type.

For Fe a slightly different situation is found. The leachable fraction is, as expected, positively correlated with the Fe oxide/hydroxide particle type. No correlation with dissolved phosphate concentration is found. Owing to the presence of an important detrital fraction, significant correlations are encountered between the abundances of the aluminosilicate particle types and the

bulk detrital fraction. Obviously, the weak acid attack is successful in dividing the total Fe content into a fraction present, at least partly, as Fe oxides/hydroxides particles and into the detrital part.

The leachable, total and excess Zn contents correlate negatively with the oxygen saturation and positively with the relative abundance of the quartz particle type.

All four Ba variables are negatively correlated with the temperature. The detrital and excess fractions are also negatively correlated with the salinity, which supports the findings of the individual particle analysis where it was stated that relatively more barite particles were present at the central Baltic Sea. However, only between the Ba bulk concentrations and the relative abundance of the aluminosilicates significant correlations were seen. No significant correlations between the barite particle type identified by EPXMA and the bulk Ba fractions were found. The significant negative correlations of the barite particle type abundance with the bulk contents of detrital and total Al and with the leachable, detrital and total Fe, is an indication that the occurrence of barite in the suspended particulate matter has an important impact on the bulk contents and is a relevant part of it. Probably, the reason for the fact that no correlation was found between the barite particle type and the Ba bulk concentration is that the strong acid attack was not efficient enough in dissolving the stable barite lattice for AAS analysis.

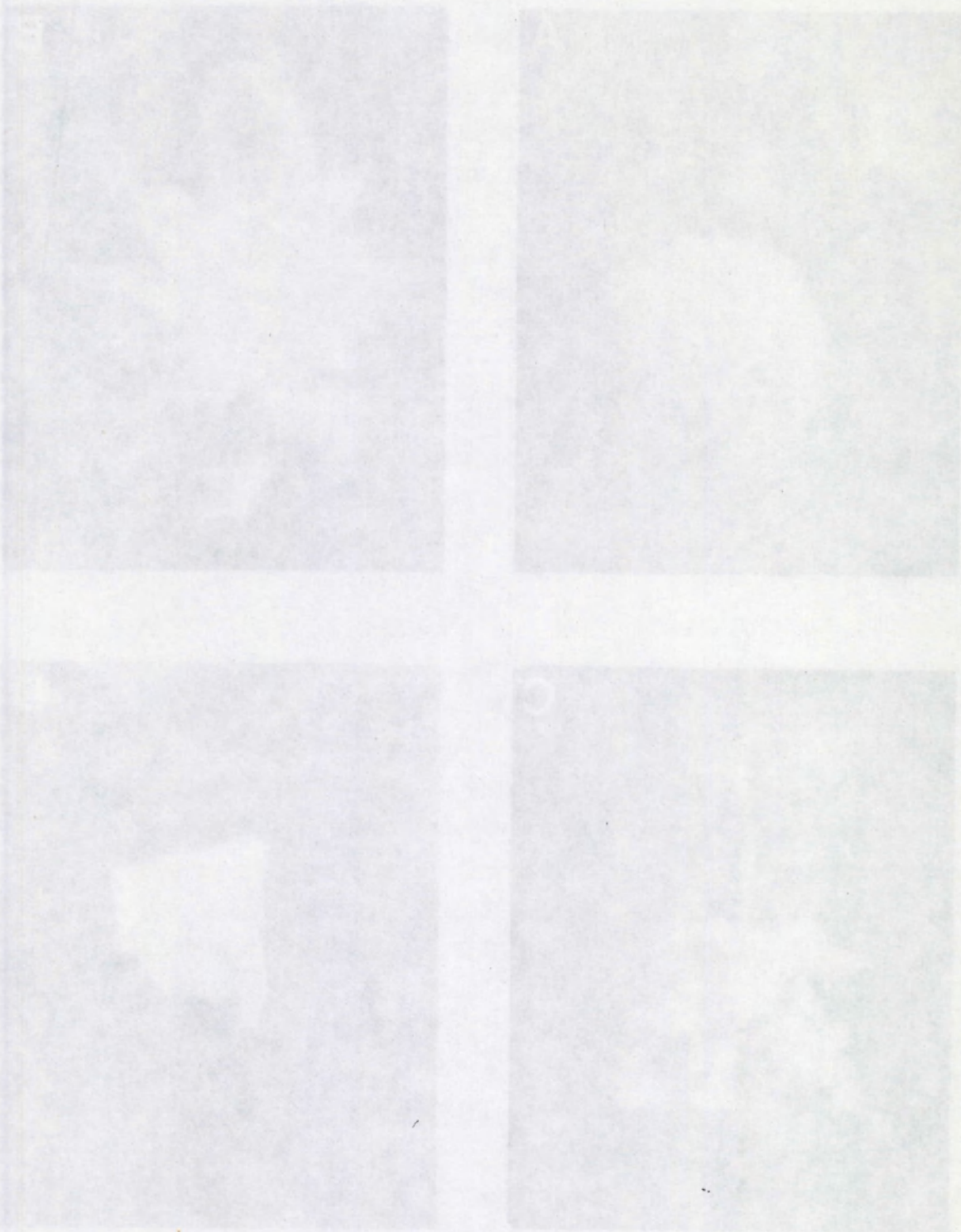


Figure 1. Electron micrographs of individual particles: (A) 1.5 μm particle; (B) 1.2 μm particle; (C) 1.8 μm particle; (D) 1.5 μm particle.

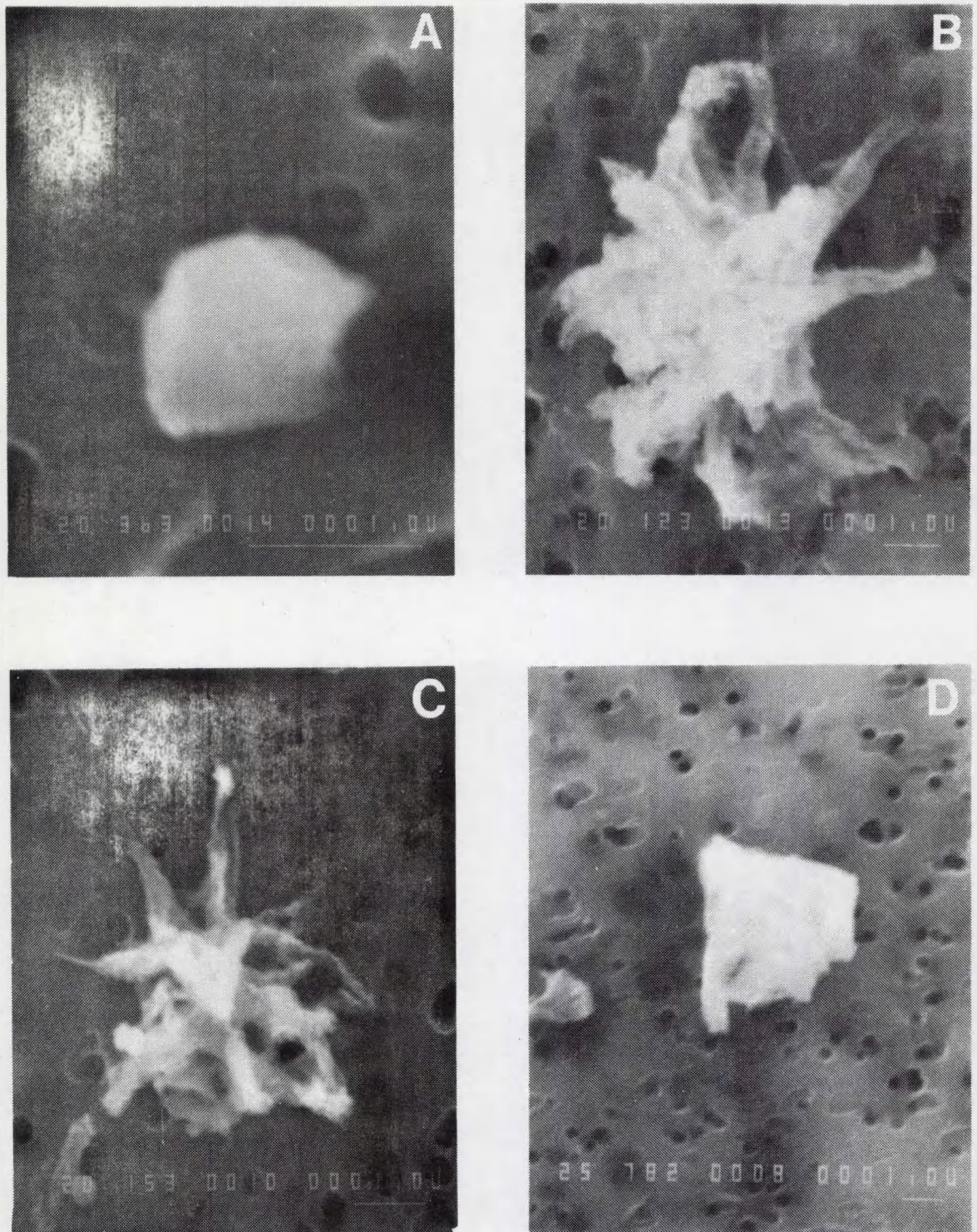


Figure 4.19 : Electron micrograph of (A) BaSO_4 -particle, (B) Fe-rich particle, (C) Mn-rich particle and (D) Zn-rich particle.

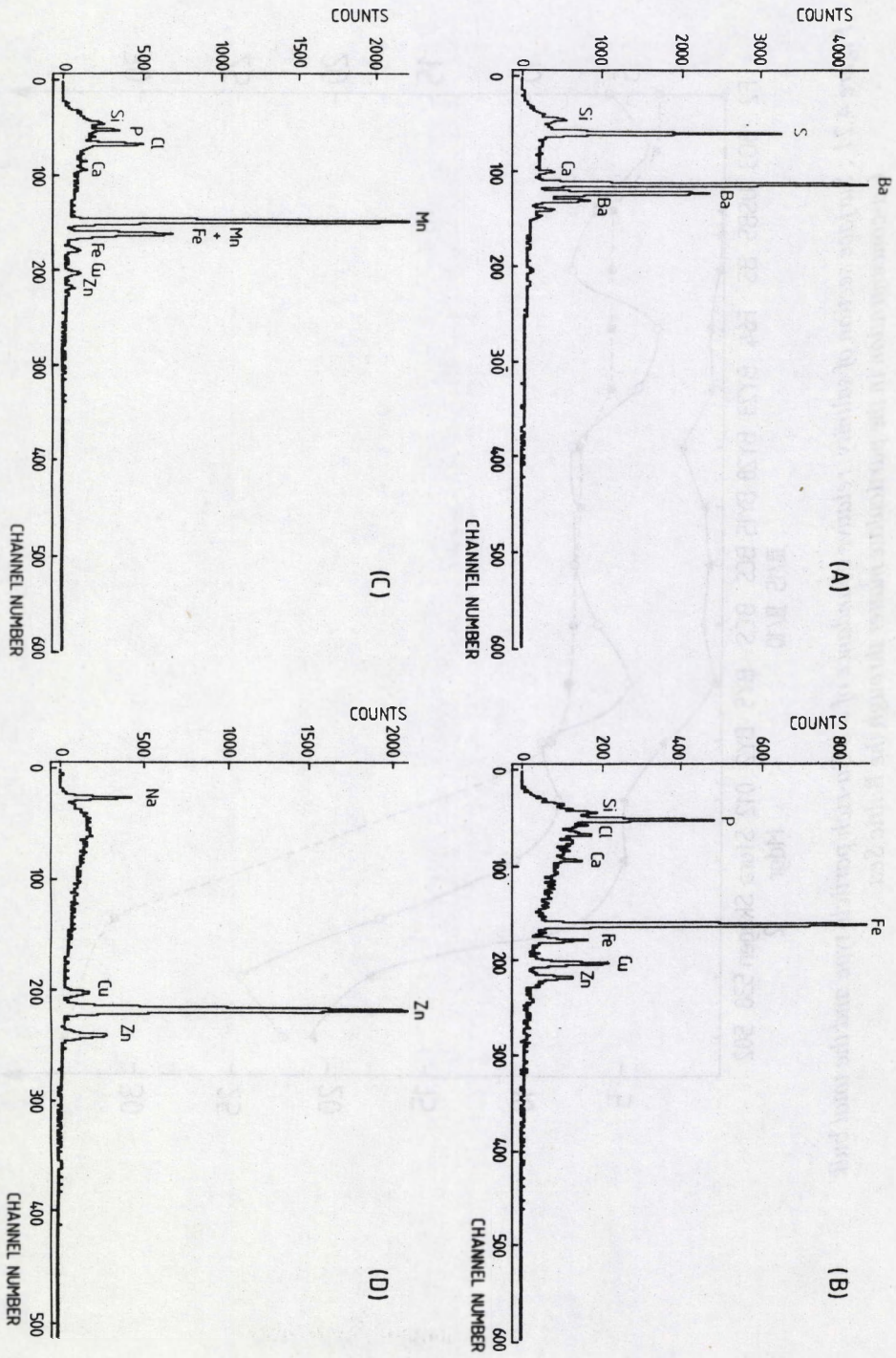


Figure 4.20 : EPXMA-spectra of the particles shown in Figure 4.19.

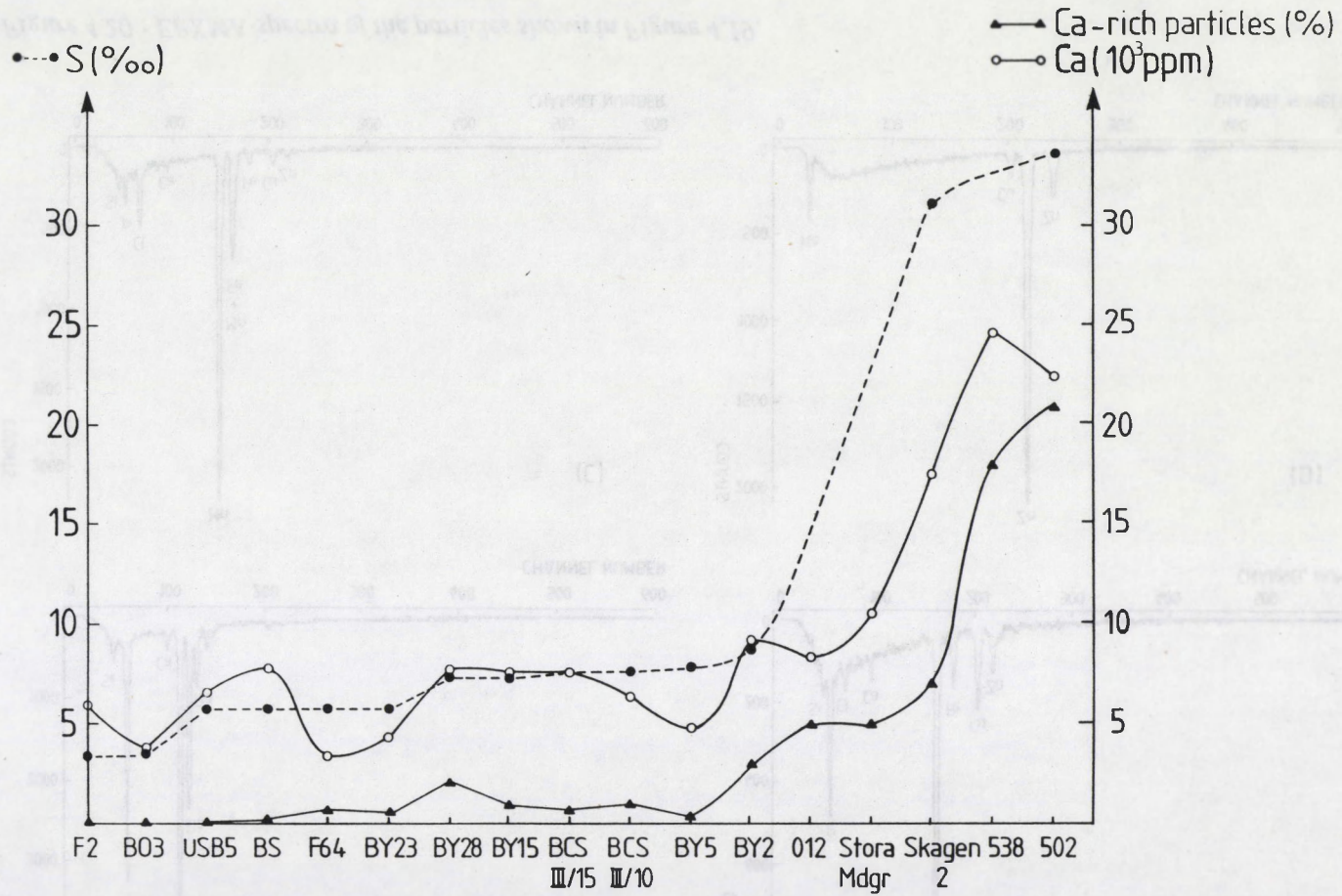


Figure 4.21 : Surface section of salinity, relative abundance of the Ca-rich particle type and the total bulk Ca-concentration in the particulate matter through the Baltic Sea.

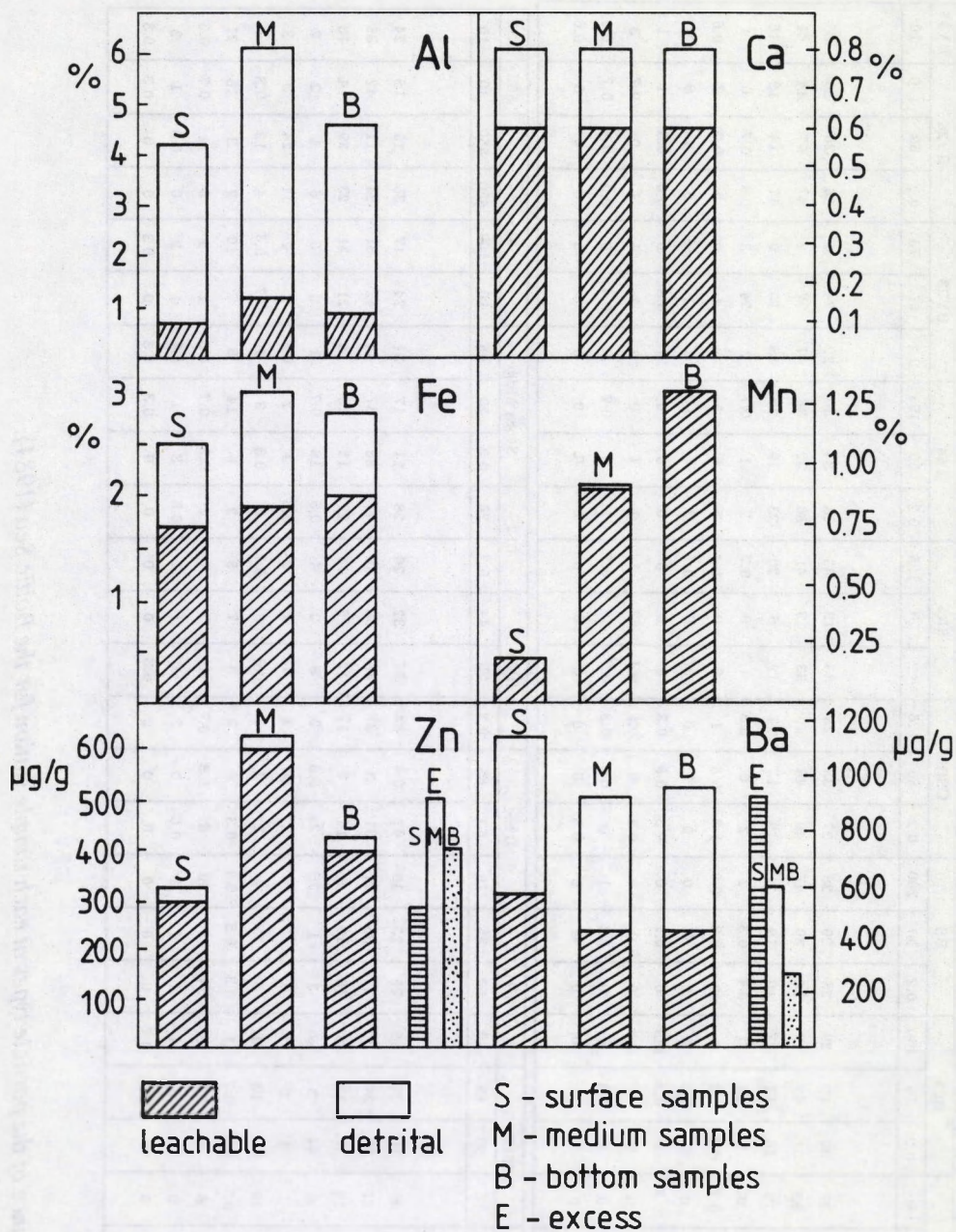


Figure 4.22 : Leachable and detrital fractions, total and "excess" contents for some elements in particulate matter from different depths of the Baltic Sea (bulk analysis by AAS).

Station	F2			H03			BS			USB5			SR5			F64			BY23			BY28			BY15	
Depth (m)	0.2	50	80	0.2	50	100	0.2	50	200	0.2	50	125	0.2	50	125	0.2	50	155	0.2	55	75	0.2	50	170	10	
Particle type number																										
1	27	37	27	30	19	29	28	29	28	27	33	25	35	13	35	28	34	30	22	24	6	26	26	26	30	
2	49	44	52	51	42	42	54	50	47	49	48	49	33	13	41	36	32	36	47	37	2	47	57	44	41	
3	20	17	19	10	12	27	16	19	21	19	17	24	19	6	20	23	19	28	18	10	0	17	14	19	16	
4	0	0	0	1	25	0	0.7	0.3	2	2	0	0.3	1	0	0.7	2	1	0.7	2	24	3	0.9	0.7	0	4	
5	0.7	1	0.7	0.7	0.3	1	2	0.3	0.9	1.3	0.6	1	6	0	1.3	5	6	5	5	1	0	2	0.7	2	0.6	
6	0.3	0.3	0	2	0.3	0	0	0	0	0	0	0	5	0	0.7	3	7	0.3	2	1	88	6	1	8	2	
7	0.7	0.3	0.7	0	0.3	0.3	0	0.7	0	0.3	0.9	0.3	0	0	0	0	0	0	2	0.8	0	0.6	0.3	1	1	
8	0.3	1	0	2	1	0.3	0	0	0	0.3	0	0.6	0.4	63	1	1	1	0	2	1	1	1	0	0.7	3	
9	1	0	0	1	0.3	0	0	0.3	1	0	0.6	0.3	0.7	0	0.7	1	0	0.7	0	0.4	0	0.3	0.3	0.7	0.9	
10	0.3	0	0	0	0	0	0	0	0	0.3	0	0	0	0	0	0	0	0	0	0	0	0	0	0	0.6	

Station	BY15		BCSIII/10			BCSIII/15			BY5			BY2		012		Stora Mdgr			Skagen				502	538		
Depth (m)	100	235	10	50	85	10	50	95	10	50	85	0.2	20	44	0.2	20	0.2	20	45	10	100	450	550	10	10	
Particle type number																										
1	27	60	39	10	35	29	25	23	16	42	0.9	34	37	32	26	28	21	17	31	24	17	30	15	18	24	
2	15	16	21	27	30	36	22	35	27	31	3	37	35	38	46	41	38	37	44	42	31	24	11	42	36	
3	9	6	10	8	13	8	13	13	5	14	2	17	12	16	13	22	12	23	18	21	31	23	29	14	13	
4	4	16	8	44	3	8	3	1	26	2	0.6	2	3	2	4	0.5	18	0.7	1	0	0	6	1	2	2	
5	2	1	3	3	2	4	3	2	4	2	86	3	4	2	2	0.8	3	2	0.3	2	2	11	24	3	2	
6	41	0	10	0.3	13	4	8	22	5	2	7	2	0.6	0	0.7	3	0.3	3	1	0.7	0.6	4	12	0.3	0	
7	0	0	0.7	0.3	0.3	1	0.3	0.3	0.4	0.3	0	3	3	7	5	2	5	14	3	7	10	2	3	18	21	
8	3	0	8	5	0.3	8	24	2	16	6	0.3	0.7	1	2	1	2	0.3	0.7	0.3	1	5	0	4	0.7	0.3	
9	0	0	0	3	3	1	1	1	1	0.6	0	2	3	1	1	0.5	3	1	0.7	1	2	0	0.3	1	2	
10	0	0	0	0	0.3	0.7	0	0	0	0	0	0	0.3	0	0	0	0	0.3	0.3	0	0.3	0	0	0.3	0.3	

Table 4.6b : Abundance of the particle types at each sample station for the Baltic Sea (1984).

group no.	% Abun.	SiO ₂ %	Al ₂ O ₃ %	CaO %	Fe ₂ O ₃ %	MnO ₂ %	TiO ₂ %	MgO %	Na ₂ O %	K ₂ O %	Ba %	SO ₄ %	PO ₄ %	MAD μm	MID μm	AVD μm	SF
1	27	86 (7)	4 (5)	1.0 (1.4)	1.2 (1.8)	0.8 (1.5)	0.8 (1.3)	0.6 (1.2)	1.0 (1.2)	1.3 (1.6)	0.7 (1.3)	1.6 (1.4)	0.6 (0.7)	1.9 (1.5)	1.0 (0.8)	1.3 (0.9)	1.6 (0.8)
2	37	62 (7)	13 (6)	3 (4)	4 (4)	1.0 (1.8)	1 (2)	1.1 (1.6)	1 (2)	10 (9)	0.7 (1.7)	1.8 (2.2)	0.9 (1.4)	2.0 (1.6)	1.0 (0.8)	1.4 (1.1)	1.7 (0.9)
3	16	47 (8)	12 (5)	4 (7)	15 (9)	2 (5)	2 (4)	4 (3)	2.3 (2.6)	5 (5)	1 (3)	3 (4)	1.9 (2.4)	2.1 (1.7)	1.0 (0.8)	1 (1)	1.8 (0.9)
4	5	10 (7)	2 (2)	1.1 (2.4)	3 (6)	1.5 (2.6)	0.05 (0.45)	1.5 (1.3)	1.5 (1.8)	1.0 (2.2)	39 (12)	38 (8)	1 (2)	1.5 (1.2)	0.9 (0.7)	1.2 (0.9)	1.25 (0.35)
5	4	15 (8)	3 (3)	2 (3)	49 (13)	7 (10)	1.4 (2.6)	2.6 (1.6)	3.5 (2.2)	1.6 (2.2)	1.4 (2.7)	3 (5)	10 (7)	1 (1)	0.6 (0.5)	0.8 (0.7)	2 (1)
6	5	13 (7)	3 (2)	2 (3)	10 (7)	51 (14)	1 (2)	2.6 (1.6)	6 (3)	1.8 (2.6)	1.1 (2.7)	4 (4)	3 (3)	1.8 (1.2)	0.9 (0.6)	1.2 (0.8)	1.8 (0.7)
7	2	10 (7)	3 (2)	72 (13)	1.7 (2.2)	1.0 (1.4)	1.0 (1.3)	2.8 (3.3)	0.9 (0.7)	0.9 (1.6)	1 (2)	1.3 (3.3)	5 (7)	1.8 (1.6)	0.8 (0.7)	1.1 (0.9)	1.7 (0.9)
8	2	15 (11)	4 (4)	10 (11)	4 (7)	4 (7)	4 (7)	6 (7)	7 (5)	9 (11)	4 (7)	13 (13)	20 (17)	1.1 (1.2)	0.5 (0.6)	0.7 (0.8)	2.1 (1.1)
9	0.8	15 (10)	4.1 (2.5)	2 (4)	7 (10)	1 (2)	58 (17)	2 (1)	1.0 (0.5)	1.3 (1.8)	5 (6)	2 (4)	1.0 (1.3)	1.1 (1.3)	0.6 (0.6)	0.8 (0.8)	1.42 (0.45)
10	0.1	12 (14)	50 (18)	3 (3)	2 (3)	2 (4)	4 (4)	0.5 (0.8)	0.7 (1.3)	1.2 (1.9)	0 (0)	4 (6)	22 (18)	1.5 (1.2)	0.8 (0.7)	1.1 (0.9)	1.4 (0.5)

Table 4.6a : Average composition of the particle types (normalized to 100 weight %) for the Baltic Sea (1984).

MAD = maximum diameter; MID = minimum diameter; AVD = average diameter; SF = shape factor

	Principal Components					
	1	2	3	4	5	6
Cum. Per.	25	45	62	70	77	83
Variables	Loadings					
Depth (%)	-0.51	0.05	-0.67	0.00	0.34	0.20
Temperature (°C)	0.01	0.59	0.48	0.00	0.12	-0.06
Salinity (ppt)	-0.03	0.89	-0.03	-0.16	-0.12	0.07
Oxygen saturation (%)	0.87	0.07	0.27	-0.13	-0.12	0.11
Phosphate ($\mu\text{mol/l}$)	-0.86	0.24	-0.21	0.25	-0.10	0.00
Nitrate ($\mu\text{mol/l}$)	0.09	0.39	-0.68	-0.19	-0.35	0.27
Nitrite ($\mu\text{mol/l}$)	0.19	0.72	0.17	0.43	0.18	-0.08
Suspended matter (mg/l)	0.13	0.15	-0.68	0.23	0.54	0.14
Particle type number						
1	0.34	-0.36	-0.29	0.45	0.05	-0.26
2	0.79	-0.17	-0.18	0.15	0.03	-0.02
3	0.55	0.16	-0.65	-0.33	-0.22	0.01
4	-0.12	-0.16	0.56	-0.02	0.19	0.75
5	-0.48	0.14	0.11	-0.65	0.39	-0.35
6	-0.78	0.00	-0.02	0.28	-0.46	-0.01
7	0.24	0.88	0.14	0.18	0.02	-0.05

Table 4.7 : Cumulative eigenvalues and the loadings for the first six principal components derived from the correlation matrix of the hydrographical and individual particle analysis data.

Elements	Al			Ca				Mn			
	Leachable	Detrital	Total	Leachable	Detrital	Total	Excess	Leachable	Detrital	Total	Excess
Depth (%)	0.11	-0.10	-0.02	-0.13	-0.03	-0.15	-0.05	0.25	-0.06	0.00	0.00
Temperature (°C)	-0.36	-0.02	-0.21	0.50	-0.53	0.36	0.37	-0.11	-0.03	-0.06	-0.05
Salinity (ppt)	-0.16	0.26	0.11	0.88	-0.40	0.81	0.22	-0.04	0.00	-0.01	-0.01
Oxygen saturation (%)	0.10	0.29	0.28	0.14	0.16	0.19	-0.21	-0.61	-0.20	-0.33	-0.34
Phosphate (μmol/l)	-0.21	-0.24	-0.30	0.14	-0.34	0.04	0.32	0.75	0.30	0.46	0.47
Nitrate (μmol/l)	0.23	0.32	0.38	0.27	0.04	0.30	-0.27	-0.10	0.08	0.05	0.04
Nitrite (μmol/l)	-0.04	0.14	0.09	0.57	-0.12	0.56	0.14	-0.06	-0.08	-0.09	-0.09
Suspended matter (mg/l)	0.22	0.32	0.37	-0.18	0.31	-0.09	-0.42	-0.08	-0.17	-0.18	-0.19
Particle type number											
1	0.13	0.00	0.07	-0.30	0.08	-0.30	-0.20	-0.39	0.01	-0.08	0.09
2	0.17	0.61	0.57	-0.28	0.39	-0.17	-0.65	-0.51	-0.18	-0.28	-0.30
3	0.26	0.54	0.56	0.10	0.37	0.23	-0.49	-0.39	-0.14	-0.23	-0.25
4	-0.19	-0.37	-0.39	-0.03	-0.27	-0.12	0.35	-0.08	0.05	0.03	0.04
5	-0.06	-0.24	-0.22	0.14	-0.11	0.11	0.27	0.12	-0.07	-0.03	-0.03
6	-0.09	-0.34	-0.31	0.03	-0.15	-0.02	0.31	0.93	0.28	0.48	0.49
7	-0.07	0.34	0.22	0.77	-0.18	0.76	0.09	-0.13	-0.04	-0.07	-0.08

Table 4.8a : Correlation coefficients between the abundance of the identified particle types, the elemental bulk concentrations and the hydrographical data.

Elements	Fe				Zn				Ba			
	Leachable	Detrital	Total	Excess	Leachable	Detrital	Total	Excess	Leachable	Detrital	Total	Excess
Depth (%)	0.09	-0.10	0.05	0.06	0.10	-0.03	0.09	0.09	-0.10	-0.07	-0.10	-0.11
Temperature (° C)	-0.27	0.03	-0.23	0.03	0.03	-0.35	-0.02	-0.01	-0.50	-0.48	-0.40	-0.40
Salinity (ppt)	-0.05	0.28	0.03	-0.09	-0.10	-0.17	-0.12	-0.13	-0.24	-0.45	-0.35	-0.40
Oxygen saturation (%)	-0.12	0.35	-0.01	-0.34	-0.53	0.12	-0.51	-0.52	-0.09	0.10	0.17	0.13
Phosphate (μmol/l)	-0.10	-0.28	-0.16	0.20	0.28	-0.24	0.25	0.26	-0.05	-0.28	-0.27	-0.25
Nitrate (μmol/l)	0.10	0.42	0.20	-0.25	-0.28	0.04	-0.28	-0.30	0.19	-0.04	-0.11	-0.19
Nitrite (μmol/l)	-0.07	0.32	0.02	-0.08	-0.12	0.00	-0.12	-0.12	-0.13	-0.22	-0.14	-0.16
Suspended matter (mg/l)	0.23	0.31	0.28	-0.17	-0.19	0.07	-0.18	-0.20	0.76	0.26	0.21	0.17
Particle type number												
1	-0.18	0.04	-0.15	-0.22	0.48	0.13	0.50	0.49	0.05	0.06	0.11	0.11
2	0.13	0.46	0.23	-0.43	-0.26	0.21	-0.23	-0.26	0.34	0.48	0.50	0.44
3	0.27	0.50	0.37	-0.30	-0.33	0.13	-0.32	-0.35	0.43	0.33	0.34	0.27
4	-0.37	-0.36	-0.42	0.05	0.16	-0.16	0.13	0.15	-0.15	-0.22	-0.23	-0.18
5	0.48	-0.17	0.38	0.61	0.00	-0.06	-0.01	0.01	-0.15	-0.21	-0.22	-0.21
6	-0.17	-0.32	-0.23	0.14	0.07	-0.10	0.05	0.07	-0.18	-0.12	-0.17	-0.13
7	-0.06	0.43	0.06	-0.20	-0.16	-0.06	-0.17	-0.18	-0.02	-0.29	-0.21	-0.27

Table 4.8b : Correlation coefficients between the abundance of the identified particle types, the elemental bulk concentrations and the hydrographical data.

4.6 REFERENCES

- Allen, G., Sauzay, G., Castaing, P., and Jouanneau, J. M., 1977. Transport and deposition of suspended sediment in the Gironde estuary, France. In : M. Wiley (Editor). *Estuarine Processes*, volume II, Academic Press, New York, pp. 63-81.
- Andrulewicz, E., Brzezinska, A., and Frzosinska, A., 1979. Some aspects of the chemical composition of particulate matter in the Southern Baltic, ICES C.M./C:9.
- Bettinelli, M., Pastorelli, N., and Baroni, V., 1986. STPF determination of trace metals in fly ash samples. *At. Spectrosc.*, 7 : 45-48.
- Bishop, J. K. B., and Biscaye, P. E., 1982. Chemical characterization of individual particles from the nepheloid layer in the Atlantic Ocean. *Earth and Planetary Science Letters*, 58 : 265-275.
- Boström, K., Farquharson, B., and Eyl, W., 1971. Submarine hot springs, a source of active ridge sediments. *Chem. Geol.*, 10 : 189-203.
- Boström, K., Burman, J.-O., Ponter, C., and Ingri, J., 1981. Selective removal of trace elements from the Baltic by suspended matter. *Mar. Chem.*, 10 : 335-354.
- Boström, K., Burman, J.-O., and Ingri, J., 1983. A chemical mass balance for the Baltic. In : R.O. Hallberg (editor), *Environmental Biogeochemistry, Proc. 5th Int. Symp. Env. Biogeochemistry (ISEB)*, Ecol. Bull., Stockholm, 35 : pp. 39-58.
- Brügmann, L., 1986. Particulate trace metals in waters of the Baltic Sea and parts of the adjacent NE Atlantic. *Beitr. Meeresk.*, 55 : 3-18.
- Brügmann, L., and Niemistö, L., 1987. Cooperative contaminant-related sediment studies in the Baltic Sea. ICES Coop. Res. Rep. Ser. : in press.
- Brügmann, L., Geyer, E., and Kay, R., 1987. A new teflon sampler for trace metal studies in seawater - "WATES". *Mar. Chem.*, 21 : 91-99.
- Brzezinska, A., Trzosinska, A., Zmijewska, W., and Wodkiewicz, L., 1984. Trace metals in suspended matter and surficial bottom sediments from the Southern Baltic. *Oceanologia*, 18 : 59-77.

- Chow, T. J., 1976. Barium in Southern-California coastal waters : a potential indicator of marine drilling contamination. *Science*, 193 : 57-8.
- Davison, W., Heany, S. I., Talling, J. F., and Rigg, E., 1980 : Seasonal transformations and movement of iron in a productive English lake with deepwater anoxia. *Schweiz. Z. Hydrol.*, 42/2 : 196-224.
- Dehairs, F., Chesselet, R., and Jedwab, J. 1980. Discrete suspended particles of barite and the barium cycle in the open ocean. *Earth Planet. Sci. Lett.*, 49 : 528-550.
- Desaulniers, J. A. H., Sturgeon, R. E., and Berman, S. S., 1985. Atomic absorption determination of trace metals in marine sediments and biological tissues using a stabilized temperature platform furnace. *At. Spectrosc.*, 6 : 125-127.
- Eggiman, D. W., and Betzer, P. R., 1976. Decomposition and analysis of refractory oceanic suspended materials. *Anal. Chem.*, 48 : 886-890.
- Eisma, D., Boon, J. J., Groenewegen, R., Ittekkot, V., Kalf, J., and Mook, W. G., 1984a. Observations on macro-aggregates, particle size and organic composition of suspended matter in the Ems estuary. In : E. T. Degens, S. Kempe and R. Herrera (Editors). *Transport of Carbon and Minerals in Major World Rivers*, part 3, *Mitteilungen aus dem Geologisch-Paläontologischen Institut der Universität Hamburg*, SCOPE/UNEP Sonderband, Heft 52, Krause-Druk, Stade, pp. 483-505.
- Eisma, D., Skei, J., Westerlund, S., Kalf, J., Magnusson, B., Naes, K., and Sørensen K., 1984b. Distribution and composition of suspended particulate matter and trace metals in the Skagerrak, Paper presented at the ICES Working Group Meeting of the WGMS, Rostock.
- Eisma, D., Bernard, P, Boon, J. J., Van Grieken, R., Kalf, J., and Mook, W. G., 1985. Loss of particulate organic matter in estuaries. In : E. T. Degens, S. Kempe and R. Herrera (Editors). *Transport of Carbon and Minerals in Major World Rivers*, part 3, *Mitteilungen aus dem Geologisch-Paläontologischen Institut der Universität Hamburg*, SCOPE/UNEP Sonderband, Heft 58, Krause-Druk, Stade, pp. 397-412.
- Emelyanov, E., 1974. Distribution of Fe, Al, Ti, Mn, Cu, Ni, Co in suspension of the Baltic Sea waters. *Vopros. Tchetwer. Geol. (Riga)*, 7 : 81-98.

- Emelyanov, E. M., and Pustelnikov O. S., 1975. Amount of suspended forms of elements (Org. C., SiO₂ amorph., Fe, Al, Ti, Mn, Ni, Cu, Co) in the waters of the Baltic Sea. *Geokhimiya*, 7 : 1049-1063.
- Emelyanov, E. M., and Trimonis, E. S., 1981. Mineral composition of late quaternary deposits of the Baltic Sea obtained by X-ray diffractometric analysis. In : A.P. Lisitzin and E.M. Emelyanov (Editors), *Formation of Sediments in the Baltic Sea*, Nauka, Moscow, pp. 180-188 (in Russian).
- Emelyanov, E. M., 1986. Basins of the Baltic Sea - traps for elements. *Finn. Mar. Res.*, 253 : 79-96.
- Filipek, L. H., and Owen, R. H., 1981. Diagenetic controls of phosphorus in outer continental shelf sediments from the Gulf of Mexico. *Chem. Geol.*, 33 : 181-204.
- Goldberg, E. D. (Editor), 1978. Biogeochemistry of estuarine sediments. Proc. Workshop in Melreux/Belgium Nov. 29 - Dec. 3, 1976 UNESCO press, Paris, 293 pp.
- Gordeev, V. V., Miklishansky, A. S., and Tambiev, S. B., 1984. Geochemistry of particulates and waters of the Gulf of Riga. In : A.P. Lisitzyn (Editor), *Geological History and Geochemistry of the Baltic Sea*, Nauka, Moscow-Leningrad, pp. 18-32 (in Russian).
- Grasshoff, K., (1975). The hydrochemistry of landlocked basins and fjords. In : J.P. Riley and G. Skirrow (Editors), *Chemical Oceanography*, Acad. Press, London, pp. 455-597.
- Gustavsson, I., and Notter, M., 1978. Tungmetaller i vattenburen partikulär substans i Rönnskärsområdet, Naturvårdsverket Rapport SNV 1026, Solna.
- Gustavsson, I., 1981. Koncentrationen av några tungmetaller i kustvattnen utanför Oxelösund och Vallvik 1980/81, Naturvårdsverket Rapport SNV PM 1465, Solna.
- HELCOM, 1982. Guidelines for the Baltic Monitoring Programme (BMP) for the first stage (updated version), Baltic Marine Environment Protection Commission, Helsinki.
- Holmes, C. W., 1982. Geochemical indices of fine sediment transport in the North-West Gulf of Mexico. *J. Sedim. Petrol.*, 52 : 307-321.

- Ingri, J., Ponter, C., Burman, J.-O., and Bostrom, K., 1984. Manganese pathways in the Baltic Sea. Proc. ICES Symposium on Contaminant Fluxes through the coastal zone, Nantes.
- Ingri, J., 1985. Geochemistry of ferromanganese concretions and associated sediments in the Gulf of Bothnia, Doctoral thesis, University of Luleo, Luleo, 374 pp.
- Ingri, J., and Ponter, C., 1986. Iron and manganese layering in recent sediments in the Gulf of Bothnia. *Chem. Geology*, 56 : 105-116.
- Jedwab, J., 1980. Rare anthropogenic and natural particles suspended in deep ocean waters. *Earth Planet. Sci. Lett.*, 49 : 551-564.
- Jonasz, M., 1983. Particle-size distributions in the Baltic. *Tellus*, 35B : 346-358.
- Jouanneau, J.-M., 1982. Matières en suspension et oligo-elements metalliques dans le système estuarien Girondin : comportement et flux. Ph.D. Dissertation, University of Bordeaux I, No. 732, 150 pp. (in French).
- Kelly, J. F., Lee, R. J., and Lentz, S., 1980. Automated characterization of fine particulates. *Scanning Electron Microscopy*, I : 311-322.
- Klossa, 1977. Contribution à l'étude de la matière particulaire par une méthode d'analyses ponctuelles combinées. Ph.D. Dissertation, Université Paris-7.
- Lambert, C. E., Bishop, J. K. B., Biscaye, P. E., and Chesselet, R., 1984. Particulate aluminium, iron and manganese chemistry at the deep Atlantic boundary layer. *Earth and Planetary Science Letters*, 70 : 237-248.
- Lowenstam, H. A., 1974. Impact of life on chemical and physical processes. In : E. D. Goldberg (Editor), *The Sea*, Wiley Interscience, New York, pp. 715-796.
- Meade, R. H., 1972. Transport and deposition of sediments in estuaries. *Geol. Soc. Am. Memoir.*, 133 : 91-120.
- Melvasalo, T., Pawlak, J., Grasshoff, K., Thorell, L., and Tsyban, A., 1981. Assessment of the effects of pollution on the natural resources of the Baltic Sea, 1980. *Baltic Sea Environment Proceedings*, No. 5B : 426 pp.

- Oreshkin, V. N., Belyaev, Yu. I., Tatsiy, Yu. G., and Vnukovskaya, G. L., 1980. A direct simultaneous determination of cadmium, lead and silver in sea, river and eolian suspended matter by the non-flame atomic absorption analysis. *Okeanologiya*, 20 : 36-742.
- Postma, H., 1980. Sediment transport and sedimentation. In : E. Olausson and I. Cato (Editors), *Chemistry and Biogeochemistry of Estuaries*. Wiley & Sons, Chichester, pp. 153-186.
- Price, N. B., and Skei, J. M., 1975. Areal and seasonal variations in the chemistry of suspended particulate matter in a deep water fjord. *Est. Coast. Mar. Science*, 3 : 349-369.
- Pritchard, D. W., 1967. What is an estuary : Physical viewpoint. In : G. H. Lauff (Editor), *Estuaries*. Publication no. 83, American Association for the Advancement of Science, Washington D.C., pp. 3-5.
- Pustelnikov, O. S., 1977. Geochemical features of suspended matter in connection with recent sedimentation processes in the Baltic Sea, *Ambio Special Report*, 5 : 157-162.
- Roaldset, E., 1978. Ph.D. Dissertation, University of Oslo.
- Salomons, W., 1975. Chemical and isotopic composition of carbonates in recent sediments and soils from Western Europe. *Journal of Sedimentary Petrology*, 45 : 440-449.
- Salomons, W., and Förstner, U., (Editors), 1984. *Metals in the Hydrocycle*, Springer-Verlag, Berlin, 349 pp.
- Schulz, S., 1985. *Ergebnisse ökologischer Untersuchungen im pelagischen Ökosystem der Ostsee*. Dissertation, Rostock-Warnemünde, 184 pp.
- Sigg, L., 1984. Metal transfer mechanisms in lakes; the role of settling particles. In : W. Stumm (Editor), *Chemical Processes in Lakes*. John Wiley & Sons, New York, pp. 283-310.
- Singh, S. K., and Subramanian, V., 1984. Hydrous Fe and Mn oxides - scavengers of heavy metals in the aquatic environment. *CRC Critical Reviews in Environmental Control*, 14 : 33-90.

- Skei, J. M., and Melson, S., 1982. Seasonal and vertical variations in the chemical composition of suspended particulate matter in an oxygen-deficient fjord. *Est. Coast. Shelf Science*, 14 : 61-78.
- Sundby, B. N., Silverberg, N., and Chesselet, R., 1984. Pathways of manganese in an open estuarine system. *Geochim. Cosmochim. Acta*, 45 : 293-307.
- Taylor, R., 1964. Abundance of chemical elements in the continental crust : a new table. *Geochim. Cosmochim. Acta*, 28 : 1273-1285.
- Turekian, K. K., and Taush, E. H., 1964. Barium in deep sea sediments of the Atlantic Ocean. *Nature*, 15 : 696-697.
- Upchurch, J. B., Edzwald, J. K., and O'Melia, C. R., 1974. Phosphates in sediments of Palmico estuary. *Environ. Sci. Technol.*, 8 : 56-68.
- Voipio, A., 1981. *The Baltic Sea*, Elsevier Oceanography Ser. No. 30, Amsterdam.
- Weigel, H.-P., 1976. Atomabsorptionsmessungen von Blei, Cadmium, Kupfer, Eisen und Zink im Seston der Ostsee. *Helgoländer wiss. Meeresunters*, 28 : 206-216.
- Weigel, H.-P., 1977. On the distribution of particulate metals, chlorophyll and seston in the Baltic Sea. *Mar. Biol.*, 44 : 217-222.
- Williams, J. D. H., Jacquet, J. M., and Thomas, R. L., 1976. Forms of phosphorus in the surficial sediments of Lake Erie. *J. Fisheries Research Board of Canada*, 33 : 413-429.
- Yeats, P. A., and Dalziel, J. A., 1985. ICES Intercalibration for Metals in Suspended Particulate Matter, ICES/ACMP Preliminary Report, 14 pp.
- Yurkovsky, A. K., and Pinkule, A. Ya., 1980. On the formation, metamorphization and distribution of allochthonous matter flocculi in the Baltic Sea. *Okeanlogiya*, 20 : 1045-1053.

Chapter 5

Summary

The primary scope of this work was to establish an unsupervised classification scheme for the reduction of the data matrix obtained by automated EPXMA. It was seen that this required the simultaneous cluster analysis of all the measured particles of all the samples. For this purpose a nonhierarchical cluster technique, the method of Forgy, a nearest centroid sorting method, was used to classify all the measured particles into particle types representative for all the studied samples, and to characterize the individual samples on the basis of the abundances of these particle types. A sequence of hierarchical cluster analysis was proposed to determine the number of clusters and the initial centroids necessary for the first step of the nearest centroid sorting method. In the past few years this method was extensively used, by a number of people to a variety of automated EPXMA data, which showed its general applicability.

To evaluate the performance of different hierarchical cluster techniques, cluster analyses were performed on a number of known mineral mixtures, and the amount of correct classification was measured quantitatively by kappa statistics. This allowed the study of the influence of a number of experimental parameters of the cluster analysis and EPXMA on the cluster result.

In practice, the combinations of the five minerals per two, ten combinations, were studied as a function of the mineral mixture ratio and the use of either normalized or unnormalized variables. For this purpose a total of 7000 cluster results were studied. It was seen that the mean kappa values of ten measurements approach the probability of good classification. Relatively high mean kappa values were found for these mineral mixtures, for which no, or minor particle overlap exists between the mineral types. This difficulty of the mineral mixtures for the cluster analysis was checked by linear discriminant analysis. In general, it seems that Ward's method was, in most cases, most successful in finding the correct classification. For mixtures which were less difficult for the cluster techniques, the mean kappa values approach each other near the upper limit of one.

For the more difficult mixtures, the Ward's method has in most cases a significantly better mean kappa value. The Furthest Neighbor, the Group Average and the Centroid method seem to be slightly better than the Simple Average, the Median and the Nearest Neighbor method. However the differences are not always significant, and the rule is not generally applicable. The influence of the relative mixing ratio could be understood on the basis of the data structure of the mixture. This data structure was studied by the use of principal component analysis, which elaborated that, as could be expected, higher mean kappa values were encountered when a higher fraction of the more compact mineral type was present, reducing in most cases also the particle overlap. In the case standardized variables were used it was seen that in most cases only the cluster results of the Ward's method were improved for a few mixtures. In general, for all other cluster techniques significantly lower mean kappa values were measured.

In a second approach one mineral mixture was used to study the effect of mixture size, of working with correlated/uncorrelated variables (principal component space) and of the quantification of the EPXMA data (different deconvolution techniques and Armstrong-Buseck ZAF-corrected results). The results of the 2100 cluster analyses were studied. These showed that there is no influence of the mixture size. Only the Nearest Neighbor method performs worse at increasing mixture size. This means, that except for the Nearest Neighbor method, all the obtained results can be extrapolated toward larger mixture sizes. Furthermore it was seen that working in the principal component space (uncorrelated variables) reduced the probability for a good classification. The cluster results of the ROI, AXIL and ZAF-corrected data were comparable, but the use of the FFA resulted in significant lower mean kappa values.

Generally, the use of the kappa statistics to the cluster results of known mineral mixtures is successful in quantitatively determining the performance of the cluster techniques and the influence of a number of experimental parameters.

For the practical part of this work, automated EPXMA combined with multivariate analysis was applied to suspended particulate matter from the aquatic environment. Geochemical studies of the Ems, Gironde and Scheldt estuary and of the Baltic Sea were performed.

In the case of the Ems estuary study, a clear distinction between the marine and river end-members was found, e.g. abundance differences between the end-members are significant. By the study of the longitudinal profile throughout the estuary, the mixing of the end-members could be followed. It was seen that the mixing of riverborne material with marine suspended particulate matter occurs entirely in the freshwater tidal area. If it is assumed that the end-members behave conservatively, the relative abundance variations of the end-members can be used as a conservative index of mixing for the suspended particulate matter. In this particular case, the results of the inorganic suspended particulate matter were used to trace the physical mixing of the river and marine suspended particulate components, to study the behavior of the organic fraction of the particulate matter. For the Ems estuary it was seen that the mixing throughout the estuary of the inorganic and organic components goes parallel. Owing to the sampling during high and low river discharge, the influence of different discharge conditions on the composition of the suspended particulate matter could be measured. It was seen that approximately the same particle types, with a significant abundance throughout the estuary, were identified by the multivariate analysis for both discharge conditions. The mixing of riverborne material with marine suspended particulate matter always appears to occur in the freshwater region, somewhat more up- or downriver depending on the river discharge. Furthermore the influence of biogenic Si-rich frustules was measurable for some samples.

The study of the Gironde estuary had the same objectives as the Ems study. The composition of the suspended particulate matter in the estuary is determined

by the mixing ratio between the Garrone, Dordogne and marine suspended matter. Sampling, throughout the estuary and in the rivers, showed that the Garrone is the principal source of the suspended particulate matter in the estuary. The abundance variations in the Gironde may at least partly be explained by the admixture of Dordogne material in different proportions. The admixture of North and South channel suspended material can also lead to fluctuations in the abundances of some of the particle types. No evidence was found for a net flux of marine suspended particulate matter into the estuary, if it is assumed that the suspended matter coming in from the sea does not have the same composition as the Garrone suspended matter. If the composition of the particulate organic matter is regarded, no uniform composition is found. The particulate inorganic suspended matter analysis indicates that this is probably not, as in the case of the Ems, caused by mixing of estuarine with marine suspended matter. Therefore probably an admixture of older estuarine suspended material or resuspended sediments with a lower organic content and different composition occurs. Or there is a process of transformation of organic matter in the estuary resulting in a different organic composition and a higher $\delta^{13}\text{C}$ ratio.

The Scheldt estuary results show that none of the identified particle types is subject to systematic abundance variations throughout the estuary. Only the abundance of the calcite and/or aragonite particle type increases gradually seaward. However its abundance fluctuates significantly. It was seen that probably the river end-member was not determined unambiguously. It is therefore recommended to sample further upriver, from Dendermonde toward Ghent to characterize pure river material. A search for particles with a relatively high mean atomic number allowed us to identify a number of particles probably formed within the anoxic region of the Scheldt or having an anthropogenic origin.

The Baltic Sea, sampled from the Bothnian Bay to the North Sea at different depth profiles, showed significant abundance variations of the identified par-

ticle types. Principal component analysis of the single particle data and the hydrochemical data revealed that most of the compositional variations can be explained by differences between deep and surface waters, the redox conditions and the influences caused by inflowing North Sea waters. Additional information about the types and sources of the suspended matter in the Baltic Sea was gained from the comparison and correlation of the single particle results with different fractions of the bulk concentrations of the elements.

Generally the use of automated EPXMA allows the advanced characterization of individual suspension particles from the aquatic environment. The study of the abundance variations of the particle types provide information about biogeochemical processes that influence the distribution of certain particle types throughout the study area.

Chapter 6

Samenvatting

De voornaamste doelstelling van dit werk was de ontwikkeling van een "unsupervised" classificatie schema voor de reductie van de gegevens matrix die resulteert uit geautomatiseerde electronen-probe X-stralen microanalyse (EPXMA). Er werd aangetoond dat dit enkel mogelijk is door een gelijktijdige clusteranalyse van alle gemeten deeltjes van alle stalen. Hiervoor werd een niet hiërarchische clustermethode gebruikt, de Forgy procedure, een nearest centroid methode, die alle gemeten deeltjes klasseerde in deeltjesklassen representatief voor alle geanalyseerde stalen. De geanalyseerde stalen worden dan gekarakteriseerd op basis van de abundanties van de deeltjesklassen. Een opeenvolging van hiërarchische clusteranalyses werd vooropgesteld om het aantal clusters en de initiële centroids, noodzakelijk voor de eerste stap van de nearest centroid methode, te bepalen. In de afgelopen jaren werd deze methode intensief toegepast door een aantal onderzoekers op een grote verscheidenheid van geautomatiseerde EPXMA data, wat de algemene versatiliteit van deze methode aantoont.

Om de prestaties van verscheidene hiërarchische clustertechnieken te evalueren, werden clusteranalyses uitgevoerd op een aantal gekende mineraalmengsels. De hoeveelheid correct geklasseerden werd kwantitatief gemeten met behulp van kappa statistiek. Deze aanpak maakt tevens de studie mogelijk van de invloed van een aantal experimentele parameters van zowel de cluster analyse als de EPXMA op het clusterresultaat. In de praktijk werden de combinaties van vijf mineralen per twee, resulterende in tien verschillende mineraalmengsels, bestudeerd in functie van de mineraalmengverhouding en het gebruik van genormaliseerde en niet genormaliseerde veranderlijken. Voor dit doel werden 7000 cluster- en kappa-analyses bestudeerd. Er werd aangetoond dat de gemiddelde kappawaarden van tien metingen een waarschijnlijkheid voor een goede classificatie benaderde. Relatief hoge kappawaarden werden gevonden bij die mengsels die geen of weinig deeltjesoverlap tussen de mineralen vertonen. De moeilijkheidsgraad van de mineraalmengsels voor de clusteranalyses werd gecontroleerd door lineaire discriminant analyses. In het algemeen was de Ward's

methode het meest succesvol om de correcte classificatie te vinden. Bij mengsels met een lage moeilijkheidsgraad voor de clustertechnieken, benaderden de gemiddelde kappawaarden van de verschillende technieken elkaar nabij de maximumlimiet van één. Voor moeilijkere mengsels gaf de Ward's methode, in de meeste gevallen, beduidend hogere kappawaarden. De Furthest Neighbor, de Group Average en de Centroid methode presteerden iets beter dan de Simple Average, de Median en de Nearest Neighbor methode. De verschillen zijn echter niet altijd beduidend en deze regel is niet algemeen toepasbaar. De invloed van de relatieve mengverhouding op het clusterresultaat kan worden begrepen aan de hand van de gegevensstructuur van het mengsel. Deze gegevensstructuur werd bestudeerd door middel van hoofdcomponenten analyse ("principal component analysis"). Deze analyses toonden aan dat, zoals verwacht, hogere kappawaarden werden bekomen indien er een groter deel van de meer compacte groep aanwezig is, wat tevens in de meeste gevallen ook de deeltjesoverlap reduceert. In het geval gestandaardiseerde veranderlijken werden gebruikt, werden in de meeste gevallen enkel de clusterresultaten van de Ward's methode verbeterd voor enkele mineraalmengsels. Voor alle andere clustertechnieken werden beduidend lagere kappawaarden gemeten.

In een tweede benadering werd één mineraalmengsel weerhouden om de invloed van de grootte van de gegevensmatrix, van het werken met gecorreleerde en niet gecorreleerde veranderlijken (hoofdcomponenten ruimte) en van het kwantificeren van de EPXMA-gegevens (verschillende deconvolutietechnieken en Armstrong-Buseck ZAF-gecorrigeerde gegevens) te bestuderen. Hiervoor werden 2100 cluster- en kappa-analyses uitgevoerd. Uit de bekomen resultaten bleek dat de afmetingen van de gegevensmatrix geen invloed heeft op het clusterresultaat. Enkel de Nearest Neighbor methode gaf slechtere resultaten bij grotere gegevensmatrices. Dit houdt in dat, behalve dan voor de Nearest Neighbor methode, de bekomen resultaten geëxtrapoleerd kunnen worden naar andere gegevensmatrixafmetingen. Verder werd er aangetoond dat het werken in de

hoofdc componenten ruimte (niet gecorreleerde veranderlijken) de waarschijnlijkheid op een goede classificatie verlaagt. De clusterresultaten van de ROI, AXIL en ZAF-gecorrigeerde gegevens waren vergelijkbaar. Het gebruik van het FFA algoritme gaf echter aanleiding tot beduidend lagere gemiddelde kappawaarden.

In het algemeen werd er aangetoond dat kappa statistiek op de clusterresultaten van gekende mineraalmengsels in staat is om de prestaties van zowel de clustertechnieken als de invloed van een aantal experimentele parameters kwantitatief te bepalen.

Voor de praktische toepassingen van dit werk, werd geautomatiseerde EPXMA gecombineerd met de multivariate analyses toegepast om het aquatisch gesuspendeerde materiaal te bestuderen. Geochemische studies werden uitgevoerd van het Eems, Gironde en Schelde estuarium en van de Baltische Zee.

Bij de Eems studie werd een duidelijk onderscheid gevonden tussen de rivier en mariene eindleden ("end-members"), m.a.w. de abundantieverschillen van bepaalde deeltjesklassen van de eindleden zijn beduidend. Indien het longitudinaal profiel doorheen het estuarium wordt bekeken, kan de menging van de eindleden worden gevolgd. Er werd aangetoond dat de menging van het riviermateriaal met het mariene gesuspendeerd materiaal volledig plaatsvindt in het zoetwatergebied van het estuarium dat door het getij beïnvloed wordt. Indien er wordt verondersteld dat de eindleden zich conservatief gedragen, dan kunnen de relatieve abundantieveranderingen van de eindleden worden gebruikt als de conservatieve mengindex voor het gesuspendeerde deeltjesmateriaal. De resultaten van de anorganische gesuspendeerde deeltjesmaterie werd gebruikt om de fysische menging van de rivier en de mariene componenten te bepalen. Voor het Eems estuarium bleek de menging van het anorganische en het organische materiaal analoog te verlopen. Daar er zowel gedurende hoge als bij lage rivier-

toevoer werd bemonsterd, kon de invloed van de verschillende toevoercondities op de samenstelling van het gesuspendeerde materiaal worden nagegaan. Er werd vastgesteld dat nagenoeg dezelfde deeltjesklassen, met een significante abundantie werden geïdentificeerd door de multivariate analyses doorheen het estuarium voor beide riviertoevoercondities. De menging van het riviermateriaal met het mariene gesuspendeerde materiaal heeft altijd plaats in het zoetwatergebied. Afhankelijk van de riviertoevoer is dit meer stroomop- of stroomafwaarts. Verder werden in enkele stalen biogene Si-rijke skeletten gevonden.

De objectieven van de studie van het Gironde estuarium waren dezelfde als deze van het Eems estuarium. Hier wordt echter de samenstelling van het gesuspendeerd materiaal bepaald door de mengverhouding van het Garrone, Dordogne en het mariene materiaal. Staalnames doorheen het estuarium, en in de rivieren toonden aan dat de Garrone de hoofdbron is van het gesuspendeerde materiaal in het estuarium. De abundantieveranderingen in de Gironde kunnen, althans gedeeltelijk, worden verklaard door de vermenging van Dordogne materiaal onder verschillende verhoudingen. De menging van gesuspendeerd materiaal van het Noord- en Zuid-kanaal kan ook tot fluctuaties van enkele deeltjesklassen leiden. Er werden geen aanwijzingen gevonden voor een netto bijdrage van het mariene gesuspendeerde materiaal naar het estuarium toe, of het mariene gesuspendeerde materiaal zou dezelfde samenstelling moeten hebben als het Garrone riviermateriaal. Wanneer echter naar de samenstelling van het organisch materiaal wordt gekeken, werd geen uniformiteit doorheen het estuarium gevonden, terwijl de analyse van het gesuspendeerd anorganisch deeltjesmateriaal aanwijst dat dit, waarschijnlijk niet, (zoals in het Eems estuarium), te wijten is aan de menging van het rivier en mariene materiaal. Daarom wordt dit toegeschreven aan een vermenging van ouder gesuspendeerd materiaal of gere-suspendeerde sedimenten uit de rivier met een lager organisch gehalte en een verschillende samenstelling. Ofwel is er een proces actief dat de transformatie

van het organisch materiaal in het estuarium mogelijk maakt, wat resulteert in een verschillende organische en isotoop samenstelling.

De Schelde resultaten wezen erop dat geen van de geïdentificeerde deeltjesklassen onderhevig is aan systematische abundantieveranderingen doorheen het estuarium. Alleen de abundantie van de calciëten en/of aragoniet groep steeg gradueel stroomafwaarts, alhoewel zijn abundantie significant fluctueerde. Tevens was het waarschijnlijk niet mogelijk om de rivier "eindleden" ontegensprekelijk te bepalen. Om zuiver riviermateriaal te bemonsteren zullen waarschijnlijk stalen tussen Dendermonde en Gent moeten worden genomen. De analyse van deeltjes met een relatief hoog atoomnummer stelde ons in staat een aantal deeltjes te identificeren die mogelijk werden gevormd in het anoxisch gebied van de Schelde of die een antropogene bron hebben.

De Baltische Zee, bemonsterd vanaf de Baai van Bothnië tot aan de Noordzee, met verschillende diepteprofielen, vertoonde significante abundantieveranderingen voor de geïdentificeerde deeltjesklassen. Hoofdcomponenten analyse van de individuele deeltjesgegevens en de hydrochemische gegevens toonden aan dat de meeste abundantieveranderingen in verband stonden met de verschillen in diepte- en oppervlakte-water, de redoxcondities en de invloed van het instromend Noordzeewater. Bijkomende informatie over de deeltjesklassen, en hun mogelijke bronnen, werd bekomen door de individuele deeltjesresultaten met de verschillende fracties van de bulkconcentraties te vergelijken en te correleren.

Algemeen kan worden besloten dat het gebruik van geautomatiseerde EPXMA de doorgedreven karakterisering van individuele deeltjes uit het aquatische milieu toelaat. De studie van de abundantieveranderingen van de geïdentificeerde deeltjesklassen levert informatie op over biogeochemische processen die een invloed uitoefenen op de verdeling van welbepaalde deeltjesklassen door-

heen een studiegebied.

Appendix

Publications

Articles.

D. Eisma, P. Bernard, J. J. Boon, R. Van Grieken, J. Kalf, W. G. Mook.
Loss of particulate organic matter in estuaries as exemplified by the Ems and Gironde estuaries.

Mitt. Geol. Palaëont. Inst. Univ. Hamburg : 58 (1985) 397-412. (SCOPE/UNEP Sonderband, Transport of Carbon and Minerals in Major World Rivers)

P. Bernard, R. Van Grieken, D. Eisma

Classification of estuarine particles using automated electron microprobe analysis and multivariate techniques.

Environmental Science & Technology : 20 (1986) 467-473.

K. Swenters, J. Verlinden, P. Bernard, R. Gijbels

Electrode surface modifications and material transport into a high voltage vacuum spark discharge.

International Journal of Mass Spectrometry and Ion Processes, 71 (1986) 85-102.

L. Wouters, P. Bernard, R. Van Grieken

Characterization of individual estuarine and marine particles by LAMMA and EPXMA.

Intern. J. Environm. Anal. Chem.: 34 (1988) 17-29.

M. F. D. Araujo, P. C. Bernard, R. E. Van Grieken

Heavy metal contamination in sediments from the Belgian coastal North Sea and the Scheldt estuary.

Marine Pollution Bulletin : 19 (1988) 269-273.

D. Eisma, J. Kalf, M. Karmini, W. G. Mook, A. Van Put, P. Bernard, R. Van Grieken

Dispersal of suspended matter in Makasa Strait and the Flores Basin.

Netherlands Journal of Sea Research, in press.

P. C. Bernard, R. E. Van Grieken, L. Brüggemann

Geochemical composition of suspended matter from the Baltic Sea : 1. Results of individual particle characterization by automated electron microprobe.

Marine Chemistry : 26 (1989) 155-177.

Proceedings.

P. C. Bernard, R. Van Grieken, D. Eisma.

Study of individual estuarine suspension particles by automated electron-probe X-ray microanalysis.

Proceedings of the Symposium Progress in Belgian Oceanographic Research, Eds. R. Van Grieken and R. Wollast, University of Antwerp, Antwerp (1985), 160-169, 1985.

P. C. Bernard, R. Van Grieken, D. Eisma.

Characterization of individual suspension particles in the Ems estuary. Proceedings of the 3rd International Symposium on River Sedimentation, Eds. S. Y. Wang, H. W. Shen, L. Z. Ding, University of Mississippi, University (1986), 488-496, 1986.

R. Van Grieken, P. Bernard, A. Van Put, L. Wouters.

Single particle analysis of suspended matter from the water environment.

Proceedings of the Symposium Analysis of Clay Minerals, Ed. P. Veniale, La Spezia, 41-51, 1987.

R. Van Grieken, P. Artaxo, P. Bernard, F. Bruynseels, Ph. Otten, H. Storms, Ch. Xhoffer.

Characterization of individual environmental particles. Proceedings of the Sixth International Conference Chemistry for Protection of the Environment 1987. Eds. L. Pawloski, E. Mentasti, W. J. Lacy, C. Sazzanini, Elsevier, Amsterdam, 307-316, 1988.

Abstracts.

P. Van Dyck, H. Storms, P. Bernard, R. Van Grieken

Automated quantitative electron microprobe analysis of particulate material

Abstracts of the 10th International Congress on X-ray Optics and Microanalysis, (1984) 218

R. Van Grieken, P. Bernard, A. Markowicz, H. Storms

Automated quantitative electron probe X-ray micro-analysis of particulate material

Abstracts of Euroanalysis V, No. III-10, (1984) 98

P. Bernard, R. Van Grieken, D. Eisma

Study of individual marine and estuarine suspension particles by automated electron-probe X-ray microanalysis.

Abstracts Symposium Progress in Belgian Oceanographic Research, (1984)

R. E. Van Grieken, P. Bernard, F. Bruynseels, H. Storms

Characterization of environmental particles by X-ray and Mass spectrometric techniques.

Abstracts of the 1st Brazilian Congress on Environmental Chemistry, Plenary Lecture no. 7, (1985) 11-12

M. F. D. Araujo, P. Bernard, R. Van Grieken

Determination of trace elements in sediments by energy-dispersive X-ray fluorescence.

Abstracts of the 10th International Symposium on Microchemical Techniques (1986) 34

L. Wouters, P. Bernard, R. Van Grieken

Characterization of the individual suspension particles from aquatic environments.

Abstracts of the 10th International Symposium on Microchemical Techniques (1986) 101

P. Bernard, R. Van Grieken, L. Brüggmann, D. Eisma

Individual suspension particle characterization by automated electron microprobe.

Abstracts of the 16th EBSA Symposium on Dynamics of Turbid Coastal Environments.

R. Van Grieken, P. Bernard, L. Wouters

Single particle analysis of estuarine and marine suspensions.

Abstracts of the 4th International Symposium Interactions between Sediments and Water (1987) 156

R. Van Grieken, P. Artaxo, P. Bernard, F. Bruynseels, L. Kolaitios, Ph. Otten, H. Storms, A. Van Put, L. Wouters, Ch. Xhoffer

Characterization of individual environmental particles.

Abstracts of the Sixth International Conference Chemistry for Protection of the Environment (1987) 19

A. Van Put, P. Bernard, R. Van Grieken

Effect of salinity and temperature on the adsorption of cadmium on estuarine suspensions.

Ibidem 197

R. Van Grieken, P. Artaxo, P. Bernard, F. Bruynseels, Ph. Otten, H. Storms, A. Van Put

Microanalysis of particulate environmental samples.

Abstracts of the VIth Spectroscopy Congress (1987) 71

M. F. D. Araujo, P. Bernard, R. Van Grieken

Trace metal analysis of sediments from the coastal Belgian zone of the North Sea and from Scheldt estuary.

Abstracts of Euroanalysis VI (1987) 401

R. Van Grieken, P. Bernard, A. Van Put, L. Wouters

Single particle analysis of estuarine and marine suspensions.

Abstract of Joint Oceanographic Assembly (1988) 357

L. Brüggemann, P. Bernard, R. Van Grieken

Geochemical composition of suspended matter from the Baltic Sea.

Abstract of the XVI conference of Baltic Oceanographers (1988)

R. Van Grieken, P. Bernard, L. Leysen, Ph. Otten, S. Scholdis, H. Storms, A. Van Put, L. Wouters, Ch. Xhoffer

Micro-analysis of individual environmental particles.

Abstract of 18th International Symposium on Environmental Analytical Chemistry (1988) 26

P. Bernard, A. Van Put, R. Van Grieken

Single particle analysis of estuarine suspended particulate matter and sediments.

Abstract of International Symposium on the Fate and Effects of Toxic Chemicals in Large Rivers and their Estuaries (1988) 6

V. Van Alsenoy, A. Van Put, P. Bernard, R. Van Grieken

Chemical characterization of suspensions and sediments in the North Sea.

Abstract van de Studiedag Noordzee (1989) 3.3

P. Bernard, A. Van Put, R. Van Grieken

The influence of data quantification on the results of cluster analysis.

Abstract of the 1st European Workshop on Modern Developments and Applications in Microbeam Analysis (1989) 185

